UNIVERSITY OF CALIFORNIA,
IRVINE

Protective Outcome of Attenuation of Kv7 Channel Suppression in the Pathology of Seizures and Epileptogenesis

DISSERTATION

submitted in partial satisfaction of the requirements
for the degree of

DOCTOR OF PHILOSOPHY

in Pharmacology and Toxicology

by

Derek Lane Greene

Dissertation Committee:
Professor Naoto Hoshi, Chair
Professor Frederick J. Ehlert
Professor Geoffrey W. Abbott

2017

TABLE OF CONTENTS

LIST OF FIGURES

ACKNOWLEDGEMENTS

I would like to express my great appreciation to my mentor and committee chair, Professor Naoto Hoshi, for providing his support and guidance as well as sharing his exemplary experience and perseverance. This dissertation would not have been possible without his efforts. I also extend my gratitude to my committee members, Professor Geoff W. Abbott and Professor Frederick J. Ehlert, for their wisdom and insight in both scientific matters and in regards to my professional development.

I would like to thank all members of the Hoshi lab, past and present. They have been colleagues as well as dear friends. I would also like to extend a special acknowledgement to my friends in the Department of Pharmacology, for their professional advice and friendship that allowed me to enjoy my time at UCI.

I thank American Society for Clinical Investigation for permission to include the originally published article originally published in the Journal of Clinical Investigation into my dissertation. The text of this dissertation is a partial reprint of the material as it appears in "M-current preservation contributes to anticonvulsant effects of valproic acid." The corresponding author listed in this publication, Naoto Hoshi, directed and supervised research which formed the basis for the dissertation. I would also like to thank the co-authors of the publication: Hee Yeon Kay, Seungwoo Kang, and Anastasia Kosenko. Additionally, I would like to thank Springer for permission to include the original article previously published in Cellular and Molecular Life Sciences. The text of this dissertation is a partial reprint of the material as it appears in "Modulation of Kv7 channels and excitability in the brain." The co-author listed in this publication, Naoto Hoshi, supervised this report. Financial support was provided by the National Institute of Health grant NS067288 to Naoto Hoshi.

Finally, a very special thanks to my family and friends for their unconditional love, support, and understanding over the years of this program. They encouraged and comforted me through the tough moments and celebrated with me in my successes.

CURRICULUM VITAE

Derek Lane Greene

Education

Ph.D. Pharmacology and Toxicology, University of California, Irvine 2017

B.S. Biological Sciences, University of California, Irvine 2009

Field of Study

Neuropharmacology and molecular mechanisms of voltage-gated ion channels in epilepsy

Research Experience

Graduate Student Researcher, Department of Pharmacology, UCI 2013-present
Laboratory of Naoto Hoshi, M.D., Ph.D.

- Discovered mechanism of inhibition for 2 common ion channel inhibitors via biochemical and electrophysiological characterization as well as live cell imaging
- Characterized novel mechanism of anticonvulsive action for valproic acid
- Examined functional role of ion channel regulation in seizure and epilepsy using animal models, molecular biology and immunohistochemistry
- Established and managed transgenic mouse lines in collaboration with UCI transgenic Mouse Facility

Laboratory Assistant, Department of Pharmacology, UCI 2009-2013
Laboratory of Naoto Hoshi, M.D., Ph.D.

- Investigated Molecular mechanisms underlying modulation of voltage-gated ion channels
- Designed and engineered proteins with site specific mutations in mammalian cells and E. coli, and used them to identify key sites of direct molecular interactions
- Discovered novel multi-protein complex and determined functional significance
- Safety on site officer
- Trained and addressed instrument related questions to undergraduate, graduate and international visiting scholars
- Improved protocols for molecular assays

Professional Development

Business of Science Certification 2016

Publications

Greene, DL, Hoshi, N (2017) Modulation of Kv7 channels and excitability in the brain. *Cellular and molecular life sciences* 74(3):495-508

Kay, HY, **Greene, DL**, Kang, S, Kosenko, A, Hoshi, N (2015) M-current preservation contributes to anticonvulsant effects of valproic acid. *J Clin Invest* 125(10): 3904-3914.

Kosenko A, Kang S, Smith IM, **Greene DL**, Langeberg LK, Scott JD, Hoshi N (2012) Coordinated signal integration at the M-type potassium channel upon muscarinic stimulation. *The EMBO Journal*, 31(14):3147-56

Greene D, Kang S, Kosenko A, Hoshi N (2012) Adrenergic regulation of HCN4 channel requires protein association with β2-adrenergic receptor. *The Journal of Biological Chemistry*, 287(28):23690-7

Oral Presentations

Protective Outcome of Attenuation of M-current Suppression in the Pathology of Seizures and Epileptogenesis — October 2016

M-current Modulation in Seizure Pathology — September 2013
8th Annual Research Day, Department of Pharmacology, UCI, Irvine, CA

Abstracts

Kosenko A, Moftakhar S, **Greene DL**, Hoshi N (2014) Deficits in M-channel regulation lead to impaired consolidation of recognition memory in mice. — November 2014
Society for Neuroscience, Washington DC

Kang S, Kosenko A, **Greene DL**, Hoshi N (2012) Modulation of M-channel via Phosphorylated calmodulin by protein kinase CK2. — November 2012
Society for Neuroscience, New Orleans, LA

Laboratory Skills

patch-clamp electrophysiology (whole cell patch on stable mammalian cells and primary neurons, perforated patch on primary neurons), live cell imaging FRET/TIRF, fluorescent microscopy, immunofluorescent imaging, immunohistochemistry, co-immunoprecipitation, Western blot, protein purification, biochemical assay development, binding assays, biotinylation, cell culture, primary neuronal culture preparation and maintenance, DNA/RNA isolation and purification, PCR, cloning, primer design, plasmid design and preparation, mutagenesis, gene expression and silencing, transfection, in vivo murine experimentation, intracardiac perfusion

Teaching experience

Teaching Assistant, Physical Biochemistry — September 2015
University of California, Irvine

Software

Adobe (Photoshop, Illustrator, Acrobat), ImageJ, pCLAMP 10 (Clampex, Clampfit), GraphPad (Prism), MetaMorph, EndNote, Microsoft Office (PowerPoint, Word, Excel), CLC Main Workbench

ABSTRACT OF THE DISSERTATION

Protective Outcome of Attenuation of Kv7 Channel Suppression
in the Pathology of Seizures and Epileptogenesis

By

Derek Lane Greene

Doctor of Philosophy in Pharmacology and Toxicology

University of California, Irvine, 2017

Professor Naoto Hoshi, Chair

The M-current is a non-inactivating voltage-gated potassium channel composed of homomeric and heteromeric assemblies of KCNQ/Kv7 subunits (KCNQ2-5). The M-current exerts pronounced control over excitability during prolonged stimulus in neurons. The channel is transiently suppressed through pathways downstream of Gq-coupled receptor activation, allowing for enhanced signaling within neural circuits. However, several mutations in this channel have been implicated in epilepsies and encephalopathies. We sought to understand the functional relevance of M-current suppression in the pathology of epilepsy. First we needed a pharmacological tool to selectively partition M-current contribution in seizures. To this end we identified the mechanism of inhibition for XE991, a popular M-current inhibitor that until know lacked sufficient characterization. XE991 was determined to be an activated-subunit inhibitor with slow binding. By using this compound the M-current could be selectively suppressed in neurons contributing to ictal activities, as XE991 would be highly efficacious on rapidly depolarizing neurons, while having minimal effect on silent or

sparsely firing neurons. Next, we identified an underlying mechanism for the widely used anticonvulsant, valproic acid. We determined that valproic acid acts as an inhibitor of palmitoylation, a posttranslational fatty acid modification. Specifically valproic acid prevented palmitoylation of a signaling scaffold protein within the Kv7 channel complex, AKAP79/150. As a result, valproic acid ablated M-current suppression from AKAP79/150-bound protein kinase C when stimulating Gq-coupled receptors, reducing neurotransmitter-induced hyperexcitability. In a kainate model of status epilepticus, the anticonvulsant action of valproic acid was transiently removed by M-current inhibition with XE991. Also, the M-current activator retigabine, which is not efficacious on neurotransmitter-suppressed channels, demonstrated anticonvulsive action even when administered after seizure induction if animals were pretreated with valproic acid. Using a transgenic mouse line carrying an alanine substitution of the key Kv7.2 phosphorylation site we confirmed that a dominant mechanism for the anticonvulsive action of valproic acid is through M-current preservation. Furthermore, prevention of M-current suppression after status epilepticus protected animals from the process of epileptogenesis. Our findings indicate that suppression of the M-current is involved in the pathology of epilepsy, and that interfering with channel suppression can robustly attenuate morbidities contributing to this neurological disorder.

Chapter One

Modulation of Kv7 channels and excitability in the brain

Introduction to Kv7/KCNQ channels

Potassium channels, being the most diverse of all ion channels, underlie a robust number of functions that control excitability in neurons. They are responsible for such aspects as setting the resting membrane potential, reducing excitability as well as controlling the duration, shape and firing frequency of action potentials. Potassium channels are localized to all subcellular compartments critical for electrical conduction in neurons. Therefore, it is not surprising that many of these channels are gated by specific activators (such as membrane potential or neurotransmitters) and regulated by complex molecular pathways.

Kv7 channels produce an outward potassium current with characteristics that make it distinctive from other voltage-gated potassium channels[1,2]. Specifically, Kv7 channels expressed in neurons lack inactivation, have slow gating kinetics (an order of magnitude slower than other voltage-gated potassium channels at room temperature as well as physiological temperatures[3,4]) and are activated near resting membrane potential[5,6]. Kv7 subunits are widely expressed in the central as well as peripheral nervous system[7,8], where its steady outwardly rectifying current functions as “brakes” for neurons receiving persistent excitatory input. A somewhat unique characteristic of the M-current was determined from the circumstances by which it was discovered. Namely,

upon activation of muscarinic acetylcholine receptors (M1 and M3), both of which being Gq-coupled receptors, there is subsequent robust suppression of the M-current, leading to a transient increase in excitability. This pathway will be of importance in chapters 3 and 4. Suppression of the M-current has been shown to lower the action potential threshold, increase afterdepolarization and depolarize axonal resting potential[2,9]. Over the past several years it has been revealed that activation of numerous Gq/11-coupled receptors suppresses the channel[10-12].

Since the initial discovery of the M-current in bullfrog sympathetic ganglion neurons there have been numerous breakthroughs identifying neuronal types expressing the M-current as well as mediators of the channel[9,13]. However, it took nearly two decades to determine the molecular identity[7]. The lapse in time that was required to elucidate Kv7 as the underling subunits of the M-current was largely due to the lack of available tools capable of linking cloned channels to native M-current[14]. On the heels of this discovery numerous facets involved in the modulation of the Kv7 channel complex have also been uncovered. However, though the M-current has consistently been discussed as playing a pivotal role in neuroplasticity, due to its prominent expression throughout the brain and its pronounced suppression via neurotransmitters, only recently have we begun to understand how dynamic Kv7 channel modulation contributes to higher brain functions.

Components of the Kv7 channel complex

The M-current is conducted through a voltage-gated potassium channel comprised of tetrameric assemblies by members of Kv7 α subunit homomers or heteromers derived from KCNQ2-5 genes. Kv7.1 is the predominant subunit of the Kv7

family found in cardiomyocytes[15,16] (Fig 1.1A). Kv7.1 channel generates the slowly activating delayed rectifier current (I_{Ks}) that contributes to the repolarization phase after action potential initiation. Kv7.1 channel is also expressed in the cochlea of the inner ear[17], and vascular smooth muscles[18].

A wide variety of neurons in the CNS as well as peripheral neurons express Kv7.2, 7.3, and 7.5 subunits, which are considered to generate the neuronal M-current[1,2]. It is widely believed that heteromeric Kv7.2/3 or Kv7.3/5 channels are the dominant subunit composition (Fig 1.1B)[1,2] since Kv7.3 has been shown to facilitate surface expression of other Kv7 subunits especially in *Xenopus* oocytes[19] and immunohistochemical studies show co-localization of these subunits in many areas[8,20]. However, a recent study using conditional knock-out mice of KCNQ2 or 3 genes showed abolished M-current in Kv7.2 deficient neurons, but normal M-current in Kv7.3 deficient neurons, which suggests that Kv7.2 homomeric channels can be fully functional without Kv7.3 subunit in CNS neurons[21].

Kv7.4 is a subtype selectively expressed in the auditory pathway including hair cells of the inner ear (Fig 1.1A)[22-24]. In addition to neurons, Kv7.4 and Kv7.5 are also expressed in various smooth muscle cells including within vascular cells[18,25] as well as the gastrointestinal tract (Fig 1.1A)[26,27].

With the advent of discovering the molecular identity of the M-current many aspects of the Kv7 channel complex have been brought to light (Fig. 1.1C-E): protein-protein and protein-lipid interactions, as well as channel phosphorylation[7,8,28]. Understanding the components of the Kv7 channel complex has provided the necessary

insight for understanding the requirements for basal channel function, its modulation, as well as the pathways involved in neurotransmitter-induced M-current suppression.

Phosphatidylinositol-4,5-bisphosphate (PIP_2) is an anionic phospholipid found on the intracellular leaflet of the plasma membrane. PIP_2 is a co-factor for numerous ion channels and transporters[29], including Kv7 channels, that alters channel function and often is obligatory for activation[30-33]. While it has been known that PIP_2 interaction with Kv7 is mandatory for channel function[34,35], more recently it was shown that PIP_2 has multiple sites of interaction within the channel, with varying effects[36]. One such PIP_2 interaction modulates coupling the voltage-sensing to the pore-gating domain[37-40]. Functionally, PIP_2 interaction within the voltage-sensing domain of the S4-S5 linker has been attributed to increasing open probability, thus voltage-conductance[40]. Another key interaction site lies within the proximal C-terminus of the Kv7.2 subunit that overlaps with the calmodulin (CaM) binding site, a key target for M-current suppression[39,41,42]. Notably, while depletion of PIP_2 in Kv7.2 and Kv7.5 homomeric channels leads to profound current suppression, heteromeric assemblies incorporating the Kv7.3 subunit, have higher affinity to PIP_2, thereby offering resistance to PIP_2 turnover[40].

Both N and C termini of Kv7 subunits are located within the intracellular side and are rich with sites of protein-protein interaction. Within the amino terminus lies a consensus site for phosphorylation by protein kinase A, which in *Xenopus* oocytes has been shown to increase Kv7 currents[19]. Protein kinase CK2 and protein phosphatase 1 (PP1) also tether to Kv7 subunits (Fig. 1.1C), and modulate the channel through the phosphorylation state of essential auxiliary unit CaM[43]. The Kv7 carboxyl terminus is relatively long compared to other potassium channels, containing numerous sites of

interaction[42]. Among these are the aforementioned sites for PIP_2, CaM, A-kinase anchoring protein 5, (AKAP5, also known as AKAP79/150), as well as ankyrin G (Fig. 1.1D). Interaction of the channel with many of these factors is highly modulated by neurotransmitters activating Gq/11–coupled receptors[44,45].

AKAPs are facilitators of second messenger signaling events that tether enzymes to target substrates at the plasma membrane, such as Kv7 channels (Fig. 1.1C)[28,46,47]. This anchoring protein is located to the plasma membrane through PIP_2 binding and a dynamic post-translational fatty acid modification known as palmitoylation[48], which will be covered in greater detail in chapter 3. AKAP5-bound Protein kinase C (PKC) is kept in proximity to neuronal Kv7 channels, which is important for the specificity of PKC-induced dissociation of CaM from Kv7.2 subunits[8,28,46].

CaM plays roles in the trafficking of Kv7 channels to the plasma membrane[49,50], functions as the Ca^{2+} sensor, and promotes channel interaction with PIP_2 (Fig 1.1C)[44,51]. CaM interacts with Kv7 subunits through two α helical regions (A and B) running antiparallel in the C-terminal tail. There has been controversy regarding whether calcium facilitates or reduces CaM binding to Kv7[52,53]. A recent crystal structure study using Kv7.1 suggests that the story is not as simple as originally impicated[54]. The study showed that the calcium-free C-lobe of CaM interacts with helix A of Kv7 and the calcium-containing N-lobe of CaM interacts with helix B of Kv7[54]. However, Kv7.2 has been shown to have higher affinity for CaM at helix B, regardless of $[Ca^{2+}]$[55], whereas the C-lobe of CaM has higher affinity to $[Ca^{2+}]$ and is dynamically bound to helix A in a calcium-dependent manner[56].

Studies over the past several years identified an increasing number of accessory proteins for the Kv7.2 subunit (Fig. 1.1D). One of the earliest examples is ankyrin G, which is an underlying molecule for anchoring Kv7.2 at the axon initial segment as well as the Node of Ranvier[57,58]. The SNARE protein syntaxin 1A is a plasma membrane protein, which serves as a docking site for synaptic vesicles. Syntaxin 1A has been demonstrated to interact with both the cytoplasmic carboxyl and amino termini of Kv7.2 subunit, which slows channel activation and decreases current amplitude (Fig. 1.1D)[59,60]. Navβ1 was originally considered to be a beta subunit unique to voltage-gated sodium channels (Nav)[61]. More recently the promiscuity of this auxiliary protein was uncovered, first in its modulation of Kv4[62], and more recently Kv1 and Kv7 subfamilies[63] (Fig. 1.1D). Navβ1 slows Kv7.2 channel activation at depolarized potentials[63]. An interesting addition to the list of accessory proteins for the Kv7.2 subunit is β-site amyloid precursor protein cleaving enzyme 1 (BACE1), which was originally identified to produce neurotoxic β-amyloid[64] and known to cleave Navβs and increase sodium currents[65]. Recently it was shown that physical interaction of BACE1, even with enzymatic inactive BACE1, can change gating kinetics and functional expression of Kv7 channels with the notable exception of Kv7.3 homomeric channels[66]. However, effects through cleavage of Kv7.2-bound Navβ have not been characterized to date.

Channel trafficking of Kv7 channels is another mechanism for regulating neuronal excitability (Fig. 1.1E). It has been noted that the majority of Kv7 channel subunits stay in cytoplasmic vesicles rather than being transported to the plasma membrane[49]. Detailed analyses of CaM-dependent regulation of Kv7 channel trafficking revealed that CaM regulates exit of Kv7 channels from ER[49,50]. In addition, our recent

proteomic study identified that tubulin dimer together with Collapsin response mediator protein-2 (CRMP-2) play a role in channel trafficking of Kv7.2 channels at post-Golgi vesicles (Fig. 1.1E)[67].

Integrated channel suppression

Various neurotransmitters activating Gq-protein coupled receptors induce profound transient suppression of the M-current[68-70]. It has been demonstrated that stimulation by luteinizing hormone releasing hormone[9], purinergic P2Y[13], substance P[71], 5-HT2 serotonin[72], as well as activation of M1/M3 muscarinic receptors[5,73,74], metabotropic glutamate receptors[75] , κ and δ opioid receptors [76], and AT1 angiotensin receptors[77,78] all suppress the M-current.

Gq/11 mediated pathway

Perhaps most well characterized is M-current suppression subsequent to activation of Gq/11-coupled muscarinic acetylcholine receptors[79,80]. It is well documented that reduction in PIP_2 leads to marked suppression of the M-current (Fig. 1.2A)[81-83]. Also, PKC was one of the first modulators proposed for neurotransmitter-induced M-current suppression[84]. This was for a time debated due to confounding and at times contradicting pharmacological data such as PKC inhibitors at times showing no interference with muscarinic suppression of the M-current[12,85]. These reports were reconciled once it was determined that AKAP-tethered PKC is protected from certain PKC inhibitors[86,87]. Indeed, a key PKC phosphorylation site on serine 559 of the mouse Kv7.2 subunit has been shown to induce inhibition equivalent to muscarinic suppression of the channel[28,44,88]. A phosphorylation deficient alanine substitution of this residue will

be described in Chapter 4. Consequently, depletion of PIP_2 and activation of PKC occur downstream of Gq-coupled receptor activation.

The Gq-protein mediated pathway occurs as follows: subsequent to activation of Gq/11-coupled receptors, such as the M1 muscarinic receptor, comes activation of phospholipase C (PLC) causing hydrolysis of PIP_2 into diacylglycerol (DAG) and inositol triphosphate (IP3), leading to the activation of PKC. Activated PKC, tethered to the M-channel complex through AKAP5, phosphorylates the C-terminus of the Kv7.2 subunit, which overlaps with the channel's CaM binding site. Phosphorylation of the Kv7.2 subunit dissociates CaM from the channel, which destabilizes its interaction with PIP_2 along with the concomitant reduction in PIP_2 due to its hydrolysis. Together, these signaling pathways downstream of Gq/11 activation lead to an amplified response that synergistically suppresses the M-channel[44].

Calcium-CaM pathway

Another well established pathway of M-current suppression is induced by increases in intracellular calcium sensed by channel-bound CaM (Fig. 1.2B)[44,89,90]. Bradykinin receptors have been demonstrated to use this pathway[90]. The physical interaction of calcium-free CaM bound to helix A of Kv7 subunits is integral to maintaining channel affinity to PIP_2[44]. Consequently, calcium-bound CaM decreases Kv7.2 channel efficacy for PIP_2, thereby inhibiting the M-current[44,90,91]. On the other hand, a recent study showed that splicing variants of Kv7.4 are differentially modulated by CaM[92]. This mechanism may explain why bradykinin induced suppression of the M-current is usually smaller than that by muscarinic agonists.

Kv7 channel physiology

The voltage dependent characteristics of the M-current lend it to various roles associated with controlling excitability in the brain. Kv7 channels activate within subthreshold potentials, approximately at –60 mV. Additionally, unlike many other voltage-gated potassium channels, Kv7 does not inactivate, therefore, as long as the membrane remains depolarized Kv7 current will persist[7]. The outcome is the effective stabilization of the membrane potential throughout the duration that neurons receive subthreshold excitatory inputs[93]. Relatively slow activation kinetics indicate that Kv7 channels do not appreciably alter single action potential amplitude or duration[94]; rather, the functional consequence of M-current is to clamp the membrane at more negative potentials, preventing repetitive action potential firing. Moreover, the persistent outward current functions to control numerous aspects of neuronal excitability as follows:

Setting membrane potential

Due to its activation at subthreshold potentials, Kv7 channels have been implicated in controlling the resting membrane potential (RMP) at the axon initial segment (AIS) and unmyelinated portions of the axons, the nodes of Ranvier as well as axon terminals. Examples have been shown in sympathetic, cortical and hippocampal neurons such as visceral sensory neurons and within the calyx of Held[95-97]. M-current control of RMP is also a major determinant for increasing the recovery of inactivated channels (i.e. axonal Na^+ and A-type K^+ channels) at the nodes of Ranvier, allowing for consecutive action potential spiking[4,97,98]. Therefore, axonal Kv7 channels at nodes of Ranvier exert two contradicting functions: increasing the action potential threshold but also increasing excitability by promoting recovery of sodium channels from inactivation[4,20]. In addition, Kv7 channels are known to express at the axon terminal and

regulate synaptic release through regulating RMP[97,99]. Confusing is that inhibition of Kv7 channel sometimes facilitates synaptic transmission such as in calyx of Held[97] and hippocampal synaptosomes[99], while suppressing synaptic transmission in Schaffer neurons[100]. These contradicting effects are assumed to be results of difference in inactivation of calcium channels and sodium channels[99,100]. On the other hand, post-synaptic responses can be also affected by perisomatic Kv7 channels by changing integration of excitatory postsynaptic potentials at the AIS, dampening synaptic transmission of prolonged subthreshold stimulus[101,102].

Afterhyperpolarization

As a consequence of continuous spiking, numerous types of neurons produce three types of an afterhyperpolarization (AHP) that contribute to refractory periods: fast AHP lasting 2-5 ms, medium AHP with durations ranging from 50-100 ms (mAHP), and a slow AHP lasting 0.1-2 s (sAHP).

Medium AHP is produced through slowly activating and long-lasting outward K^+ current that is composed in part by a component that requires Ca^{2+} influx[103,104] and has been shown to control the time where neurons are refractory to further excitatory input. Channels contributing to the generation of mAHP are Kv7 channels as well as SK2 calcium-activated potassium channels and HCN channels[80,103,105]. However, it has been reported that distinct channels are responsible for mAHP depending on membrane potentials and neuronal types[104,106].

Slow AHP is involved in neuronal plasticity and is implicated as a major component during learning and establishing memory within the hippocampus[34,38]. The identity of the potassium channel responsible for the slow AHP had proven elusive until

recently. While Kv7 has been suggested as a contributor of sAHP, as afferent cholinergic stimulation reduces effective sAHP amplitude[107], one confounding factor discredited its involvement: the sAHP is active at membrane potentials more negative than M-current activity is typically observed. Activation of the sAHP is known to have a Ca^{2+} dependent component, and neuronal calcium sensor proteins such as hippocalcin have been implicated in the activation of potassium channels that constitute the sAHP[108,109]. A physiological consequence of hippocalcin activation is the downstream production of PIP_2. In recent reports evidence was given for shifting Kv7 open probability to more negative potentials through increased interaction with PIP_2[40,110]. It has also been observed that BACE1 knockout mice have reduced sAHP. This provides further evidence since BACE1 has been shown to cause a leftward shift in Kv7 voltage activation, within the voltage range where sAHP is active[66].

Interspike interval

High frequency bursts of action potentials lead to Kv7 channel activation. This gradually increases spike interval, which is also known as spike frequency adaptation[80,111]. Recently M-current was also shown to regulate the firing frequency of tonically firing neurons in rat entorhinal cortex layer II stellate cells[112], as well as neurons of the retrotrapezoid nucleus[113], which, during continuous current input, initially fire with short interspike intervals that quickly lead to refractory periods with minimal firing[112]. Furthermore, Kv7 current has also been shown to control the rate of firing in dopaminergic neurons of the ventral tegmental area[94] and hippocampal neurons[114]. Thus, the M-current robustly controls the frequency at which neurons are able to fire while receiving continuous excitatory input[115].

Theta-resonance

Another physiological function of Kv7 channels, in conjunction with HCN channels, is facilitating the responsiveness to oscillating subthreshold membrane potential within theta frequencies (2-7 Hz), which functions as a band pass filter[116]. This function has predominantly been characterized in pyramidal neurons in the hippocampus[116,117]. Interestingly, two distinct channel types with different ion species, gating kinetics, and subcellular localization (somatic Kv7 channels and dendritic HCN channels) produce a synergized function[116,117]. Theta resonance has been considered integral to inducing synchronous activity within the local circuit and shown to be a necessary component of neuroplasticity as well as learning and memory[118-120]. Network oscillations at the theta frequency have been shown to be important for hippocampal function, such as exploration[121] and working memory such as navigation of mazes[122,123]. As such, disruption of M-channel activity, such as conditional knockout of Kv7.2 subunits, reduces hippocampal theta resonance and consequently impairs animal performance in spatial memory tasks[124].

Transient neuronal hyperexcitability

Suppression of Kv7 current leads to the transient removal of the channel's physiological functions, leading to neural hyperexcitability (Fig. 1.3). Consequently, channel suppression allows for the accumulation of excitatory inputs that lead to burst firing or "complex-spikes"[125]. In addition, suppression of Kv7 channels leads to concomitant reduction in action potential threshold such as what is seen in dentate granule cells after stimulation by cholinergic fibers[126]. Thus, reduction in action potential threshold by Kv7 channel suppression makes action potential propagation more

permissive, where weaker stimuli can invoke neuronal spiking with higher probability, and increases the likelihood of spontaneous firing, which underlies burst firing in some neurons[4]. Alternatively, ablation of Kv7 current by conditional knockout produces a similar effect[21]. Furthermore, since the M-current is activated during high frequency firing, M-current suppression allows neurons to respond to high frequency inputs. Moreover, This bursting has been shown to be one component of memory coding after learning in subcortical regions[14,127]. Suppression of axonal M-current also increases the likelihood of the back-propagation of action potential spikes into the apical dendrites, which has been demonstrated to promote long-term potentiation[101,128].

Kv7 channel augmentation

Just as there are multiple mediators of M-current suppression, so too are there mediators of M-channel preservation as well as enhancers of M-current activity. Early examples include neurotransmitters such as somatostatin[129], corticostatin[130] and dynorphin[131]. Since phosphorylation of certain residues of Kv7 channels are known to cause robust suppression it follows that some protein phosphatases preserve neuronal Kv7 channel activity. One example is Protein Phosphatase 2A, (PP2A), which was demonstrated to counteract channel inhibition via phosphorylation by Glycogen Synthase Kinase 3β, (GSK3β)[132,133]. While phosphorylation of Kv7 subunits is typically associated with channel suppression, phosphorylation of Kv7-bound CaM by protein kinase CK2 facilitates CaM interaction with the channel, increasing PIP_2 efficacy and increasing channel amplitude while remaining sensitive to increases in intracellular Ca^{2+} [43,134]. Another signaling pathway known to augment the M-current (specifically, channels containing Kv7.2/4/5 subunits) is through the increase in an intracellular

reactive oxygen species (ROS)[135,136]. It has been shown that the oxidation of three cysteine residues lying within the S2-S3 linker increase the P_o of Kv7 channels[135]. Another recently identified pathway for ROS induced augmentation is methylation of arginine residues of Kv7.2 subunit by arginine methyltransferase 1 (Prmt1), which promotes Kv7.2 interaction with PIP_2[136]. This study also suggests that partial methylation of arginine residues in Kv7 channels is essential for maintaining basal M-current[136].

Auxiliary units of potassium channels such as members of the KCNE family are common co-factors that associate with pore-forming subunits and alter channel activity, such as voltage dependence of activation[137,138]. Recently β-secretase BACE1 was revealed to associate with members of the Kv7 family in neurons (Fig. 1.1D). Interestingly, it is the physical interaction and not the enzymatic activity of BACE1 protein that is responsible for the leftward shift in the voltage conductance of the M-current. This leftward shift was accompanied by a change in Kv7 channel kinetics, accelerating activation as well as slowing channel deactivation[66]. While PIP_2 is necessary for M-current function, it has also been revealed that increasing PIP_2 levels caused Kv7 channels to open at deeper potentials, similar to the effect seen with BACE1[40,110]. Interestingly, the combination of BACE1 interaction with the channel along with elevating PIP_2 levels causes even greater leftward shift in channel activation[40]. These revelations bring credence to the growing consensus that Kv7 channels are a major part of the burst firing-activated outward current underlying sAHP, which is known to be active at membrane potentials lower than where the M-current has been thought to be active.

Another association with Kv7.4 subunits has recently been uncovered. Kv7 channels in vascular smooth muscle are positively regulated by G-protein βγ subunits, enhancing the rate of Kv7 channel activation and shifting the voltage dependence of activation so that the channel is open at deeper potentials[139]. While it is important to note that this phenomenon has yet to be confirmed in CNS neurons, G-protein βγ subunits may prove to be an underlying factor responsible for enhancement of Kv7 activity by as seen with G-protein coupled receptor activation by somatostatin[129] and dynorphins[131].

Subcellular localization

A key characteristic determining the roles of neuronal Kv7 channels lies in their subcellular localization. Kv7 channels are highly concentrated at the distal end of the AIS and nodes of Ranvier by the protein ankyrin-G. The AIS functions as the gatekeeper of action potential initiation by controlling the threshold at which excitatory presynaptic potentials transmit action potentials down the axon. Ankyrin G also functions to localize Kv7.2 and to a lesser extent Kv7.3 channels at unmyelinated regions of the axon, known as Nodes of Ranvier[57,58,140]. At these nodes, Kv7 channels (Kv7.2/7.3) co-cluster with voltage gated sodium channels and are thought to underlie the slow outward potassium current, stabilizing RMP[4,98]. In agreement with its axonal localization, selective suppression of axonal Kv7 channel increases spike afterdepolarization, facilitating action potential firing[125]. Interestingly, in a study where myelination of the axon was removed, Kv7 channels dispersed along the axon, which had the net effect of increasing neural excitability[141]. This was postulated to be through

stabilizing the RMP throughout the axon, thereby increasing the availability of Nav channels as previously described[4,20].

Kv7 channels have also been reported to be expressed in the perisomatic region outside the AIS[57,142,143]. Somatic function of the M-current is implicated in excitatory synaptic potential integration as well as counteracting afterdepolarization[57,144,145]. Perisomatic Kv7 channel has been shown to change the amplitude and shape of somatic EPSPs[102]. There is also accumulating evidence that Kv7 channels may be expressed at apical dendrites[142,144,146]. Due to their relative scarcity at this location, the function of Kv7 channels within dendrites is still controversial, though it has been proposed to contribute to conditions where there is dendritic hyperexcitability, as in the case of persistent excitatory presynaptic input[144,146], however, further clarification of Kv7 channel function outside the axon is still needed.

Finally, Kv7.2 has been shown to localize to presynaptic terminals[99]. Augmentation of Kv7 channels at this location attenuates neurotransmitter release[99] whereas suppression of Kv7 current by Gq activation increases activation of voltage-gated calcium channels leading to increased transmission[147].

Surface expression

Under basal conditions, Kv7.2/3 channels have very low turnover rate throughout the axon[148]. However, surface expression of Kv7 channels is upregulated after neuronal stimulation[149]. Paradoxically, persistent excitation of neurons leads to pronounced internalization of Kv7 channel at the AIS, which is largely irreversible[150]. Li and colleagues demonstrated that persistent activation through glutamate induced a Ca^{2+} and PKC-dependent internalization of Kv7 channel. Similar irreversible suppression of

Kv7 channel was observed with cholinergic stimulation onto dentate granule cells, causing an increase in their intrinsic excitability[126]. It was revealed that cholinergic stimulation onto the AIS of dentate granule neurons leads to persistent activation of T-type Ca^{2+} channels, causing robust M-current suppression that does not recover after washout. Conversely, deprivation of afferent axonal stimulus, as shown in neurons of the avian cochlear nucleus leads to pronounced increase in surface expression of Kv7.2 channels and concomitant reduction of Kv1 channels at the AIS[151]. This reduces the fast activating Kv1 currents, thereby increasing excitability, while preserving axonal RMP by Kv7 channels.

CaM tethered to Kv7 subunits is important for Kv7 channel exit from the endoplasmic reticulum and is necessary for basal surface expression of the channel at the plasma membrane[49,55]. Alternatively, a recent study uncovered a form of induced surface translocation subsequent to muscarinic suppression of the channel tested in a heterologous system in which Kv7 channels in post-Golgi vesicles were determined to be the predominant source of this form of over-recovery of the M-current, mediated through a CRMP-2 pathway[67] (Fig. 1.1E).

Pathology

The genes encoding Kv7.2 and Kv7.3 have been shown to have numerous mutations that induce epilepsies and encephalopathies. The most common of these pathologies is known as benign familial neonatal seizures (BFNS), a form of autosomal dominant idiopathic epileptic syndrome. The generalized seizures induced by these mutations occur within the first days after birth and have a high likelihood of spontaneously receding within the first two months[152-155]. Mutations leading to epileptic

activity are predominantly autosomal dominant, inducing loss of channel function such as from missense, truncation, and non-native splice variants that reduce functional Kv7 channel at the plasma membrane[156,157]. Many of these mutations lead to reduction in basal M-current and subsequent hyperexcitability[158]. This is also true in the cases of early onset epileptic encephalopathy, though usually with more severe channel suppression[154]. As of yet, encephalopathies have only been detected from missense mutations in KCNQ genes and tend to occur *de novo*[154,159,160]. One example is through an alternative substitution of a previously described select amino acid mutation, normally causing BFNS, instead leading to a severe form of encephalopathy. It was determined that the functional difference in this severe form of single amino acid mutation is derived from not only reduction of functional expression of Kv7 channels but also loss of localization of Kv7 channels to the AIS[154]. As a consequence for the growing literature on pathologies associated with Kv7 mutations there has been an effort to develop genetically engineered animals to recapitulate and understand the pathologies of the numerous implicated mutations and better understand underlying causes[161,162] as well as the effectiveness of potential therapies[163]. One such mutation will be investigated in chapter 4.

M-current activity is an important obstacle for seizure onset[164,165]. However, gain of function mutations in Kv7 channels have also been uncovered in patients suffering from epileptic encephalopathies[166-168]. One such mutation was found within the voltage-sensing domain of Kv7.2 and Kv7.3 subunits, stabilizing the channel in the open conformation, reducing the voltage dependence of activation[167]. Interestingly, while these mutations decrease the intrinsic excitability in neurons where they are expressed,

there is a marked increase in network excitability within the CA1 of the hippocampus. This suggests the grave importance in Kv7 channel control of action potential propagation, particularly at its axonal localization.

Conclusion

The specific characteristics of Kv7 channels allow it to function as brakes against continuous neural activity. In regards to this dissertation, little is known of M-current modulation during seizures. Kv7 channels expressed in the cortex should provide a major deterrent from pathological hyperactivity in the brain. Though evidence suggests that the channel is suppressed during seizure. As we will demonstrate in chapter 3, the mechanism of a robust antiepileptic drug, valproic acid, functions through disruption of M-current suppression[169]. Additionally, retigabine-induced augmentation of the M-current has been successful as an antiepileptic therapeutic[170]. Paradoxically, transient suppression of Kv7 channels is important for cognitive functions such as memory encoding, while complete removal of Kv7.2 increases susceptibility to seizures and leads to deficits in hippocampal-dependent spatial memory[124] as well as fear memory in mice[171]. Therefore, it is paramount to increase our understanding of Kv7 channel modulation throughout the brain in order to effectively determine its role in relevant pathologies as well as develop new therapeutics.

A

	heart	neurons	auditory pathway	smooth muscles
Kv7.1	+		inner ear	+/-
Kv7.2		+		
Kv7.3		+		
Kv7.4			inner ear brain stem	+
Kv7.5		+	brain stem	+

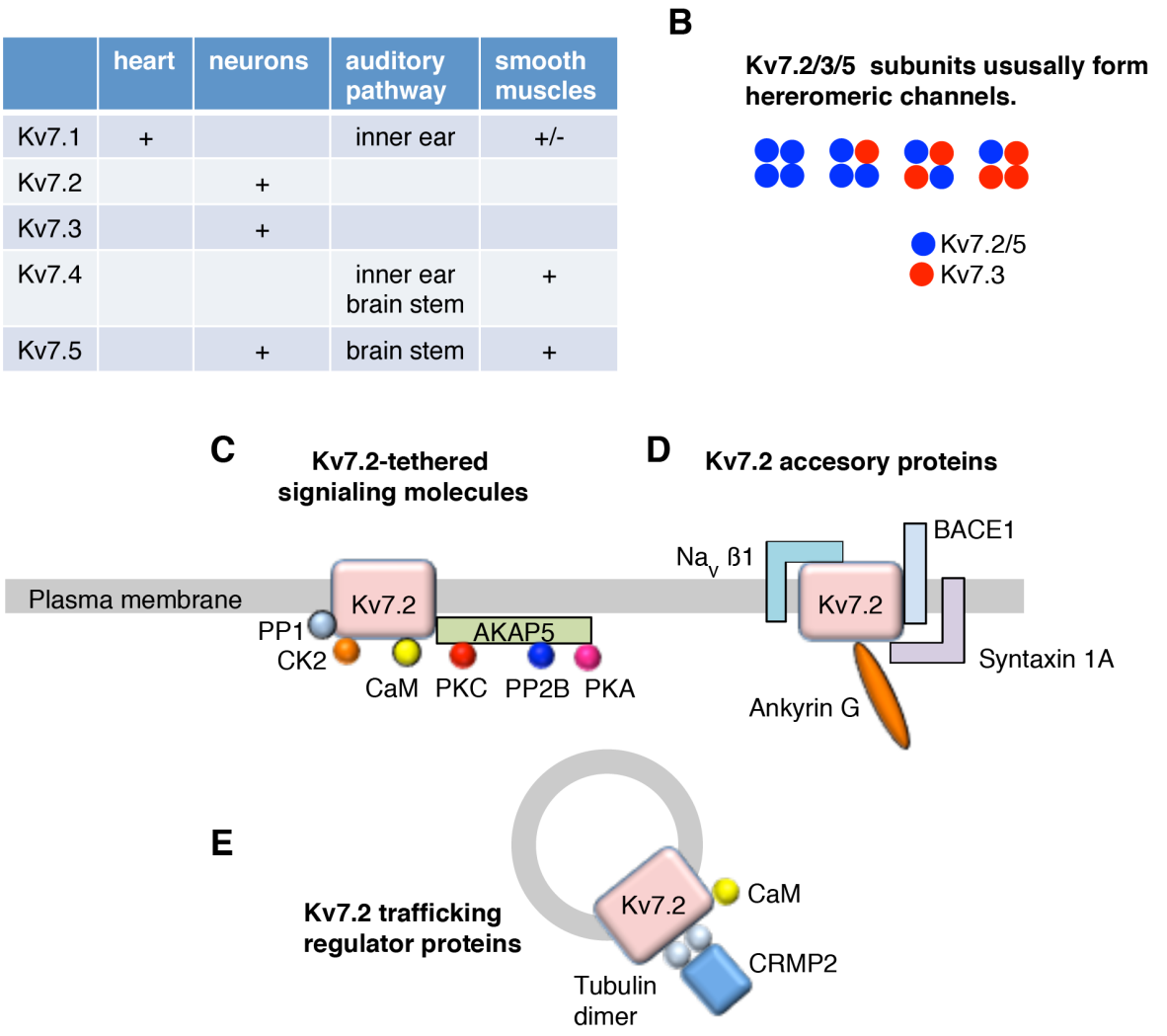

Figure 1.1. Summary of Kv7 channel family and their binding proteins.

A. Subtypes of Kv7 channel family and their expression pattern. **B.** Summary of subunit composition with Kv7.2. 7.3 and 7.5 subunits, which is widely observed in neurons. **C.** Schematic summary of signaling proteins that are tethered to Kv7.2 subunit. PP1, protein phosphatase 1. CK2, CK2 protein kinase. CaM, calmodulin. PKC, protein kinase C. PP2B, protein phosphatase 2B. PKC, protein kinase A. **D.** Schematic summary of accessory proteins for Kv7.2 subunit. Navnβ1, sodium channel β subunit 1. BACE1,β-site amyloid precursor protein cleaving enzyme 1. **E.** Schematic summary of identified regulator proteins for Kv7.2 channel trafficking. CRMP2, collapsin response mediator protein 2.

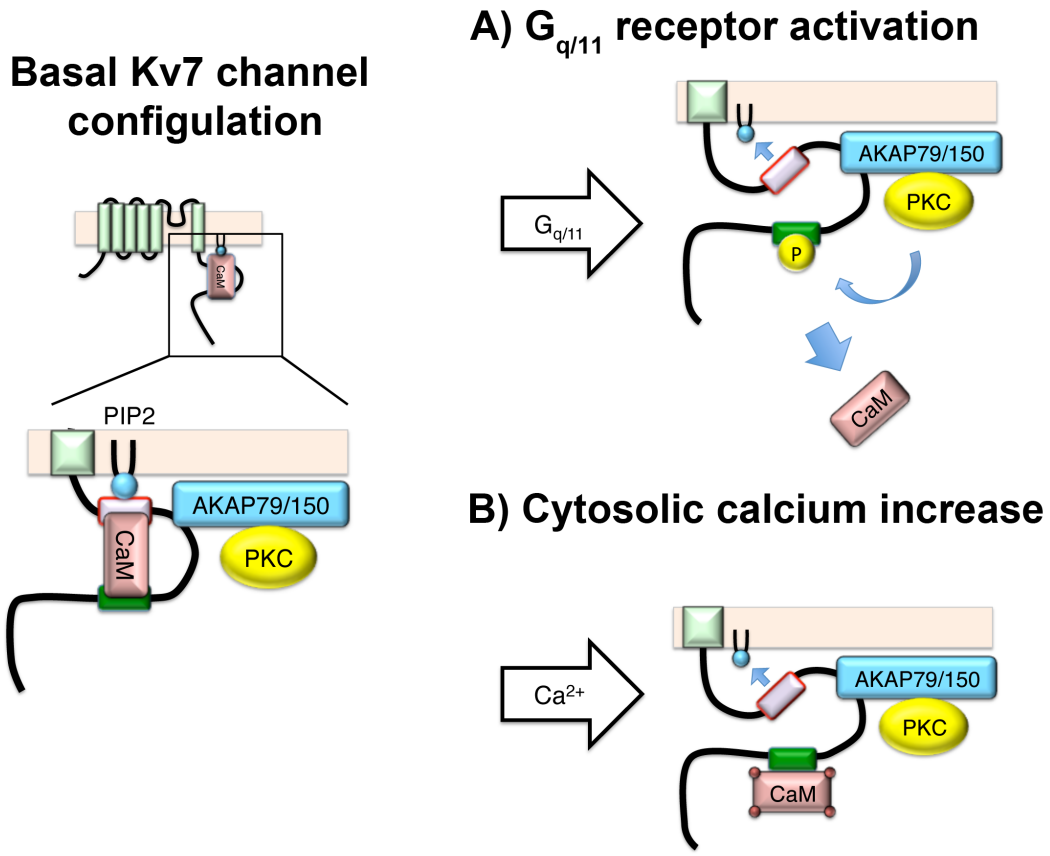

Figure 1.2. Schematic summary of molecular configuration of Kv7 channel and its modulation modified from ref 29.

A. Activation of Gq/11 coupled receptor induces depletion of PIP_2 as well as activation of PKC, which phosphorylates Kv7 channel leading to dissociation of CaM and unstabilized PIP_2 interaction. **B.** Increase in cytosolic calcium induces change in CaM conformation, and configuration between CaM and Kv7 channel, which leads to unstabilized PIP_2 interaction.

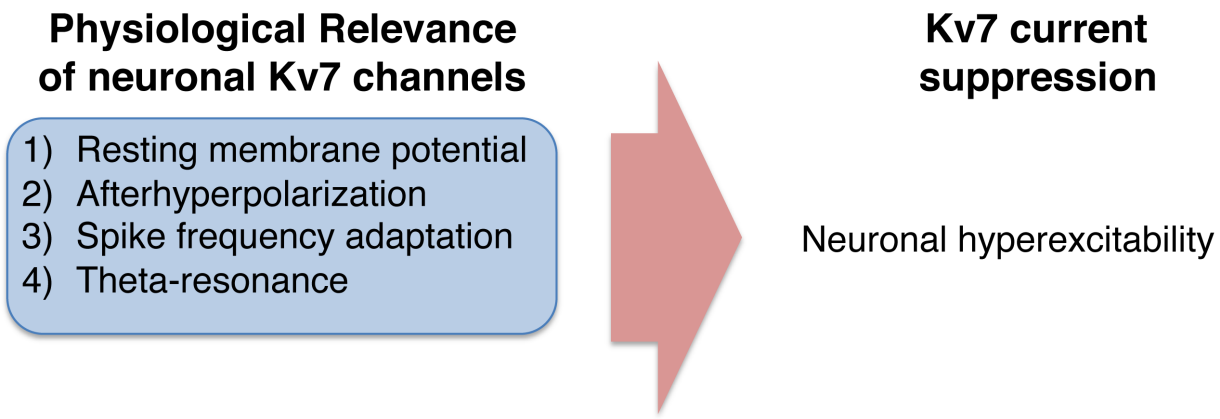

Figure 1.3. Summary of physiological relevance of neuronal Kv7 channel and its modulation.

References

1 Jentsch, T. J. Neuronal KCNQ potassium channels: physiology and role in disease. *Nat Rev Neurosci* **1**, 21-30, doi:10.1038/35036198 (2000).

2 Delmas, P. & Brown, D. A. Pathways modulating neural KCNQ/M (Kv7) potassium channels. *Nat Rev Neurosci* **6**, 850-862, doi:10.1038/nrn1785 (2005).

3 Miceli, F., Cilio, M. R., Taglialatela, M. & Bezanilla, F. Gating currents from neuronal K(V)7.4 channels: general features and correlation with the ionic conductance. *Channels (Austin, Tex.)* **3**, 274-283 (2009).

4 Battefeld, A., Tran, B. T., Gavrilis, J., Cooper, E. C. & Kole, M. H. Heteromeric Kv7.2/7.3 channels differentially regulate action potential initiation and conduction in neocortical myelinated axons. *J Neurosci* **34**, 3719-3732, doi:10.1523/JNEUROSCI.4206-13.2014 (2014).

5 Halliwell, J. V. & Adams, P. R. Voltage-clamp analysis of muscarinic excitation in hippocampal neurons. *Brain Res* **250**, 71-92 (1982).

6 Robbins, J. KCNQ potassium channels: physiology, pathophysiology, and pharmacology. *Pharmacol Ther* **90**, 1-19 (2001).

7 Wang, H. S. *et al.* KCNQ2 and KCNQ3 potassium channel subunits: molecular correlates of the M-channel. *Science* **282**, 1890-1893 (1998).

8 Cooper, E. C. *et al.* Colocalization and coassembly of two human brain M-type potassium channel subunits that are mutated in epilepsy. *Proc Natl Acad Sci U S A* **97**, 4914-4919, doi:10.1073/pnas.090092797 (2000).

9 Adams, P. R. & Brown, D. A. Luteinizing hormone-releasing factor and muscarinic agonists act on the same voltage-sensitive K+-current in bullfrog sympathetic neurones. *Br J Pharmacol* **68**, 353-355 (1980).

10 Tatulian, L., Delmas, P., Abogadie, F. C. & Brown, D. A. Activation of expressed KCNQ potassium currents and native neuronal M-type potassium currents by the anti-convulsant drug retigabine. *J Neurosci* **21**, 5535-5545 (2001).

11 Adelman, J. P., Maylie, J. & Sah, P. Small-conductance Ca2+-activated K+ channels: form and function. *Annu Rev Physiol* **74**, 245-269, doi:10.1146/annurev-physiol-020911-153336 (2012).

12 Shapiro, M. S. *et al.* Reconstitution of muscarinic modulation of the KCNQ2/KCNQ3 K(+) channels that underlie the neuronal M current. *J Neurosci* **20**, 1710-1721 (2000).

13 Adams, P. R., Brown, D. A. & Constanti, A. Pharmacological inhibition of the M-current. *J Physiol* **332**, 223-262 (1982).

14 Cook, L., Nickolson, V. J., Steinfels, G. F., Rohrbach, K. W. & Denoble, V. J. Cognition enhancement by the acetylcholine releaser DuP 996. *Drug Development Research* **19**, 301-314, doi:10.1002/ddr.430190308 (1990).

15 Sanguinetti, M. C. *et al.* Coassembly of K(V)LQT1 and minK (IsK) proteins to form cardiac I(Ks) potassium channel. *Nature* **384**, 80-83, doi:10.1038/384080a0 (1996).

16 Nakajo, K., Ulbrich, M. H., Kubo, Y. & Isacoff, E. Y. Stoichiometry of the KCNQ1 - KCNE1 ion channel complex. *Proc Natl Acad Sci U S A* **107**, 18862-18867, doi:10.1073/pnas.1010354107 (2010).

17 Neyroud, N. *et al.* A novel mutation in the potassium channel gene KVLQT1 causes the Jervell and Lange-Nielsen cardioauditory syndrome. *Nat Genet* **15**, 186-189, doi:10.1038/ng0297-186 (1997).

18 Ng, F. L. *et al.* Expression and function of the K(+) channel KCNQ genes in human arteries. *Br J Pharmacol* **162**, 42-53, doi:10.1111/j.1476-5381.2010.01027.x (2011).

19 Schroeder, B. C., Kubisch, C., Stein, V. & Jentsch, T. J. Moderate loss of function of cyclic-AMP-modulated KCNQ2/KCNQ3 K+ channels causes epilepsy. *Nature* **396**, 687-690, doi:10.1038/25367 (1998).

20 Kole, M. H. & Cooper, E. C. Axonal Kv7.2/7.3 channels: caught in the act. *Channels (Austin, Tex.)* **8**, 288-289, doi:10.4161/chan.29965 (2014).

21 Soh, H., Pant, R., LoTurco, J. J. & Tzingounis, A. V. Conditional deletions of epilepsy-associated KCNQ2 and KCNQ3 channels from cerebral cortex cause differential effects on neuronal excitability. *J Neurosci* **34**, 5311-5321, doi:10.1523/JNEUROSCI.3919-13.2014 (2014).

22 Marcotti, W., Johnson, S. L., Holley, M. C. & Kros, C. J. Developmental changes in the expression of potassium currents of embryonic, neonatal and mature mouse inner hair cells. *J Physiol* **548**, 383-400, doi:10.1113/jphysiol.2002.034801 (2003).

23 Kharkovets, T. *et al.* KCNQ4, a K+ channel mutated in a form of dominant deafness, is expressed in the inner ear and the central auditory pathway. *Proc Natl Acad Sci U S A* **97**, 4333-4338 (2000).

24 Kharkovets, T. *et al.* Mice with altered KCNQ4 K+ channels implicate sensory outer hair cells in human progressive deafness. *Embo j* **25**, 642-652, doi:10.1038/sj.emboj.7600951 (2006).

25 Brueggemann, L. I. *et al.* Differential protein kinase C-dependent modulation of Kv7.4 and Kv7.5 subunits of vascular Kv7 channels. *J Biol Chem* **289**, 2099-2111, doi:10.1074/jbc.M113.527820 (2014).

26 Ohya, S., Asakura, K., Muraki, K., Watanabe, M. & Imaizumi, Y. Molecular and functional characterization of ERG, KCNQ, and KCNE subtypes in rat stomach smooth muscle. *American journal of physiology. Gastrointestinal and liver physiology* **282**, G277-287, doi:10.1152/ajpgi.00200.2001 (2002).

27 Greenwood, I. A. & Ohya, S. New tricks for old dogs: KCNQ expression and role in smooth muscle. *Br J Pharmacol* **156**, 1196-1203, doi:10.1111/j.1476-5381.2009.00131.x (2009).

28 Hoshi, N. *et al.* AKAP150 signaling complex promotes suppression of the M-current by muscarinic agonists. *Nat Neurosci* **6**, 564-571, doi:10.1038/nn1062 (2003).

29 Suh, B. C. & Hille, B. PIP2 is a necessary cofactor for ion channel function: how and why? *Annu Rev Biophys* **37**, 175-195, doi:10.1146/annurev.biophys.37.032807.125859 (2008).

30 Suh, B. C., Inoue, T., Meyer, T. & Hille, B. Rapid chemically induced changes of PtdIns(4,5)P2 gate KCNQ ion channels. *Science* **314**, 1454-1457, doi:10.1126/science.1131163 (2006).

31 McLaughlin, S., Wang, J., Gambhir, A. & Murray, D. PIP(2) and proteins: interactions, organization, and information flow. *Annual review of biophysics and biomolecular structure* **31**, 151-175, doi:10.1146/annurev.biophys.31.082901.134259 (2002).

32 Rusten, T. E. & Stenmark, H. Analyzing phosphoinositides and their interacting proteins. *Nature methods* **3**, 251-258, doi:10.1038/nmeth867 (2006).

33 Li, Y. *et al.* KCNE1 enhances phosphatidylinositol 4,5-bisphosphate (PIP2) sensitivity of IKs to modulate channel activity. *Proc Natl Acad Sci U S A* **108**, 9095-9100, doi:10.1073/pnas.1100872108 (2011).

34 Zhang, W. & Linden, D. J. The other side of the engram: experience-driven changes in neuronal intrinsic excitability. *Nat Rev Neurosci* **4**, 885-900, doi:10.1038/nrn1248 (2003).

35 Li, Y., Gamper, N., Hilgemann, D. W. & Shapiro, M. S. Regulation of Kv7 (KCNQ) K+ channel open probability by phosphatidylinositol 4,5-bisphosphate. *J Neurosci* **25**, 9825-9835, doi:10.1523/jneurosci.2597-05.2005 (2005).

36 Eckey, K. *et al.* Novel Kv7.1-phosphatidylinositol 4,5-bisphosphate interaction sites uncovered by charge neutralization scanning. *J Biol Chem* **289**, 22749-22758, doi:10.1074/jbc.M114.589796 (2014).

37 Zaydman, M. A. *et al.* Kv7.1 ion channels require a lipid to couple voltage sensing to pore opening. *Proc Natl Acad Sci U S A* **110**, 13180-13185, doi:10.1073/pnas.1305167110 (2013).

38 Zhang, L., Ouyang, M., Ganellin, C. R. & Thomas, S. A. The slow afterhyperpolarization: a target of beta1-adrenergic signaling in hippocampus-

dependent memory retrieval. *J Neurosci* **33**, 5006-5016, doi:10.1523/jneurosci.3834-12.2013 (2013).

39 Zaydman, M. A. & Cui, J. PIP2 regulation of KCNQ channels: biophysical and molecular mechanisms for lipid modulation of voltage-dependent gating. *Front Physiol* **5**, 195, doi:10.3389/fphys.2014.00195 (2014).

40 Kim, K. S., Duignan, K. M., Hawryluk, J. M., Soh, H. & Tzingounis, A. V. The Voltage Activation of Cortical KCNQ Channels Depends on Global PIP2 Levels. *Biophys J* **110**, 1089-1098, doi:10.1016/j.bpj.2016.01.006 (2016).

41 Suh, B. C., Horowitz, L. F., Hirdes, W., Mackie, K. & Hille, B. Regulation of KCNQ2/KCNQ3 current by G protein cycling: the kinetics of receptor-mediated signaling by Gq. *J Gen Physiol* **123**, 663-683, doi:10.1085/jgp.200409029 (2004).

42 Haitin, Y. & Attali, B. The C-terminus of Kv7 channels: a multifunctional module. *J Physiol* **586**, 1803-1810, doi:10.1113/jphysiol.2007.149187 (2008).

43 Kang, S., Xu, M., Cooper, E. C. & Hoshi, N. Channel-anchored protein kinase CK2 and protein phosphatase 1 reciprocally regulate KCNQ2-containing M-channels via phosphorylation of calmodulin. *J Biol Chem* **289**, 11536-11544, doi:10.1074/jbc.M113.528497 (2014).

44 Kosenko, A. *et al.* Coordinated signal integration at the M-type potassium channel upon muscarinic stimulation. *EMBO J* **31**, 3147-3156, doi:10.1038/emboj.2012.156 (2012).

45 Hughes, S., Marsh, S. J., Tinker, A. & Brown, D. A. PIP2-dependent inhibition of M-type (Kv7. 2/7.3) potassium channels: direct on-line assessment of PIP2 depletion

by Gq-coupled receptors in single living neurons. *Pflügers Archiv-European Journal of Physiology* **455**, 115-124 (2007).

46 Hoshi, N., Langeberg, L. K. & Scott, J. D. Distinct enzyme combinations in AKAP signalling complexes permit functional diversity. *Nat Cell Biol* **7**, 1066-1073, doi:10.1038/ncb1315 (2005).

47 Wong, W. & Scott, J. D. AKAP signalling complexes: focal points in space and time. *Nat Rev Mol Cell Biol* **5**, 959-970, doi:10.1038/nrm1527 (2004).

48 Delint-Ramirez, I., Willoughby, D., Hammond, G. R., Ayling, L. J. & Cooper, D. M. Palmitoylation targets AKAP79 protein to lipid rafts and promotes its regulation of calcium-sensitive adenylyl cyclase type 8. *J Biol Chem* **286**, 32962-32975, doi:10.1074/jbc.M111.243899 (2011).

49 Etxeberria, A. *et al.* Calmodulin regulates the trafficking of KCNQ2 potassium channels. *FASEB J* **22**, 1135-1143, doi:10.1096/fj.07-9712com (2008).

50 Alaimo, A. *et al.* Calmodulin activation limits the rate of KCNQ2 K+ channel exit from the endoplasmic reticulum. *J Biol Chem* **284**, 20668-20675, doi:10.1074/jbc.M109.019539 (2009).

51 Alberdi, A. *et al.* Uncoupling PIP2-calmodulin regulation of Kv7.2 channels by an assembly destabilizing epileptogenic mutation. *J Cell Sci* **128**, 4014-4023, doi:10.1242/jcs.176420 (2015).

52 Levitan, I. B. Signaling protein complexes associated with neuronal ion channels. *Nat Neurosci* **9**, 305-310, doi:10.1038/nn1647 (2006).

53 Kosenko, A. & Hoshi, N. A change in configuration of the calmodulin-KCNQ channel complex underlies Ca2+-dependent modulation of KCNQ channel activity. *PLoS One* **8**, e82290, doi:10.1371/journal.pone.0082290 (2013).

54 Sachyani, D. *et al.* Structural basis of a Kv7.1 potassium channel gating module: studies of the intracellular c-terminal domain in complex with calmodulin. *Structure* **22**, 1582-1594, doi:10.1016/j.str.2014.07.016 (2014).

55 Alaimo, A. *et al.* Cooperativity between calmodulin-binding sites in Kv7.2 channels. *J Cell Sci* **126**, 244-253, doi:10.1242/jcs.114082 (2013).

56 Alaimo, A. *et al.* Pivoting between calmodulin lobes triggered by calcium in the Kv7.2/calmodulin complex. *PLoS One* **9**, e86711, doi:10.1371/journal.pone.0086711 (2014).

57 Devaux, J. J., Kleopa, K. A., Cooper, E. C. & Scherer, S. S. KCNQ2 is a nodal K+ channel. *J Neurosci* **24**, 1236-1244, doi:10.1523/JNEUROSCI.4512-03.2004 (2004).

58 Pan, Z. *et al.* A common ankyrin-G-based mechanism retains KCNQ and NaV channels at electrically active domains of the axon. *J Neurosci* **26**, 2599-2613, doi:10.1523/jneurosci.4314-05.2006 (2006).

59 Regev, N. *et al.* Selective interaction of syntaxin 1A with KCNQ2: possible implications for specific modulation of presynaptic activity. *PLoS One* **4**, e6586, doi:10.1371/journal.pone.0006586 (2009).

60 Etzioni, A. *et al.* Regulation of neuronal M-channel gating in an isoform-specific manner: functional interplay between calmodulin and syntaxin 1A. *J Neurosci* **31**, 14158-14171, doi:10.1523/jneurosci.2666-11.2011 (2011).

61 Brackenbury, W. J. & Isom, L. L. Na Channel beta Subunits: Overachievers of the Ion Channel Family. *Frontiers in pharmacology* **2**, 53, doi:10.3389/fphar.2011.00053 (2011).

62 Marionneau, C. *et al.* The sodium channel accessory subunit Navbeta1 regulates neuronal excitability through modulation of repolarizing voltage-gated K(+) channels. *J Neurosci* **32**, 5716-5727, doi:10.1523/jneurosci.6450-11.2012 (2012).

63 Nguyen, H. M. *et al.* Modulation of voltage-gated K+ channels by the sodium channel beta1 subunit. *Proc Natl Acad Sci U S A* **109**, 18577-18582, doi:10.1073/pnas.1209142109 (2012).

64 Luo, Y. *et al.* Mice deficient in BACE1, the Alzheimer's beta-secretase, have normal phenotype and abolished beta-amyloid generation. *Nat Neurosci* **4**, 231-232, doi:10.1038/85059 (2001).

65 Wong, H. K. *et al.* beta Subunits of voltage-gated sodium channels are novel substrates of beta-site amyloid precursor protein-cleaving enzyme (BACE1) and gamma-secretase. *J Biol Chem* **280**, 23009-23017, doi:10.1074/jbc.M414648200 (2005).

66 Hessler, S. *et al.* beta-Secretase BACE1 regulates hippocampal and reconstituted M-currents in a beta-subunit-like fashion. *J Neurosci* **35**, 3298-3311, doi:10.1523/JNEUROSCI.3127-14.2015 (2015).

67 Jiang, L. *et al.* Activation of m1 muscarinic acetylcholine receptor induces surface transport of KCNQ channels through a CRMP-2-mediated pathway. *J Cell Sci* **128**, 4235-4245, doi:10.1242/jcs.175547 (2015).

68 Brown, D. M-currents: an update. *Trends Neurosci* **11**, 294-299 (1988).

69 Marrion, N. V. Control of M-current. *Annu Rev Physiol* **59**, 483-504, doi:10.1146/annurev.physiol.59.1.483 (1997).

70 Zaika, O. *et al.* Angiotensin II regulates neuronal excitability via phosphatidylinositol 4,5-bisphosphate-dependent modulation of Kv7 (M-type) K+ channels. *J Physiol* **575**, 49-67, doi:10.1113/jphysiol.2006.114074 (2006).

71 Jones, S. W. Muscarinic and peptidergic excitation of bull-frog sympathetic neurones. *J Physiol* **366**, 63-87 (1985).

72 Colino, A. & Halliwell, J. V. Differential modulation of three separate K-conductances in hippocampal CA1 neurons by serotonin. *Nature* **328**, 73-77, doi:10.1038/328073a0 (1987).

73 Marrion, N. V., Smart, T. G., Marsh, S. J. & Brown, D. A. Muscarinic suppression of the M-current in the rat sympathetic ganglion is mediated by receptors of the M1-subtype. *Br J Pharmacol* **98**, 557-573 (1989).

74 Bernheim, L., Mathie, A. & Hille, B. Characterization of muscarinic receptor subtypes inhibiting Ca2+ current and M current in rat sympathetic neurons. *Proc Natl Acad Sci U S A* **89**, 9544-9548 (1992).

75 Charpak, S., Gahwiler, B. H., Do, K. Q. & Knopfel, T. Potassium conductances in hippocampal neurons blocked by excitatory amino-acid transmitters. *Nature* **347**, 765-767, doi:10.1038/347765a0 (1990).

76 Moore, S. D., Madamba, S. G., Schweitzer, P. & Siggins, G. R. Voltage-dependent effects of opioid peptides on hippocampal CA3 pyramidal neurons in vitro. *J Neurosci* **14**, 809-820 (1994).

77 Constanti, A. & Brown, D. A. M-Currents in voltage-clamped mammalian sympathetic neurones. *Neurosci Lett* **24**, 289-294 (1981).

78 Shapiro, M. S., Wollmuth, L. P. & Hille, B. Angiotensin II inhibits calcium and M current channels in rat sympathetic neurons via G proteins. *Neuron* **12**, 1319-1329 (1994).

79 Brown, D. A. & Adams, P. R. Muscarinic suppression of a novel voltage-sensitive K+ current in a vertebrate neurone. *Nature* **283**, 673-676 (1980).

80 Storm, J. F. Potassium currents in hippocampal pyramidal cells. *Prog Brain Res* **83**, 161-187 (1990).

81 Suh, B. C. & Hille, B. Recovery from muscarinic modulation of M current channels requires phosphatidylinositol 4,5-bisphosphate synthesis. *Neuron* **35**, 507-520 (2002).

82 Zhang, H. *et al.* PIP(2) activates KCNQ channels, and its hydrolysis underlies receptor-mediated inhibition of M currents. *Neuron* **37**, 963-975 (2003).

83 Winks, J. S. *et al.* Relationship between membrane phosphatidylinositol-4,5-bisphosphate and receptor-mediated inhibition of native neuronal M channels. *J Neurosci* **25**, 3400-3413, doi:10.1523/jneurosci.3231-04.2005 (2005).

84 Higashida, H. & Brown, D. A. Two polyphosphatidylinositide metabolites control two K+ currents in a neuronal cell. *Nature* **323**, 333-335, doi:10.1038/323333a0 (1986).

85 Bosma, M. M. & Hille, B. Protein kinase C is not necessary for peptide-induced suppression of M current or for desensitization of the peptide receptors. *Proc Natl Acad Sci U S A* **86**, 2943-2947 (1989).

86 Hoshi, N., Langeberg, L. K., Gould, C. M., Newton, A. C. & Scott, J. D. Interaction with AKAP79 modifies the cellular pharmacology of PKC. *Mol Cell* **37**, 541-550, doi:10.1016/j.molcel.2010.01.014 (2010).

87 Smith, I. M. & Hoshi, N. ATP competitive protein kinase C inhibitors demonstrate distinct state-dependent inhibition. *PLoS One* **6**, e26338, doi:10.1371/journal.pone.0026338 (2011).

88 Tunquist, B. J. *et al.* Loss of AKAP150 perturbs distinct neuronal processes in mice. *Proc Natl Acad Sci U S A* **105**, 12557-12562, doi:10.1073/pnas.0805922105 (2008).

89 Kirkwood, A. & Lisman, J. E. Action potentials produce a long-term enhancement of M-current in frog sympathetic ganglion. *Brain Res* **580**, 281-287 (1992).

90 Gamper, N. & Shapiro, M. S. Calmodulin mediates Ca2+-dependent modulation of M-type K+ channels. *J Gen Physiol* **122**, 17-31, doi:10.1085/jgp.200208783 (2003).

91 Bal, M., Zhang, J., Hernandez, C. C., Zaika, O. & Shapiro, M. S. Ca2+/calmodulin disrupts AKAP79/150 interactions with KCNQ (M-Type) K+ channels. *J Neurosci* **30**, 2311-2323, doi:10.1523/JNEUROSCI.5175-09.2010 (2010).

92 Sihn, C. R. *et al.* Mechanisms of Calmodulin Regulation of Different Isoforms of Kv7.4 K+ Channels. *J Biol Chem* **291**, 2499-2509, doi:10.1074/jbc.M115.668236 (2016).

93 Brown, D. A. & Passmore, G. M. Neural KCNQ (Kv7) channels. *Br J Pharmacol* **156**, 1185-1195, doi:10.1111/j.1476-5381.2009.00111.x (2009).

94 Koyama, S. & Appel, S. B. Characterization of M-current in ventral tegmental area dopamine neurons. *J Neurophysiol* **96**, 535-543, doi:10.1152/jn.00574.2005 (2006).

95 Wladyka, C. L. & Kunze, D. L. KCNQ/M-currents contribute to the resting membrane potential in rat visceral sensory neurons. *J Physiol* **575**, 175-189, doi:10.1113/jphysiol.2006.113308 (2006).

96 Guan, D., Higgs, M. H., Horton, L. R., Spain, W. J. & Foehring, R. C. Contributions of Kv7-mediated potassium current to sub- and suprathreshold responses of rat layer II/III neocortical pyramidal neurons. *J Neurophysiol* **106**, 1722-1733, doi:10.1152/jn.00211.2011 (2011).

97 Huang, H. & Trussell, L. O. KCNQ5 channels control resting properties and release probability of a synapse. *Nat Neurosci* **14**, 840-847, doi:10.1038/nn.2830 (2011).

98 Schwarz, J. R. *et al.* KCNQ channels mediate IKs, a slow K+ current regulating excitability in the rat node of Ranvier. *J Physiol* **573**, 17-34, doi:10.1113/jphysiol.2006.106815 (2006).

99 Martire, M. *et al.* M channels containing KCNQ2 subunits modulate norepinephrine, aspartate, and GABA release from hippocampal nerve terminals. *J Neurosci* **24**, 592-597, doi:10.1523/JNEUROSCI.3143-03.2004 (2004).

100 Vervaeke, K., Gu, N., Agdestein, C., Hu, H. & Storm, J. F. Kv7/KCNQ/M-channels in rat glutamatergic hippocampal axons and their role in regulation of excitability and transmitter release. *J Physiol* **576**, 235-256, doi:10.1113/jphysiol.2006.111336 (2006).

101 Shah, M. M., Migliore, M., Valencia, I., Cooper, E. C. & Brown, D. A. Functional significance of axonal Kv7 channels in hippocampal pyramidal neurons. *Proc Natl Acad Sci U S A* **105**, 7869-7874, doi:10.1073/pnas.0802805105 (2008).

102 Shah, M. M., Migliore, M. & Brown, D. A. Differential effects of Kv7 (M-) channels on synaptic integration in distinct subcellular compartments of rat hippocampal pyramidal neurons. *J Physiol* **589**, 6029-6038, doi:10.1113/jphysiol.2011.220913 (2011).

103 Storm, J. F. An after-hyperpolarization of medium duration in rat hippocampal pyramidal cells. *J Physiol* **409**, 171-190 (1989).

104 Gu, N., Vervaeke, K., Hu, H. & Storm, J. F. Kv7/KCNQ/M and HCN/h, but not KCa2/SK channels, contribute to the somatic medium after-hyperpolarization and excitability control in CA1 hippocampal pyramidal cells. *J Physiol* **566**, 689-715, doi:10.1113/jphysiol.2005.086835 (2005).

105 Stocker, M., Krause, M. & Pedarzani, P. An apamin-sensitive Ca2+-activated K+ current in hippocampal pyramidal neurons. *Proc Natl Acad Sci U S A* **96**, 4662-4667 (1999).

106 Mateos-Aparicio, P., Murphy, R. & Storm, J. F. Complementary functions of SK and Kv7/M potassium channels in excitability control and synaptic integration in rat hippocampal dentate granule cells. *J Physiol* **592**, 669-693, doi:10.1113/jphysiol.2013.267872 (2014).

107 Sanchez, G., Rodriguez, M. J., Pomata, P., Rela, L. & Murer, M. G. Reduction of an afterhyperpolarization current increases excitability in striatal cholinergic

interneurons in rat parkinsonism. *J Neurosci* **31**, 6553-6564, doi:10.1523/jneurosci.6345-10.2011 (2011).

108 Tzingounis, A. V., Kobayashi, M., Takamatsu, K. & Nicoll, R. A. Hippocalcin gates the calcium activation of the slow afterhyperpolarization in hippocampal pyramidal cells. *Neuron* **53**, 487-493, doi:10.1016/j.neuron.2007.01.011 (2007).

109 Andrade, R., Foehring, R. C. & Tzingounis, A. V. The calcium-activated slow AHP: cutting through the Gordian knot. *Front Cell Neurosci* **6**, 47, doi:10.3389/fncel.2012.00047 (2012).

110 Zhang, Q. *et al.* Dynamic PIP2 interactions with voltage sensor elements contribute to KCNQ2 channel gating. *Proc Natl Acad Sci U S A* **110**, 20093-20098, doi:10.1073/pnas.1312483110 (2013).

111 Aiken, S. P., Lampe, B. J., Murphy, P. A. & Brown, B. S. Reduction of spike frequency adaptation and blockade of M-current in rat CA1 pyramidal neurones by linopirdine (DuP 996), a neurotransmitter release enhancer. *Br J Pharmacol* **115**, 1163-1168 (1995).

112 Nigro, M. J., Mateos-Aparicio, P. & Storm, J. F. Expression and functional roles of Kv7/KCNQ/M-channels in rat medial entorhinal cortex layer II stellate cells. *J Neurosci* **34**, 6807-6812, doi:10.1523/JNEUROSCI.4153-13.2014 (2014).

113 Hawryluk, J. M. *et al.* KCNQ channels determine serotonergic modulation of ventral surface chemoreceptors and respiratory drive. *J Neurosci* **32**, 16943-16952, doi:10.1523/jneurosci.3043-12.2012 (2012).

114 Lawrence, J. J. *et al.* Somatodendritic Kv7/KCNQ/M channels control interspike interval in hippocampal interneurons. *J Neurosci* **26**, 12325-12338, doi:10.1523/JNEUROSCI.3521-06.2006 (2006).

115 Madison, D. V. & Nicoll, R. A. Control of the repetitive discharge of rat CA 1 pyramidal neurones in vitro. *J Physiol* **354**, 319-331 (1984).

116 Hu, H., Vervaeke, K. & Storm, J. F. Two forms of electrical resonance at theta frequencies, generated by M-current, h-current and persistent Na+ current in rat hippocampal pyramidal cells. *J Physiol* **545**, 783-805 (2002).

117 Ge, L. & Liu, X. D. Electrical resonance with voltage-gated ion channels: perspectives from biophysical mechanisms and neural electrophysiology. *Acta Pharmacol Sin* **37**, 67-74, doi:10.1038/aps.2015.140 (2016).

118 Winson, J. Loss of hippocampal theta rhythm results in spatial memory deficit in the rat. *Science* **201**, 160-163 (1978).

119 Huerta, P. T. & Lisman, J. E. Heightened synaptic plasticity of hippocampal CA1 neurons during a cholinergically induced rhythmic state. *Nature* **364**, 723-725, doi:10.1038/364723a0 (1993).

120 Buzsaki, G. Theta oscillations in the hippocampus. *Neuron* **33**, 325-340 (2002).

121 Bland, B. H. The physiology and pharmacology of hippocampal formation theta rhythms. *Prog Neurobiol* **26**, 1-54 (1986).

122 Sarnthein, J., Petsche, H., Rappelsberger, P., Shaw, G. L. & von Stein, A. Synchronization between prefrontal and posterior association cortex during human working memory. *Proc Natl Acad Sci U S A* **95**, 7092-7096 (1998).

123 Olvera-Cortes, E., Guevara, M. A. & Gonzalez-Burgos, I. Increase of the hippocampal theta activity in the Morris water maze reflects learning rather than motor activity. *Brain research bulletin* **62**, 379-384, doi:10.1016/j.brainresbull.2003.10.003 (2004).

124 Peters, H. C., Hu, H., Pongs, O., Storm, J. F. & Isbrandt, D. Conditional transgenic suppression of M channels in mouse brain reveals functions in neuronal excitability, resonance and behavior. *Nat Neurosci* **8**, 51-60, doi:10.1038/nn1375 (2005).

125 Yue, C. & Yaari, Y. KCNQ/M channels control spike afterdepolarization and burst generation in hippocampal neurons. *J Neurosci* **24**, 4614-4624, doi:10.1523/JNEUROSCI.0765-04.2004 (2004).

126 Martinello, K. *et al.* Cholinergic afferent stimulation induces axonal function plasticity in adult hippocampal granule cells. *Neuron* **85**, 346-363, doi:10.1016/j.neuron.2014.12.030 (2015).

127 Young, M. B. & Thomas, S. A. M1-muscarinic receptors promote fear memory consolidation via phospholipase C and the M-current. *J Neurosci* **34**, 1570-1578, doi:10.1523/JNEUROSCI.1040-13.2014 (2014).

128 Frick, A., Magee, J. & Johnston, D. LTP is accompanied by an enhanced local excitability of pyramidal neuron dendrites. *Nat Neurosci* **7**, 126-135, doi:10.1038/nn1178 (2004).

129 Moore, S. D., Madamba, S. G., Joels, M. & Siggins, G. R. Somatostatin augments the M-current in hippocampal neurons. *Science* **239**, 278-280 (1988).

130 de Lecea, L. *et al.* A cortical neuropeptide with neuronal depressant and sleep-modulating properties. *Nature* **381**, 242-245, doi:10.1038/381242a0 (1996).

131 Madamba, S. G., Schweitzer, P. & Siggins, G. R. Dynorphin selectively augments the M-current in hippocampal CA1 neurons by an opiate receptor mechanism. *J Neurophysiol* **82**, 1768-1775 (1999).

132 Borsotto, M. *et al.* PP2A-Bgamma subunit and KCNQ2 K+ channels in bipolar disorder. *Pharmacogenomics J* **7**, 123-132, doi:10.1038/sj.tpj.6500400 (2007).

133 Wildburger, N. C. & Laezza, F. Control of neuronal ion channel function by glycogen synthase kinase-3: new prospective for an old kinase. *Frontiers in molecular neuroscience* **5**, 80, doi:10.3389/fnmol.2012.00080 (2012).

134 Zhang, M. *et al.* Selective phosphorylation modulates the PIP2 sensitivity of the CaM-SK channel complex. *Nature chemical biology* **10**, 753-759, doi:10.1038/nchembio.1592 (2014).

135 Gamper, N. *et al.* Oxidative modification of M-type K(+) channels as a mechanism of cytoprotective neuronal silencing. *Embo j* **25**, 4996-5004, doi:10.1038/sj.emboj.7601374 (2006).

136 Kim, H. J. *et al.* Protein arginine methylation facilitates KCNQ channel-PIP2 interaction leading to seizure suppression. *eLife* **5**, doi:10.7554/eLife.17159 (2016).

137 Schroeder, B. C. *et al.* A constitutively open potassium channel formed by KCNQ1 and KCNE3. *Nature* **403**, 196-199, doi:10.1038/35003200 (2000).

138 Abbott, G. W. *et al.* KCNQ1, KCNE2, and Na+-coupled solute transporters form reciprocally regulating complexes that affect neuronal excitability. *Sci Signal* **7**, ra22, doi:10.1126/scisignal.2005025 (2014).

139 Stott, J. B., Povstyan, O. V., Carr, G., Barrese, V. & Greenwood, I. A. G-protein betagamma subunits are positive regulators of Kv7.4 and native vascular Kv7 channel activity. *Proc Natl Acad Sci U S A* **112**, 6497-6502, doi:10.1073/pnas.1418605112 (2015).

140 Roper, J. & Schwarz, J. R. Heterogeneous distribution of fast and slow potassium channels in myelinated rat nerve fibres. *J Physiol* **416**, 93-110 (1989).

141 Hamada, M. S. & Kole, M. H. Myelin loss and axonal ion channel adaptations associated with gray matter neuronal hyperexcitability. *J Neurosci* **35**, 7272-7286, doi:10.1523/jneurosci.4747-14.2015 (2015).

142 Shah, M., Mistry, M., Marsh, S. J., Brown, D. A. & Delmas, P. Molecular correlates of the M-current in cultured rat hippocampal neurons. *J Physiol* **544**, 29-37 (2002).

143 Kapfhamer, D. *et al.* Protein Phosphatase 2a and glycogen synthase kinase 3 signaling modulate prepulse inhibition of the acoustic startle response by altering cortical M-Type potassium channel activity. *J Neurosci* **30**, 8830-8840, doi:10.1523/jneurosci.1292-10.2010 (2010).

144 Yue, C. & Yaari, Y. Axo-somatic and apical dendritic Kv7/M channels differentially regulate the intrinsic excitability of adult rat CA1 pyramidal cells. *J Neurophysiol* **95**, 3480-3495, doi:10.1152/jn.01333.2005 (2006).

145 Hu, H., Vervaeke, K. & Storm, J. F. M-channels (Kv7/KCNQ channels) that regulate synaptic integration, excitability, and spike pattern of CA1 pyramidal cells are located in the perisomatic region. *J Neurosci* **27**, 1853-1867, doi:10.1523/jneurosci.4463-06.2007 (2007).

146 Chen, X. & Johnston, D. Properties of single voltage-dependent K(+) channels in dendrites of CA1 pyramidal neurones of rat hippocampus. *J Physiol* **559**, 187-203, doi:10.1113/jphysiol.2004.068114 (2004).

147 Sun, J. & Kapur, J. M-type potassium channels modulate Schaffer collateral-CA1 glutamatergic synaptic transmission. *J Physiol* **590**, 3953-3964, doi:10.1113/jphysiol.2012.235820 (2012).

148 Benned-Jensen, T. *et al.* Live Imaging of Kv7.2/7.3 Cell Surface Dynamics at the Axon Initial Segment: High Steady-State Stability and Calpain-Dependent Excitotoxic Downregulation Revealed. *J Neurosci* **36**, 2261-2266, doi:10.1523/JNEUROSCI.2631-15.2016 (2016).

149 Zhang, J. & Shapiro, M. S. Activity-dependent transcriptional regulation of M-Type (Kv7) K(+) channels by AKAP79/150-mediated NFAT actions. *Neuron* **76**, 1133-1146, doi:10.1016/j.neuron.2012.10.019 (2012).

150 Li, C. *et al.* Activity-dependent downregulation of M-Type (Kv7) K(+) channels surface expression requires the activation of iGluRs/Ca(2)(+)/PKC signaling pathway in hippocampal neuron. *Neuropharmacology* **95**, 154-167, doi:10.1016/j.neuropharm.2015.03.004 (2015).

151 Kuba, H., Yamada, R., Ishiguro, G. & Adachi, R. Redistribution of Kv1 and Kv7 enhances neuronal excitability during structural axon initial segment plasticity. *Nat Commun* **6**, 8815, doi:10.1038/ncomms9815 (2015).

152 Biervert, C. *et al.* A potassium channel mutation in neonatal human epilepsy. *Science* **279**, 403-406 (1998).

153 Castaldo, P. *et al.* Benign familial neonatal convulsions caused by altered gating of KCNQ2/KCNQ3 potassium channels. *J Neurosci* **22**, RC199 (2002).

154 Abidi, A. *et al.* A recurrent KCNQ2 pore mutation causing early onset epileptic encephalopathy has a moderate effect on M current but alters subcellular localization of Kv7 channels. *Neurobiol Dis* **80**, 80-92, doi:10.1016/j.nbd.2015.04.017 (2015).

155 Borgatti, R. *et al.* A novel mutation in KCNQ2 associated with BFNC, drug resistant epilepsy, and mental retardation. *Neurology* **63**, 57-65 (2004).

156 Schwake, M., Pusch, M., Kharkovets, T. & Jentsch, T. J. Surface expression and single channel properties of KCNQ2/KCNQ3, M-type K+ channels involved in epilepsy. *J Biol Chem* **275**, 13343-13348 (2000).

157 Chung, H. J., Jan, Y. N. & Jan, L. Y. Polarized axonal surface expression of neuronal KCNQ channels is mediated by multiple signals in the KCNQ2 and KCNQ3 C-terminal domains. *Proc Natl Acad Sci U S A* **103**, 8870-8875, doi:10.1073/pnas.0603376103 (2006).

158 Soldovieri, M. V., Miceli, F. & Taglialatela, M. Driving with no brakes: molecular pathophysiology of Kv7 potassium channels. *Physiology (Bethesda, Md.)* **26**, 365-376, doi:10.1152/physiol.00009.2011 (2011).

159 Dedek, K., Fusco, L., Teloy, N. & Steinlein, O. K. Neonatal convulsions and epileptic encephalopathy in an Italian family with a missense mutation in the fifth transmembrane region of KCNQ2. *Epilepsy Res* **54**, 21-27 (2003).

160 Weckhuysen, S. *et al.* Extending the KCNQ2 encephalopathy spectrum: clinical and neuroimaging findings in 17 patients. *Neurology* **81**, 1697-1703, doi:10.1212/01.wnl.0000435296.72400.a1 (2013).

161 Singh, N. A. *et al.* Mouse models of human KCNQ2 and KCNQ3 mutations for benign familial neonatal convulsions show seizures and neuronal plasticity without synaptic reorganization. *J Physiol* **586**, 3405-3423, doi:10.1113/jphysiol.2008.154971 (2008).

162 Tomonoh, Y. *et al.* The kick-in system: a novel rapid knock-in strategy. *PLoS One* **9**, e88549, doi:10.1371/journal.pone.0088549 (2014).

163 Ihara, Y. *et al.* Retigabine, a Kv7.2/Kv7.3-Channel Opener, Attenuates Drug-Induced Seizures in Knock-In Mice Harboring Kcnq2 Mutations. *PLoS One* **11**, e0150095, doi:10.1371/journal.pone.0150095 (2016).

164 Lothman, E. W., Bertram, E. H., 3rd & Stringer, J. L. Functional anatomy of hippocampal seizures. *Prog Neurobiol* **37**, 1-82 (1991).

165 Meriaux, C. *et al.* Human temporal lobe epilepsy analyses by tissue proteomics. *Hippocampus* **24**, 628-642, doi:10.1002/hipo.22246 (2014).

166 Weckhuysen, S. *et al.* KCNQ2 encephalopathy: emerging phenotype of a neonatal epileptic encephalopathy. *Ann Neurol* **71**, 15-25, doi:10.1002/ana.22644 (2012).

167 Miceli, F. *et al.* Early-onset epileptic encephalopathy caused by gain-of-function mutations in the voltage sensor of Kv7.2 and Kv7.3 potassium channel subunits. *J Neurosci* **35**, 3782-3793, doi:10.1523/JNEUROSCI.4423-14.2015 (2015).

168 Devaux, J. *et al.* A Kv7.2 mutation associated with early onset epileptic encephalopathy with suppression-burst enhances Kv7/M channel activity. *Epilepsia*, doi:10.1111/epi.13366 (2016).

169 Kay, H. Y., Greene, D. L., Kang, S., Kosenko, A. & Hoshi, N. M-current preservation contributes to anticonvulsant effects of valproic acid. *J Clin Invest* **125**, 3904-3914, doi:10.1172/JCI79727 (2015).

170 Wickenden, A. D., Yu, W., Zou, A., Jegla, T. & Wagoner, P. K. Retigabine, a novel anti-convulsant, enhances activation of KCNQ2/Q3 potassium channels. *Molecular pharmacology* **58**, 591-600 (2000).

171 Santini, E. & Porter, J. T. M-type potassium channels modulate the intrinsic excitability of infralimbic neurons and regulate fear expression and extinction. *J Neurosci* **30**, 12379-12386, doi:10.1523/jneurosci.1295-10.2010 (2010).

Chapter Two

XE991 and Linopirdine are activated-subunit inhibitors of Kv7/KCNQ channels

Introduction

As detailed in chapter 1, Kv7/KCNQ channels regulate neuronal excitability[1-3] and activation of Gq-coupled receptors such as muscarinic acetylcholine receptors (m1 and m3) suppresses the M-current and induces transient hyperexcitability in a wide range of neurons[2]. Accordingly, M-channel inhibitors were developed in hopes of ameliorating defective neuronal activity such as in Alzheimer's dementia. Linopirdine is one such prototypical compound that was found to have a cognitive enhancing effect in an animal model[4]. However, linopirdine did not pass phase 3 clinical trials[5]. XE991 was developed as an improved compound with a similar chemical structure[6]. Although no clinical trials have been conducted for this compound, XE991 has increasingly been used in cell culture and animal experiments to investigate physiological[7-9] and pathological roles[10,11] of the M-current.

It has been shown that KCNQ2 gene knockout is lethal[12,13]. However, administration of linopirdine is well tolerated in humans[5,14], as well as animals for linopirdine and XE991[4,6]. In addition, even though XE991 is a highly potent inhibitor, it sometimes requires prolonged incubation to inhibit[15], or may have no observed effect[16].

These lines of evidence suggest that there are conditions where these Kv7 channel inhibitors are not efficacious.

XE991 will be utilized in proceeding chapters in order to determine M-current contribution in seizure and epileptogenesis. Since there remains uncertainty on the proper use of XE991, as made apparent by inconsistencies in the literature, there is a need to further characterize its mode of inhibition. To this end we performed an electrophysiological study in a heterologous expression system using Chinese hamster ovary cells transiently expressing Kv7 channels. We determined the conditions where these compounds are efficacious, their mode of interaction and addressed the past inconsistencies regarding the washout of these compounds. The determined characteristics of XE991 and linopirdine should be pertinent for experimenters utilizing these compounds.

Experimental Procedures

Reagents and Plasmids.

Linopirdine (1,3-Dihydro-1-phenyl-3,3-bis(4-pyridinylmethyl)-2H-indol-2-one dihydrochloride), XE991 dihydrochloride (10,10-bis(4-Pyridinylmethyl)-9(10H)-anthracenone dihydrochloride), and Exo1 were purchased from Tocris (Bristol, UK). Retigabine (Ethyl N-[2-amino-4-[(4-fluorophenyl)methylamino]phenyl]carbamate) was purchased from Alomone Labs (Jerusalem, Israel). Concanavalin A, was purchased from Sigma-Aldrich (St. Louis, MO, USA). Mammalian expression plasmids containing rat Kv7.2, Kv7.3[17] and Kv7.2-mCit[18] have been described. Kv7.2 mutation (R214D) was generated using QuickChange II XL site-directed mutagenesis (Agilent Technologies, San Diego, CA, USA), and was validated by DNA sequencing.

Cell Culture.

Chinese hamster ovary hm1 cells[19] were cultured in α minimum essential media containing 5% fetal calf serum and 500 μg/ml G418 sulfate. Cells were maintained in a humidified incubator at 37 °C with 5% CO_2. CHO cells were grown to 30% confluence on 35 mm plates before being transfected with 1 μg plasmid DNA and 4 μl LT1 reagent (Mirus Bio LLC, Madison, WI, USA).

Pre-incubation Treatments.

For pretreatment experiments using XE991, culture dishes were washed for 1 minute with Q2 solution containing 144 mM NaCl, 5 mM KCl, 2 mM $CaCl_2$, 0.5 mM $MgCl_2$, 10 mM glucose, and 10 mM HEPES (pH 7.4), the solution was then replaced with distinct experimental solutions. For the treatment group with 10 mM KCl, NaCl was reduced to 139 mM to maintain osmolarity. 10 μM XE991 ± 10 μM retigabine were

incubated for 10 minutes at 37 °C, then thoroughly washed with constant perfusion of Q2 solution for 5 minutes before proceeding with whole cell patch clamp. For Exo1 experiments, cells were pretreated with 100 μM Exo1 in Q2 solution at room temperature for 2 minutes prior to proceeding with experiments.

Electrophysiology.

All patch clamp recordings were performed at room temperature on isolated CHO cells using an Axon Multiclamp 700B patch clamp amplifier (Molecular Devices). Data were acquired using pClamp software (version 10; Molecular Devices). Signals for current traces with ≤1 second duration were sampled at 2 kHz and low pass-filtered at 1 kHz. Current recordings between 1-15 seconds were sampled at 500 Hz and those longer than 15 seconds was sampled at 250 Hz. Whole cell patch clamp recordings on CHO hm1 cells has been described previously[18]. Briefly, cells were constantly perfused with the Q2 solution detailed above. Patch pipettes (3–4 MΩ) were filled with intracellular solution containing 135 mM potassium aspartate, 2 mM $MgCl_2$, 3 mM EGTA, 1 mM $CaCl_2$, 4 mM ATP, 0.1 mM GTP, 10 mM HEPES (pH 7.2). Successful patches that maintained Rs <6 MΩ were selected for experiments. Liquid junction potential is not corrected in this study.

Live Cell Imaging.

Protocol for TIRF-based assessment of surface transport of Kv7.2 channel has been described previously[19]. Briefly, one day after transfection cells were replated onto 18 mm round cover-glasses. On the second day after transfection, cells were used for TIRF experiments. For recording, medium was replaced with Q2 solution. Fluorescence emission was acquired using an inverted microscope IX-81 (Olympus Tokyo, Tokyo,

Japan) with an ImageEM CCD camera (Hamamatsu Photonics, Hamamatsu, Shizuoka Japan) controlled by MetaMorph 7.6.3 (Molecular Devices, Sunnyvale, CA, USA). For excitation in TIRF experiments, a 515 nm diode-pumped solid-state laser (Cobolt, Stockholm, Sweden) with an acousto-optic tunable filter was used with a TIRF module (Olympus). Emission images were obtained through a dual-view module (Photometrics, Tucson, AZ, USA) with ET535/30m, ET480/40m emission filters and a T505lpxr dichroic mirror (Chroma Technology, Bellows Falls, VT, USA). 100 ms exposure time of images was taken every 10 seconds for time-lapse imaging measurements.

Data Analysis.

The activation curves were obtained by non-linear regression to a Boltzmann equation, $Y = 1\text{-}1/(1+\exp((x\text{-}V_{1/2})/k))$ where x is membrane potential, $V_{1/2}$ is the half activation potential, and k is the slope factor unless stated otherwise in the text. All results are expressed as the mean ± s.e.m. Statistical significance of the results was assessed by non-parametric ANOVA (Kruskal-Wallis test) followed by Dunn's multiple comparisons test or Mann-Whitney test. Two-sample comparison was determined by Student t-test with Welch's correction. All statistical tests were performed by a computer program Prism 6 (GraphPad, La Jolla, CA, USA). $P < 0.05$ is considered significant.

Results

Inhibition of Kv7 channels by XE991 requires membrane depolarization.

It has previously been reported that M-current inhibition by XE991 is voltage dependent and that under some conditions it does not inhibit the M-current[16]. We alternatively reasoned that these characteristics of XE991 are derived from state-dependent inhibition rather than voltage-dependent inhibition since the activation threshold of Kv7 channel is very close to the resting membrane potential.

Treatment with channel inhibitors in cultured dish is a common procedure for inhibiting ion channel activities. Indeed, previous studies incubated with XE991 to suppress the M-current prior to starting experiments[20-23]. We first confirmed whether incubating with XE991 at resting potential is efficacious at suppressing the M-current. This was assessed using Kv7.2 channels expressed in Chinese hamster ovary (CHO) cells. Kv7.2-transfected cells were first voltage-clamped to measure control Kv7.2 current. The configuration was then switched to current clamp mode (I = 0 pA) to hold cells at resting membrane potential and 10 μM XE991 was applied for 1 minute. After a 10 second wash, configuration was reverted back to voltage clamp mode and Kv7.2 current was re-measured. As expected, this procedure did not show significant Kv7.2 current inhibition (4.65 ± 1.42% inhibition, n = 8, Fig. 2.1A). These results indicate that treatment with XE991 to cells at resting membrane potential is not an effective method to inhibit Kv7.2 current.

Voltage-dependence of XE991 inhibition is closely related to activation of Kv7 channels rather than the membrane potential per se.

To further investigate determinants of XE991 potency, we compared the voltage range of Kv7.2 homomeric and Kv7.2/3 heteromeric channel activation to XE991-mediated inhibition. Exposure to 10 μM XE991 for 25 seconds was ineffective when cells were held at -70 mV (Fig. 2.1B), while showing nearly complete inhibition when XE991 was administered at potentials more positive than -30 mV (Fig. 2.1C). XE991-mediated inhibition of Kv7.2 or Kv7.2/3 channels showed voltage-dependence consistent with a previous report[16] (Fig. 2.1D & E). Half-inhibition potentials were -51.6 ± 0.0 mV for Kv7.2 channels, and -50.7 ± 0.9 mV for Kv7.2/3 channels. When XE991-mediated inhibition is plotted against relative activation of Kv7.2 and Kv7.2/3 channels (Fig. 2.1F), it indicates that XE991 is only effective when cells are held at potentials where Kv7 channels are activated more than 1%.

To further characterize activation-dependent inhibition of XE991, we pharmacologically induced a change in the activation voltage of Kv7 channels to more hyperpolarized potentials with retigabine and evaluated whether it changed the efficacy of XE991 (Fig. 2.2). 10 μM retigabine shifted the half-activation voltage of Kv7.2 to -47.0 ± 0.8, a -24 mV shift from the control (Fig. 2.2B). The half-inhibition potential of XE991 (-75.2 ± 0.6 mV, n = 5) also shifted -24 mV from the control (Fig. 2.2B). Importantly, XE991 inhibited Kv7.2 current at a holding potential of -70 mV in the presence of retigabine (Fig. 2.2A), a potential at which XE991 did not inhibit Kv7.2 current in control (Fig. 2.1B). Furthermore, activation-inhibition plots show that the close relationship between inhibition by XE991 and Kv7.2 activation is maintained in the presence of retigabine (Fig. 2.2C).

An additional characterization of voltage-dependent inhibition by XE991 was assessed in a mutant Kv7.2 channel (R214D), which had a 26 mV right-shift in the activation potential compared to WT (half-activation potential 3.4 ± 14.0 mV, Fig. 2.3). Accordingly, the rightward shift in the voltage-dependence of activation coincided with an equivalent rightward shift (26 mV) in the half-inhibition potential (-26.3 ± 0.27 mV) (Fig. 2.3B). Relationships between inhibition by XE991 and channel activation was maintained in this condition (Fig. 2.3C). Interestingly, the voltage dependence of Kv7 channel activation vs. inhibition by XE991 followed a linear function with a slope = 0.97 ± 0.03, when comparing wild-type, retigabine-treated and Kv7.2(R214D) channels (Fig 2.3D), indicating that voltage-dependence of Kv7.2 channel activation and efficacy of XE991 are closely related.

Kinetics of XE991 interaction with Kv7.2.

We then tested the effect of membrane potential on the rate of interaction between Kv7.2 channel and XE991. To examine this, we measured the time course of current inhibition induced by XE991 at various potentials (Fig. 2.4). Cells were held at -70 mV, a potential where XE991 was ineffective, followed by a 20 second depolarization to various test potentials with or without XE991 and then analyzed relative current. XE991 inhibited Kv7.2 currents with time constants that decreased with increasing depolarization (Fig. 2.4A–C). Since many state-dependent ion channel inhibitors such as open channel inhibitors alter gating kinetics[24,25], we also measured the activation and deactivation kinetics of Kv7.2 channel in the presence of XE991. Neither activation nor deactivation time constants of Kv7.2 current were affected by 10 μM XE991 (Figure 2.5) as described previously[24].

Kv7.2 current inhibition mediated by XE991 followed a single exponential decay (Fig. 2.4A & B) with some degree of voltage dependence (Fig. 2.4C). Single exponential decay suggests a single step reaction for XE991-mediated inhibition, which can be summarized as the reaction scheme

$$\text{Kv7.2} + \text{XE991} \underset{k_{off}}{\overset{k_{on}}{\rightleftharpoons}} \text{Kv7.2:XE991}$$

where k_{on} ($M^{-1}s^{-1}$) is the second-order association rate constant and k_{off} (s^{-1}) is the first-order dissociation rate constant. Thus, this reaction can be described as

$$t^{-1} = k_{on}[\text{XE991}] + k_{off} \quad (1)$$

using the inhibition time constant (t) and concentration of XE991, [XE991], as described[26,27]. To determine these constants, we measured time course of current inhibition for wash-in and washout of XE991 at several concentrations (Fig. 2.4D & E). k_{off} was measured directly from the rate of washout from a holding potential of 0 mV (Fig. 2.4E), which was extremely slow and apparently limited. k_{on} was determined subsequently utilizing above reaction equation. If dissociation of XE991 is indeed limited then Kd values cannot be calculated. Therefore, the Kd value observed in a previous report[28] needs to be amended, both because the slow association kinetics of the channel require several minutes to reach steady state at low concentrations and dissociation of the compound may be limited (Fig. 2.4D).

Slow recovery of Kv7 current after washout of XE991 is predominantly due to channel trafficking.

There are conflicting reports regarding recovery of Kv7 currents from XE991 after washout. Some groups considered inhibition by XE991 to be reversible[15,29,30], while others considered it irreversible[23,31]. Our washout experiments with XE991 showed no difference at the concentrations tested (Fig. 2.4E). To further analyze current recovery after washout, we treated CHO cells expressing Kv7.2 channels with 10 μM XE991 at 0 mV for 25 seconds, and then held cells at holding potentials of either -70 or -30 mV during wash to assess the contribution of the activation states of Kv7.2 channels to dissociation (Fig. 2.6). Washout experiments revealed that current recovery observed during washout was voltage-independent, unlike the voltage-dependence of wash-in kinetics. Kv7.2 currents showed 20.2 ± 3.9% and 18.2 ± 2.9% recovery after 10 minute washout when held at -70 mV and -30 mV holding potential respectively (Fig. 2.6A & B). Control experiments without XE991 showed stable Kv7.2 current in our recording condition (Fig. 2.6B) as we reported previously[18]. Kv7.2 current recovery was best fit with a single exponential function (Fig. 2.6B), with recovery time constants of 16.6 ± 12 minutes (-70 mV, n = 8), and 14.1 ± 0.1 minutes (-30 mV, n = 6) with estimated maximal recovery ~35% of control, further suggesting irreversible association of the compound. Similar slow and limited recovery after washout was also observed with Kv7.2/3 heteromeric channels [33.4 ± 5.9% (n = 6) recovery at -70 mV, 37.8 ± 3.8% (n = 6) at -30 mV after 10 minute wash].

30% turnover of Kv7.2 channel in 10 minutes is comparable to surface transport of Kv7 subunit by constitutive exocytosis in CHO cells that we described previously[19]. To evaluate the contribution of Kv7.2 channel trafficking during washout, exocytosis was inhibited by 100 μM Exo1. We first confirmed the effects of 100 μM Exo1 on surface

transport of Kv7.2 channel by total internal reflection fluorescence (TIRF) measurements using monomeric citrine-tagged Kv7.2 channel, Kv7.2-mCit. TIRF selectively illuminates <100 nm from the cover glass, which can be used to monitor Kv7.2 surface transport at the bottom surface of cells as we described previously[19]. To assess Exo1 ability to suppress exocytosis, we inhibited constitutive endocytosis by 50 μg/mL concanavalin A, which induced a gradual increase of TIRF signal of Kv7.2-mCit (Fig. 2.6C), reflecting constitutive exocytosis[19]. 2 minute pretreatment with 100 μM Exo1 resulted in a 75 ± 5% reduction in concanavalin A-induced increase in TIRF signals of Kv7.2-mCit (Fig. 2.6C), confirming that the majority of exocytosis is inhibited in this condition. Using this condition, we examined whether Exo1 prevents recovery of Kv7.2 current after XE991 washout. In the control condition, Kv7.2 current recovered 20.2 ± 3.5% after 10 washout of XE991. When pretreated with Exo1, recovery was reduced to 10.7 ± 1.2%, approximately half of control (Fig. 2.6D). We concluded that current recovery after washout of XE991 is mostly derived from new Kv7 channels surfaced to the plasma membrane rather than dissociation of XE991 from Kv7.2 channel.

Linopirdine shares common features with XE991.

Linopirdine is a prototypical M-channel inhibitor that was developed prior to XE991 and is considered to be structurally similar to XE991[6]. Therefore, we examined whether linopirdine has similar state-dependent inhibition. As summarized in Fig. 2.7, 30 μM linopirdine showed voltage-dependent inhibition of Kv7.2 current with a half-inhibition potential at -55.7 ± 0.4 mV (Fig. 2.7A & B), which is very close to that of XE991. Unlike XE991, linopirdine appreciably inhibited Kv7.2 current at -70 mV, 16 ± 1.8% (n = 6) inhibition with 55-second incubation (Fig. 2.7A–C). Inhibition at -70 mV was

further facilitated by 10 μM retigabine to 81.4 ± 3.4% inhibition (n = 6, P < 0.0001). For an accurate comparison of linopirdine and XE991 at -70 mV we used the same 25 second treatment that was used for XE991 in Fig. 2.1C. We confirmed that at -70 mV 30 μM linopirdine inhibition of Kv7.2 current was significantly larger (8.1 ± 1.9%, P < 0.05, n=6) than 10 μM XE991 (-0.8 ± 2.1%, n = 9, Fig. 2.1B), which indicates that linopirdine is less strict for its voltage-dependent inhibition.

The differences from XE991 became apparent in washout experiments. When linopirdine-treated CHO cells were washed at a holding potential of -70 mV, Kv7.2 currents showed 24.2 ± 4% recovery after 10 minutes (n = 6) (Fig. 2.7D & E), comparable to that of XE991. However, when cells were held at -30 mV, Kv7.2 currents showed almost full recovery after 10 minute wash (93.4 ± 4.2%, n = 5, Fig. 6D & E). Similar recovery profile was observed with Kv7.2/3 heteromeric channels (Fig. 2.7F). These results suggest that the linopirdine binding site is reversibly accessible when Kv7.2 channel is held above the activation potential.

We then assessed binding kinetics of linopirdine interaction. Following the same procedure as with XE991 in Fig. 2.4, we measured the time course of current inhibition induced by 30 μM linopirdine at various potentials (Fig. 2.8). Relative current during a 20 second depolarization step was compared with or without linopirdine and wash-in tau was compared between potentials (Fig. 2.8A-C). As with XE991, rate of linopirdine inhibition was increased at more depolarized potentials (Fig. 2.8C). In contrast, washout experiments indicate that the degree of channel activation facilitates the rate of washout for linopirdine as expected from results shown in Fig. 6 (Fig. 2.8D & E, P = 0.014, n = 5).

Quantitative model for XE991 and linopirdine.

We have demonstrated that inhibition kinetics of XE991 and linopirdine were closely related with the activation state of Kv7.2 channel. A common mechanism of state-dependent ion channel inhibitors is open channel inhibition. Therefore, we first assessed this mechanism. If XE991 and linopirdine interact with the channel at the open state then wash-in and washout time constants should show close correlation with channel activation. Namely, if inhibitors indeed interact only with open channels, then the rate of association at the half-activation potential for Kv7.2 channel (-21 mV, Fig. 2.9) should be nearly twice that of the rate constant at maximal activation. As equation 1 predicts, time constants are proportional to the reciprocal of the rate constant. Thus, we plotted normalized wash-in time constants to reciprocals of the activation curve (Ch_a^{-1}, Fig. 2.9B). To our surprise, neither wash-in nor washout time constants overlapped with Ch_a^{-1} (Fig. 2.9B & C). Instead, best-fits of relative time constants were close to one-fourth power of the activation curve ($Ch_a^{1/4}$), which suggests binding interactions are related to activation of a single subunit (Fig. 2.9 B & C, orange traces, best-fit powers for wash-in were 0.19 ± 0.06 for linopirdine, 0.26 ± 0.03 for XE991, and 0.36 ± 0.006 for linopirdine washout). We excluded washout of XE991 from this analysis since it did not show voltage-dependence as described above. In order to focus on activation of a single subunit in a tetrameric channel, we re-fitted Kv7.2 activation results with the fourth power Boltzmann equation:

$$Y = (1+\exp((V_{1/2}-x)/k))^{-4} \quad (2)$$

where x is the membrane potential, $V_{1/2}$ is the half activation potential of a single subunit, and k is the slope factor. Best-fit curve is shown as purple curve in Fig. 2.9A (Sub_a^4), and red curve shows a derived activation curve for a single subunit (Sub_a). Predicted single subunit activation curves were also in good agreement with the interaction kinetics of XE991 and linopirdine (Fig. 2.9B & C, red curve). This analysis suggests that XE991 and linopirdine bind to an activated subunit rather than open channels. Indeed, when relationships between half-inhibition potentials of XE991 and half-activation potentials of Kv7.2 channel by retigabine and channel mutant Kv7.2(R214D), shown in Fig. 2.3D, were recalculated against half-activation potentials of a single subunit, paired $V_{1/2}$ values were nearly identical (Figure 2.10).

Discussion

It has been previously reported that efficacy of linopirdine and XE991 is voltage-dependent[16]. We confirmed similar voltage-dependent inhibition by these inhibitors. On the other hand, we also found that altering voltage-dependency of Kv7.2 channels changed the half-inhibition potential of these inhibitors. Namely, shifts in half-inhibition potential corresponded with equivalent shifts in half-activation voltage by retigabine or Kv7.2(R214D), which suggests that such change in efficacy is derived from conformational changes of Kv7.2 channel subunits, rather than from voltage differences across the plasma membrane. Hence, our results suggest that these inhibitors detect state-changes of Kv7 channel subunits.

The most common class of state-dependent ion channel inhibitor is open channel inhibitors. Therefore, we first suspected this mechanism. In fact, transient channel activation in the presence of inhibitors, as we demonstrated in Fig. 2.4 & 2.8, is a signature profile for open channel inhibition[32]. However, our interaction kinetics did not match with open channel inhibition (Fig. 2.9). Rather, it is well described by binding to a single activated subunit (Fig. 2.9B & C).

If these inhibitors bind a single activated subunit, how many molecules can bind to each Kv7 channel? Since Kv channels are composed of four alpha subunits, each subunit may bind a single inhibitor molecule. However, our XE991 (Fig. 2.4E) and linopirdine (Fig. 2.7E & 2.8D) washout experiments showed a single exponential recovery, rather than a hyperbolic recovery reported for multiple inhibitor binding[33,34]. Therefore, our results are consistent with a single molecule binding to each Kv7.2 channel.

Inhibition by binding an activated subunit also explains why these inhibitors have a half-inhibition potential for these inhibitors at approximately -50 mV, which is very close to the half-activation potential of a single subunit (Fig. 2.9 & 2.10). However, this model does not sufficiently explain why XE991 is ineffective at membrane potentials below -70 mV or why these two inhibitors have a very steep voltage-dependent efficacy around -50 mV (Fig. 2.1D & E). The slope of single subunit activation curve is much milder than that of the channel activation curve (Fig. 2.9A). Therefore, if binding to a single activated subunit is the only mechanism of inhibition, we should observe Kv7 current inhibition at potentials as negative as -70 or -80 mV. One possible explanation for this mystery is that these inhibitors favor distinct active states. On the other hand, single channel recording have demonstrated that linopirdine inhibits both high and low conducting states of Kv7.2/3 channels[35]. Alternatively, since these inhibitors are molecules with one-axis symmetry, these inhibitors might have dual functions: one-side functions as a binding domain, and the other side functions as an open pore inhibitor. However, further structure-function analyses would be required to elucidate this mystery.

Although, results from linopirdine mirror the majority of findings from XE991, we did identify differences in interaction characteristics, beyond their potencies. A key difference is that inhibition by linopirdine is reversible at depolarized potentials. Notably, linopirdine-treated Kv7.2 current could only recover when membrane potential was depolarized (Fig. 2.7 & 2.8). This, together with our findings from voltage-dependent wash-in kinetics, suggests that linopirdine can reversibly interact with Kv7.2 channel only when subunits are at the active conformation, but is trapped within Kv7.2 channels

when subunits are in the resting conformation after binding. On the other hand, results from our XE991 washout study were puzzling. Unlike linopirdine, we did not observe voltage-dependent recovery for this compound. Considering that 1) XE991 has slow binding compared to that of linopirdine, which is evident from wash-in experiments (Fig. 2.4 vs. 2.8) and 2) since XE991 is a much more potent inhibitor than linopirdine, dissociation of XE991 would be considerably slower than that of linopirdine. It is likely that naïve channel translocation to the cell surface overwhelms slow recovery of Kv7 channel from XE991 mediated inhibition. However, we cannot rule out the possibility that XE991 binding is irreversible.

A deliberative from this study is that XE991 is often not efficacious for cells in physiological conditions, unless they are depolarized. Therefore, when designing experiments using these compounds additional manipulation would be necessary for effective inhibition by XE991 and linopirdine. For animal experiments, to inhibit Kv7 channels in silent or scarcely firing neurons, co-administration of XE991 and retigabine would be effective even at resting membrane potential. For cultured neurons, holding at depolarized potentials while voltage clapped or co-administration of XE991 and retigabine or high potassium would effectively inhibit Kv7 current during experiments. In the proceeding chapters, the characteristics of XE991 will be important for selectively inhibiting rapidly spiking neurons that contribute to ictal activities during seizure without increasing excitability in other areas of the cortex. Indeed, activated subunit inhibition and slow binding kinetics of these inhibitors may explain why these compounds are well tolerated in animals[7,8,10,11] without causing lethal seizures, as seen in KCNQ2 gene knockout mice[12,13]. This model of XE991 and linopirdine inhibition would preferentially

target highly active neurons, exaggerating their neuronal activities, which may underlie the cognitive enhancing action of these compounds.

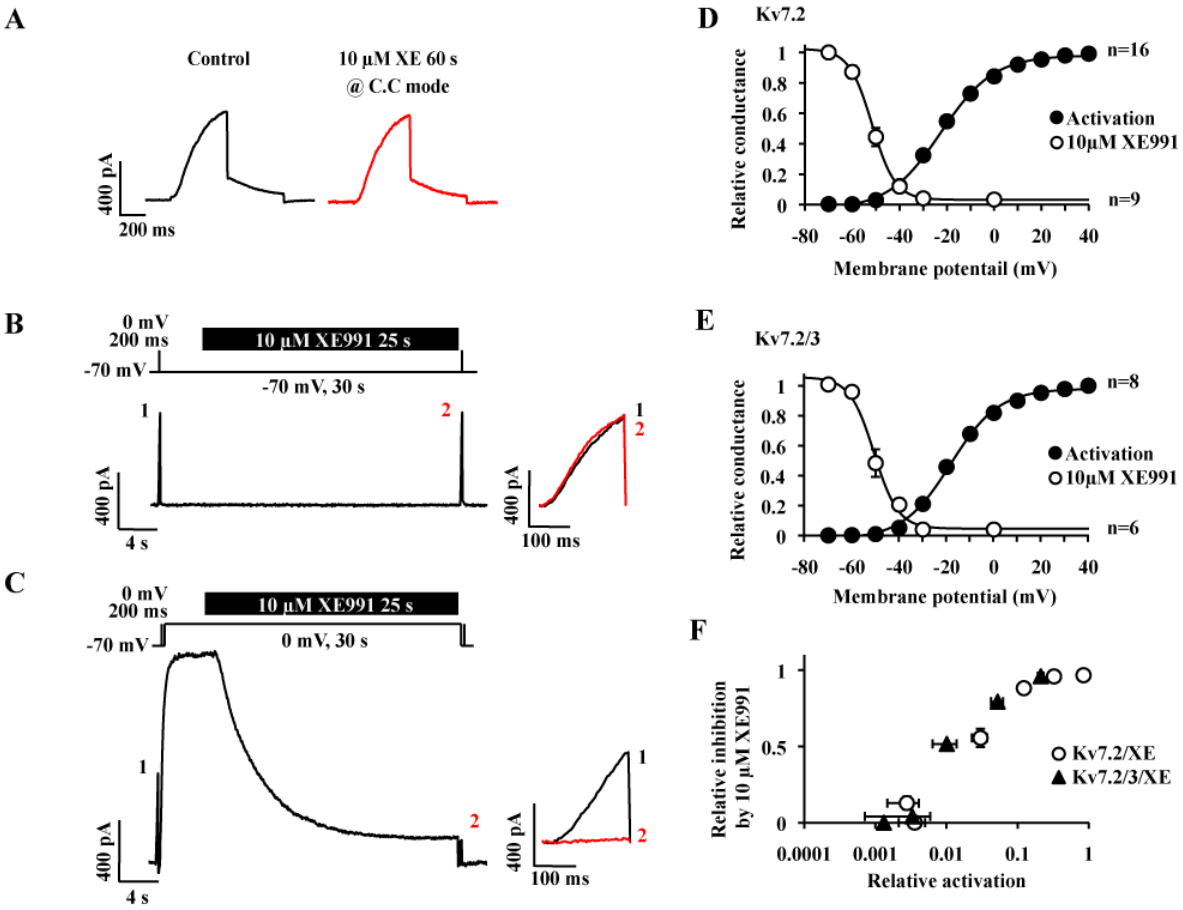

Figure 2.1. XE991 inhibits homomeric Kv7.2 and heteromeric Kv7.2/3 channels only in conditions where the channel is activated.

A. Representative current traces showing 10 µM XE991 did not inhibit Kv7.2 current when exposed at resting membrane potential. CHO cells were first voltage clamped at -70 mV, given a test potential of 0 mV for 500 ms, followed by -60 mV for 500 ms, then current clamped (I = 0 pA) while perfusing 10 µM XE991 for 60 seconds, and then voltage clamped at -70 mV for another step depolarization. **B.** Voltage protocol and representative traces showing exposure to 10 µM XE991 at -70 mV for 25 seconds, indicated as black box, was ineffective on Kv7.2 current. Expanded traces show 200 ms test potential to 0 mV from indicated time points (1 and 2). **C.** Voltage protocol and representative traces showing 10 µM XE991 completely blocked Kv7.2 current when exposed to XE991 at 0 mV for 25 seconds, indicated as black box. Expanded current traces also shown. **D.** Summary graph showing voltage–XE991 inhibition relationships and activation curve for Kv7.2 homomeric channels. **E.** Voltage–XE991 inhibition relationships and activation curve for Kv7.2/3 heteromeric channels. **F.** Results shown in panels C and D re-plotted for relative inhibition by XE991 vs. relative activation of channels. Inhibition of XE991 is closely correlated with activation of Kv7 channels in a semi-log plot (Kv7.2: r = 0.94, Kv7.2/3: r = 0.90). Data shown as average values ± SEM.

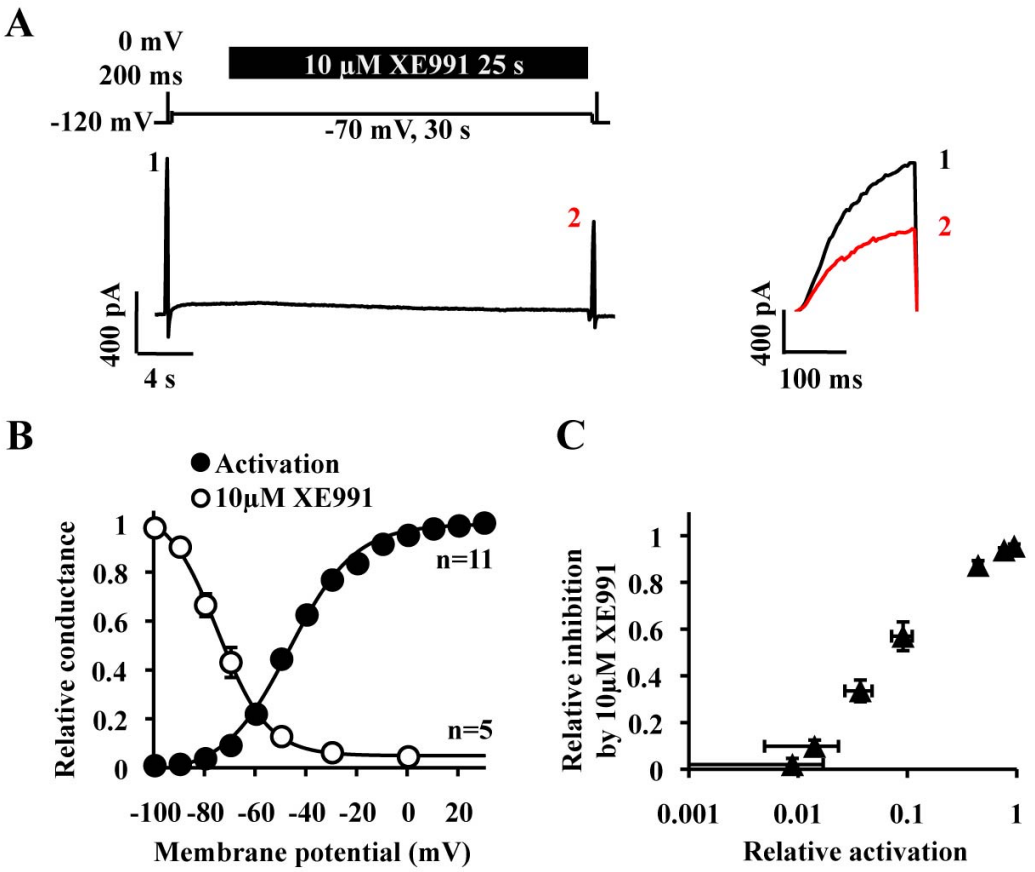

Figure 2.2. Retigabine sensitized Kv7.2 to XE991 at more negative potentials.

A. Voltage protocol and representative traces showing when cells were pretreated with 10 µM retigabine, 25 second treatment with 10 µM XE991 (black box) inhibited Kv7.2 current at a holding potential of -70 mV. **B.** Voltage–XE991 inhibition relationships and activation curve for Kv7.2 channels pretreated with 10 µM retigabine. **C.** Activation–XE991 inhibition relationships for Kv7.2 channel from results shown in B. Error bars show SEM.

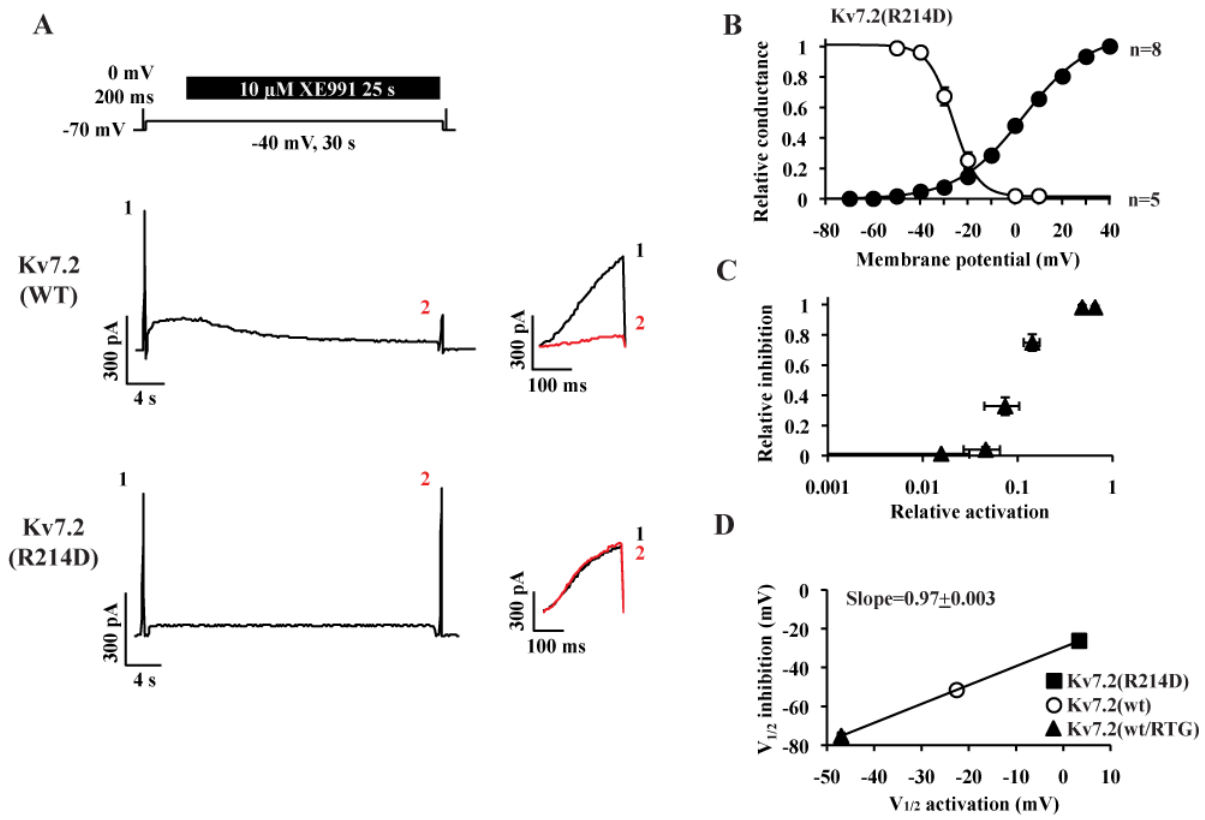

Figure 2.3. Kv7.2 mutant (R214D) shifted voltage dependence of activation and XE991 inhibition to more positive potentials.

A. Voltage protocol and representative traces showing that 25 second treatment with 10 µM XE991 (black box) inhibited WT Kv7.2 current at a holding potential of -40 mV while Kv7.2(R214D) mutant channel had minimal inhibition at same holding potential **B.** Voltage–XE991 inhibition relationships and activation curve for Kv7.2(R214D) channels. **C.** Activation–XE991 inhibition relationships for Kv7.2(R214D) channel from results shown in B. **D.** Pooled results for $V_{1/2}$ inhibition and $V_{1/2}$ activation potentials of Kv7.2, retigabine treated Kv7.2 and Kv7.2(R214D) channel. Slope of regression line is also shown. Error bars show SEM.

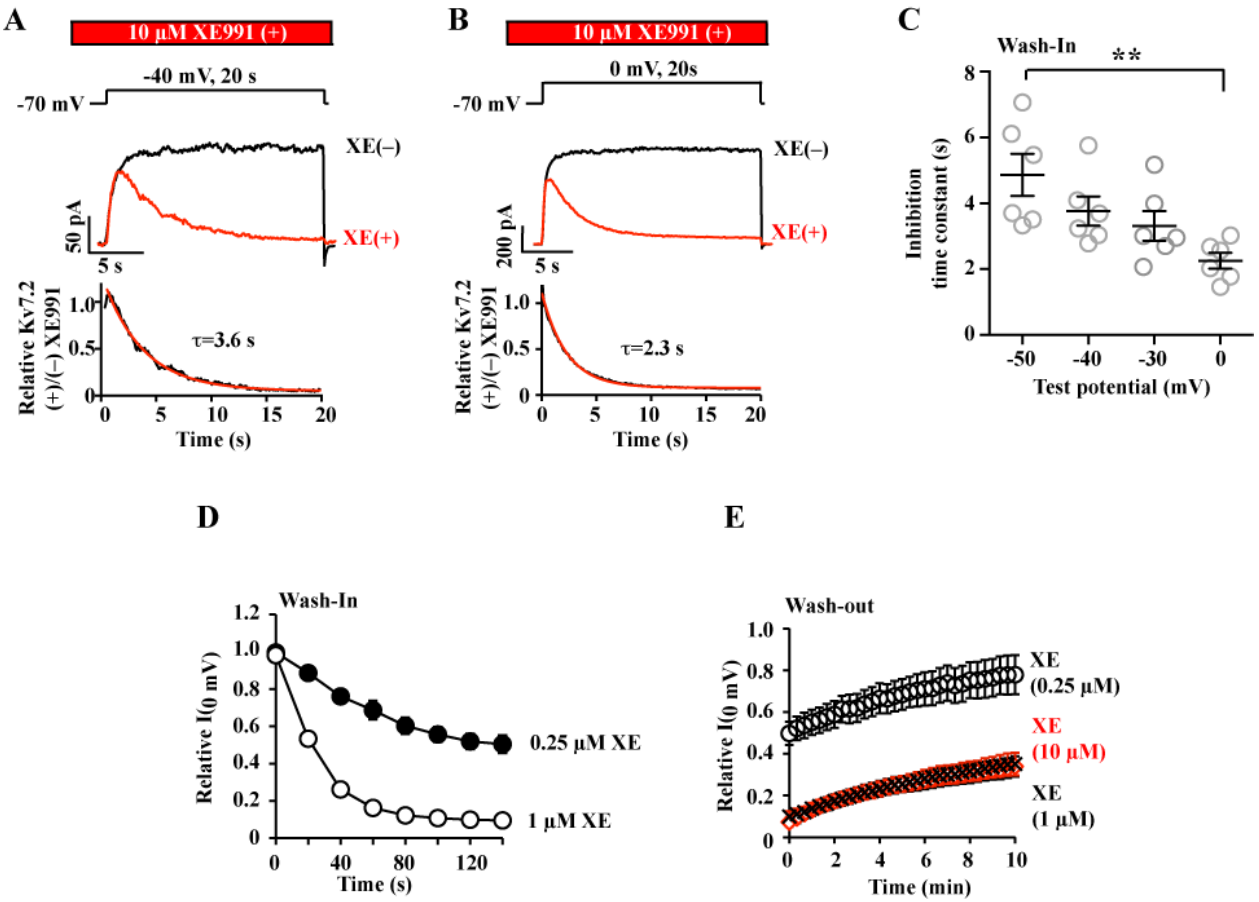

Figure 2.4. XE991 interaction kinetics with Kv7.2 channels and relationships to membrane potential.

A. Voltage protocol and representative Kv7.2 current traces from 20 second test potential to -40 mV during absence, XE(–), and presence, XE(+), of 10 µM XE991 (red box). Note that in the presence of XE991, the initial activation phase of Kv7.2 current is unaffected. Relative Kv7.2 current ratio of XE(+)/XE(–) showing that current inhibition followed a single exponential decay (lower graph, red line) with the indicated time constant. **B.** Same as A with voltage step to 0 mV. **C.** Inhibition time constants of Kv7.2 current from wash-in experiments at indicated holding potentials measured as shown in A and B. ** <0.01, non-parametric ANOVA (Kruskal-Wallis test) followed by Mann–Whitney test, n = 6. **D.** Kv7.2 current inhibition time courses at lower doses of XE991 as indicated. XE991 was applied at T = 0. Cells were held at 0 mV and current was measured by 500 ms repolarizing potentials to -60 mV in 20 second intervals, n = 5-6. **E.** Current recovery by washout from indicated XE991 concentrations using same voltage protocol as in D. T = 0 indicates start of washout, n = 5-6. Error bars show SEM.

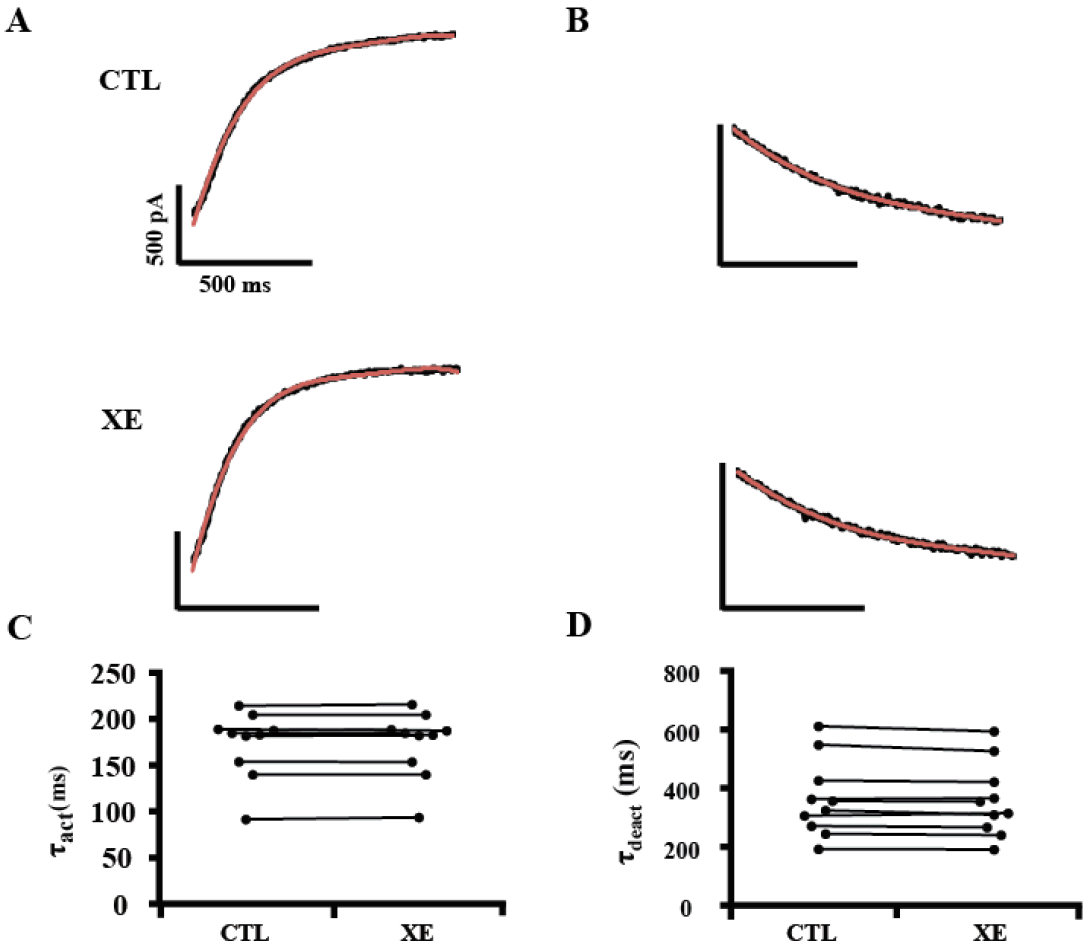

Figure 2.5. XE991 does not interfere with Kv7.2 channel kinetics.

A. Representative paired traces for activation of Kv7.2 current with a step depolarization to 0 mV for 1 s, subsequent depolarization from same cell was measured in presence of 10 μM XE991. **B.** Representative paired traces for tail currents of Kv7.2 current from a 1 s step repolarization from 0 mV to -50 mV for 1 s, without and subsequently with 10 μM XE991. **C.** Pooled results for activation tau from single exponential line of best fit before and after XE991. **D.** Pooled results for deactivation tau from single exponential line of best fit before and after XE991 treatment. No significant difference. Red line represents best-fit single exponential function. Error bars show SEM.

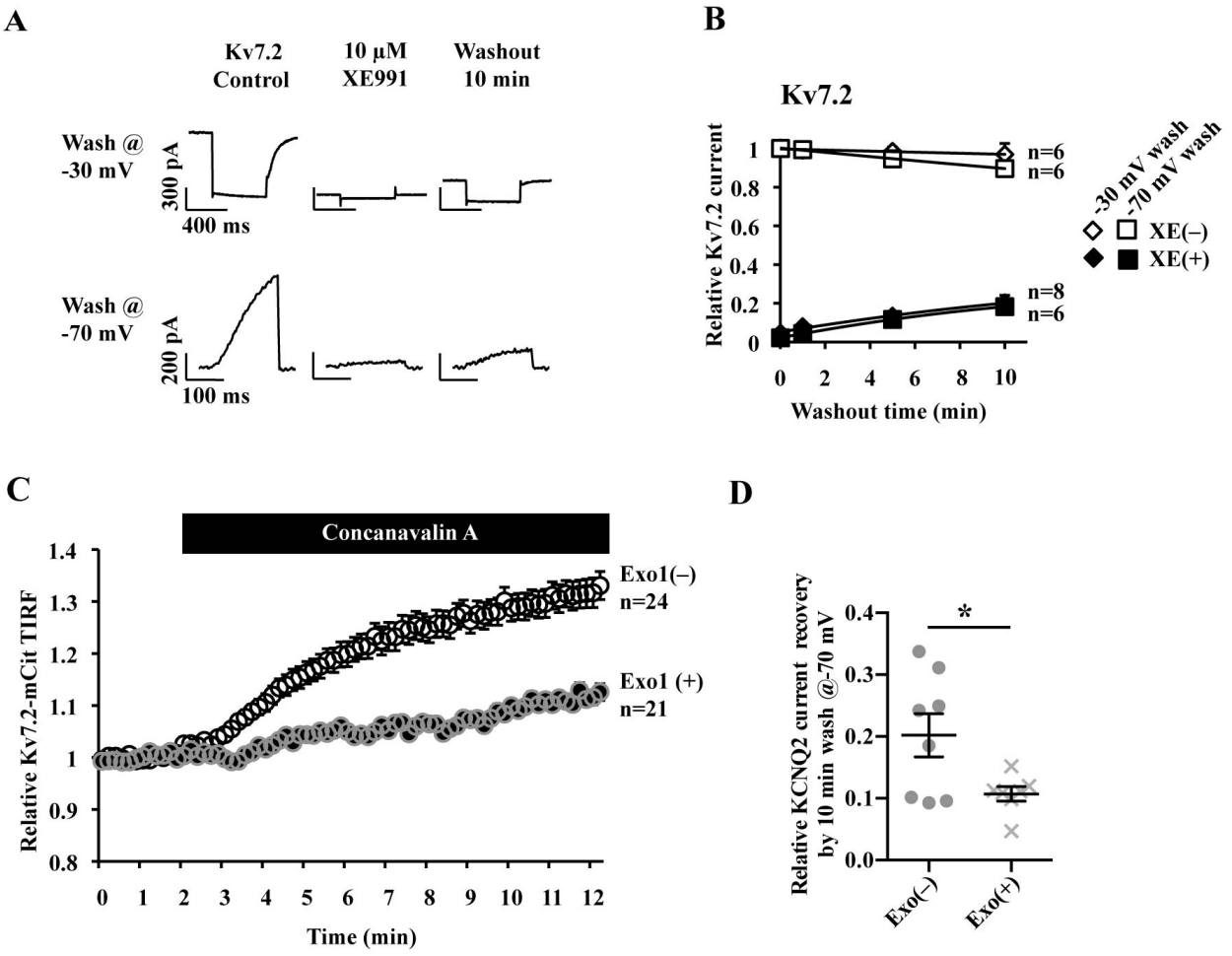

Figure 2.6. Kv7.2 current recovery from XE991 washout is extremely slow.

A. Representative Kv7.2 current traces showing control, 10 µM XE991 inhibited, and after 10 minute washout at indicated holding potentials. For washout at -30 mV, current was measured by 1-second test potential to -60 mV from a holding potential of -30 mV. For washout at -70 mV, cells were depolarized to 0 mV for 200 ms from a holding potential of -70 mV. **B.** Summary showing slow and limited recovery of Kv7.2 current after washout in cells held at -30 mV or -70 mV. **C.** TIRF experiments showing 100 µM Exo1 suppressed constitutive exocytosis of mCit tagged Kv7.2 (KCNQ2-mCit) by 50 µg/mL concanavalin A (black box) applied at t = 2 minutes. **D.** 100 µM Exo1 suppressed recovery of Kv7.2 current from XE991 during 10-minute wash at a holding potential of -70 mV. * < 0.05 Student's t-test with Welch's correction, n = 8. Data shown as average values ± SEM.

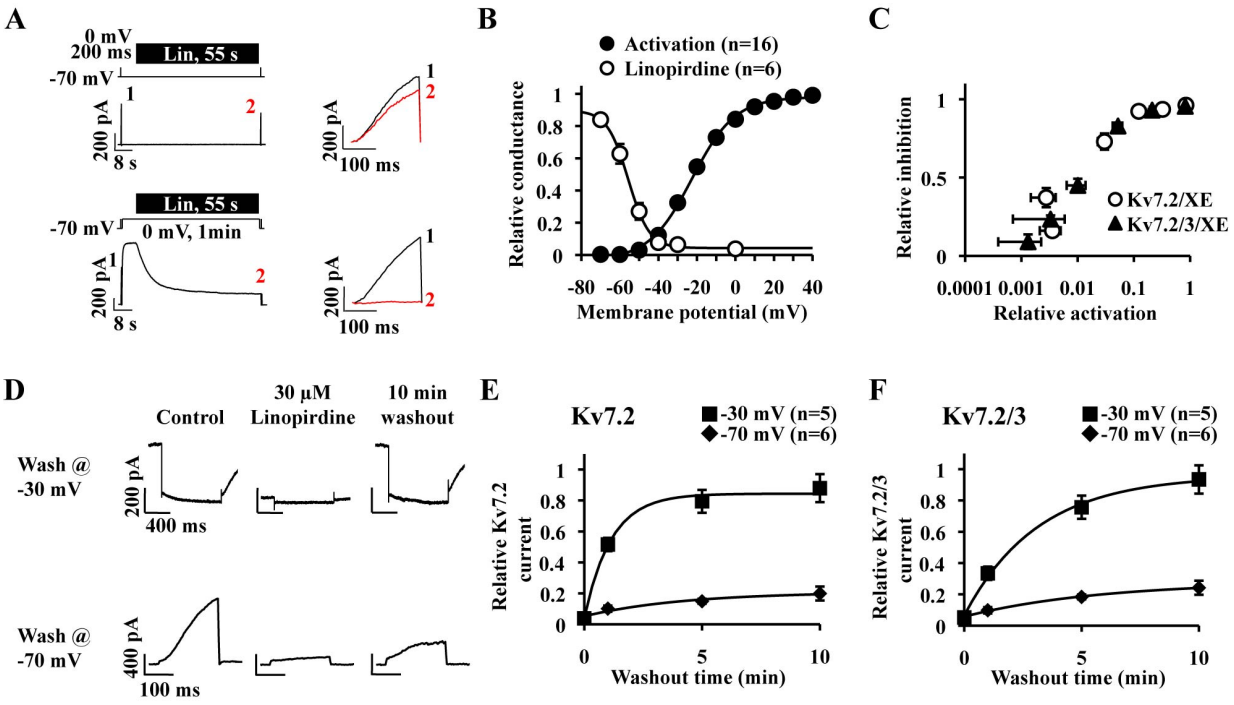

Figure 2.7. Linopirdine replicated most effects from XE991 inhibition.

A. Voltage protocol and representative Kv7.2 current traces showing voltage-dependent inhibition of 30 µM linopirdine (black box). Right traces show expanded currents from indicated time points 1 and 2. **B.** Pooled results for voltage-inhibition relationships of linopirdine and activation curve for Kv7.2 channels as measured in A. **C.** Results shown in B re-plotted as relative activation against relative inhibition of Kv7.2 by linopirdine. Results of Kv7.2/3 are also included. **D.** Representative current traces showing Kv7.2 current recovery after washout of 30 µM linopirdine from cells held at -30 mV or -70 mV. For -30 mV holding potential during washout, Kv7.2 currents were monitored by 1-second step hyperpolarizations to -60 mV. For -70 mV holding potential, cells received a 200-ms step depolarization to 0 mV. **E.** Summary showing almost full recovery of Kv7.2 current when cells were washed at -30 mV, while showing slow and limited recovery at -70 mV. **F.** Similar full recovery was observed with Kv7.2/3 heteromeric channels. Error bars show SEM.

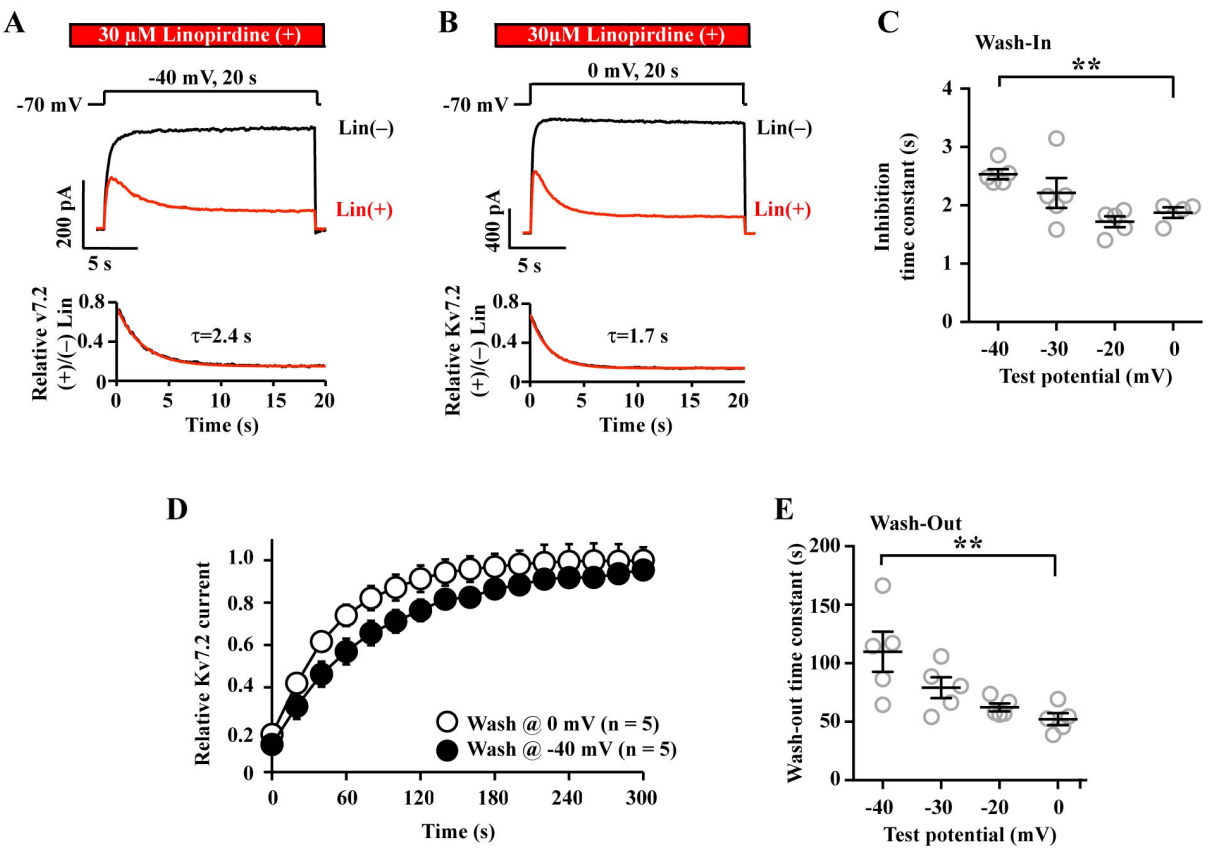

Figure 2.8. Linopirdine interaction kinetics with Kv7.2 channels in relation to membrane potential.

A. Voltage protocol and representative Kv7.2 current traces with a test potential to -40 mV during absence, Lin(–), and presence, Lin(+), of 30 µM linopirdine (red box). Relative Kv7.2 current ratio Lin(+)/Lin(–) showing that current inhibition followed a single exponential decay with the indicated time constant (bottom graph, red line). **B.** Same as A with a test potential to 0 mV. **C.** Inhibition time constants of wash-in from Kv7.2 current measured as shown in A and B. Like with XE991, time constants decreased with depolarizing potentials. ** <0.01, non-parametric ANOVA (Kruskal-Wallis test) followed by Mann–Whitney test, n = 5. **D.** Current recovery during washout after steady-state inhibition with 30 µM linopirdine at indicated holding potentials. T = 0 indicates beginning of washout. Current was determined from 500 ms repolarizing potentials to -60 mV at 20 second intervals from indicated holding potentials. **E.** Current recovery time constants from experiments in D. ** <0.01, non-parametric ANOVA (Kruskal-Wallis test) followed by Mann–Whitney test, n = 5. Error bars show SEM.

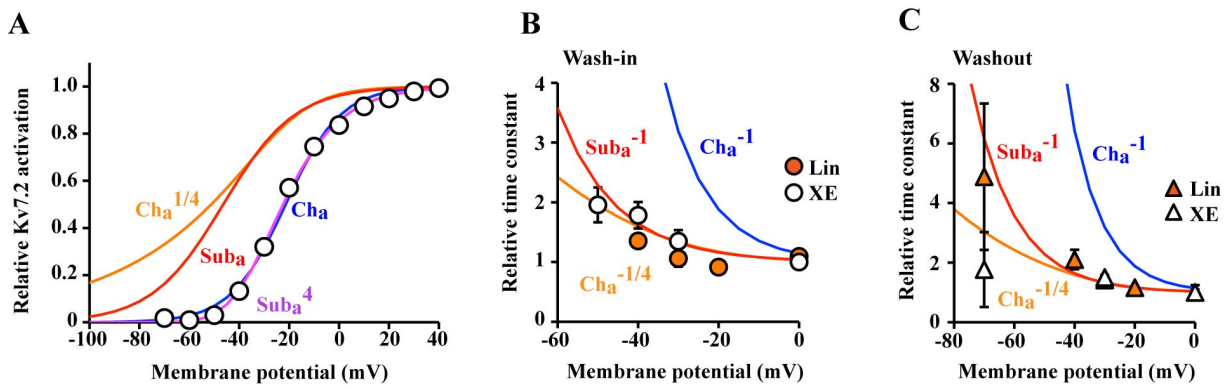

Figure 2.9. XE991 and linopirdine interaction with Kv7.2 relates with activation of single subunit.

A. Activation curve for Kv7.2 channel (blue curve, Ch_a), and one-quarter power of its Boltzmann function (orange curve, $Ch_a^{1/4}$). Activation curve for a single subunit (red curve, Sub_a) and its fourth power function (Sub_a^4) are also shown (see text for details). **B.** Relative inhibition time constants calculated from Fig. 4C (XE991, open circle) and Fig. 7C (linopirdine, orange circle) normalized to those from 0 mV plotted as a function of voltage. The reciprocal of the activation curves of Ch_a, $Ch_a^{1/4}$ and Sub_a shown in panel A are also shown. **C.** Relative recovery time constants calculated from experiments shown in Fig. 4 & 5B (XE991, open triangle) and Fig. 6E & 7E (linopirdine, orange triangle), overlaid with the reciprocal of the activation curves of Ch_a, $Ch_a^{1/4}$ and Sub_a. Error bars show SEM.

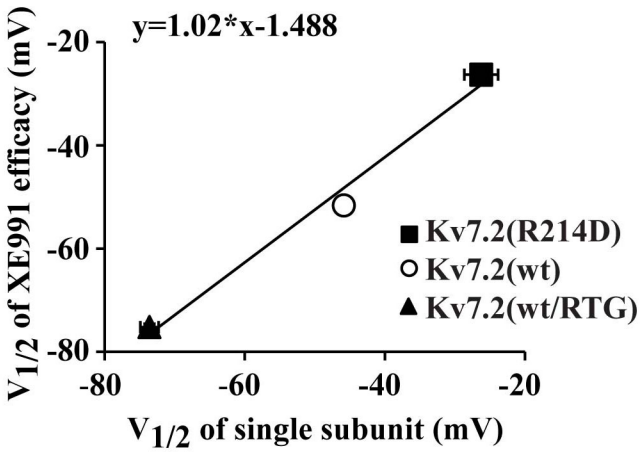

Figure 2.10. Relationships between $V_{1/2}$ of XE991 efficacy and single subunit activation.

Pooled results from Fig. 3D reevaluated for single subunit activation. $V_{1/2}$ of subunit activation showed almost complete match to that of XE efficacy in al three conditions. Best-fit linear regression equation is shown. Error bars show SEM.

References

1 Jentsch, T. J. Neuronal KCNQ potassium channels: physiology and role in disease. *Nat Rev Neurosci* **1**, 21-30, doi:10.1038/35036198 (2000).

2 Delmas, P. & Brown, D. A. Pathways modulating neural KCNQ/M (Kv7) potassium channels. *Nat Rev Neurosci* **6**, 850-862, doi:10.1038/nrn1785 (2005).

3 Greene, D. L. & Hoshi, N. Modulation of Kv7 channels and excitability in the brain. *Cellular and molecular life sciences : CMLS*, doi:10.1007/s00018-016-2359-y (2016).

4 Fontana, D. J., Inouye, G. T. & Johnson, R. M. Linopirdine (DuP 996) improves performance in several tests of learning and memory by modulation of cholinergic neurotransmission. *Pharmacology, biochemistry, and behavior* **49**, 1075-1082 (1994).

5 Rockwood, K. *et al.* A randomized, controlled trial of linopirdine in the treatment of Alzheimer's disease. *The Canadian journal of neurological sciences. Le journal canadien des sciences neurologiques* **24**, 140-145 (1997).

6 Zaczek, R. *et al.* Two new potent neurotransmitter release enhancers, 10,10-bis(4-pyridinylmethyl)-9(10H)-anthracenone and 10,10-bis(2-fluoro-4-pyridinylmethyl)-9(10H)-anthracenone: comparison to linopirdine. *J Pharmacol Exp Ther* **285**, 724-730 (1998).

7 Vetter, I. *et al.* Amplified cold transduction in native nociceptors by M-channel inhibition. *J Neurosci* **33**, 16627-16641, doi:10.1523/JNEUROSCI.1473-13.2013 (2013).

8 Young, M. B. & Thomas, S. A. M1-muscarinic receptors promote fear memory consolidation via phospholipase C and the M-current. *J Neurosci* **34**, 1570-1578, doi:10.1523/JNEUROSCI.1040-13.2014 (2014).

9 Martinello, K. *et al.* Cholinergic afferent stimulation induces axonal function plasticity in adult hippocampal granule cells. *Neuron* **85**, 346-363, doi:10.1016/j.neuron.2014.12.030 (2015).

10 Mani, B. K. *et al.* Vascular KCNQ (Kv7) potassium channels as common signaling intermediates and therapeutic targets in cerebral vasospasm. *Journal of cardiovascular pharmacology* **61**, 51-62, doi:10.1097/FJC.0b013e3182771708 (2013).

11 Kay, H. Y., Greene, D. L., Kang, S., Kosenko, A. & Hoshi, N. M-current preservation contributes to anticonvulsant effects of valproic acid. *J Clin Invest* **125**, 3904-3914, doi:10.1172/JCI79727 (2015).

12 Watanabe, H. *et al.* Disruption of the epilepsy KCNQ2 gene results in neural hyperexcitability. *J Neurochem* **75**, 28-33 (2000).

13 Soh, H., Pant, R., LoTurco, J. J. & Tzingounis, A. V. Conditional deletions of epilepsy-associated KCNQ2 and KCNQ3 channels from cerebral cortex cause differential effects on neuronal excitability. *J Neurosci* **34**, 5311-5321, doi:10.1523/JNEUROSCI.3919-13.2014 (2014).

14 Pieniaszek, H. J., Jr. *et al.* Single-dose pharmacokinetics, safety, and tolerance of linopirdine (DuP 996) in healthy young adults and elderly volunteers. *Journal of clinical pharmacology* **35**, 22-30 (1995).

15 Yue, C. & Yaari, Y. KCNQ/M channels control spike afterdepolarization and burst generation in hippocampal neurons. *J Neurosci* **24**, 4614-4624, doi:10.1523/JNEUROSCI.0765-04.2004 (2004).

16 Romero, M., Reboreda, A., Sanchez, E. & Lamas, J. A. Newly developed blockers of the M-current do not reduce spike frequency adaptation in cultured mouse sympathetic neurons. *Eur J Neurosci* **19**, 2693-2702, doi:10.1111/j.1460-9568.2004.03363.x (2004).

17 Hoshi, N. *et al.* AKAP150 signaling complex promotes suppression of the M-current by muscarinic agonists. *Nat Neurosci* **6**, 564-571, doi:10.1038/nn1062 (2003).

18 Kosenko, A. *et al.* Coordinated signal integration at the M-type potassium channel upon muscarinic stimulation. *EMBO J* **31**, 3147-3156, doi:10.1038/emboj.2012.156 (2012).

19 Jiang, L. *et al.* Activation of m1 muscarinic acetylcholine receptor induces surface transport of KCNQ channels through a CRMP-2-mediated pathway. *J Cell Sci* **128**, 4235-4245, doi:10.1242/jcs.175547 (2015).

20 Chen, X., Li, W., Hiett, S. C. & Obukhov, A. G. Novel Roles for Kv7 Channels in Shaping Histamine-Induced Contractions and Bradykinin-Dependent Relaxations in Pig Coronary Arteries. *PLoS One* **11**, e0148569, doi:10.1371/journal.pone.0148569 (2016).

21 Hedegaard, E. R. *et al.* Inhibition of KV7 Channels Protects the Rat Heart against Myocardial Ischemia and Reperfusion Injury. *J Pharmacol Exp Ther* **357**, 94-102, doi:10.1124/jpet.115.230409 (2016).

22 Namkung, W. *et al.* In situ measurement of airway surface liquid [K+] using a ratioable K+-sensitive fluorescent dye. *J Biol Chem* **284**, 15916-15926, doi:10.1074/jbc.M808021200 (2009).

23 Wladyka, C. L. & Kunze, D. L. KCNQ/M-currents contribute to the resting membrane potential in rat visceral sensory neurons. *J Physiol* **575**, 175-189, doi:10.1113/jphysiol.2006.113308 (2006).

24 Hu, H. N. *et al.* Discovery of a retigabine derivative that inhibits KCNQ2 potassium channels. *Acta Pharmacol Sin* **34**, 1359-1366, doi:10.1038/aps.2013.79 (2013).

25 Jeong, I., Choi, B. H. & Hahn, S. J. Rosiglitazone inhibits Kv4.3 potassium channels by open-channel block and acceleration of closed-state inactivation. *Br J Pharmacol* **163**, 510-520, doi:10.1111/j.1476-5381.2011.01210.x (2011).

26 Hille, B. *Ion channels of excitable membranes*. (Sinauer Associates, Inc., 2001).

27 Goldstein, S. A. & Miller, C. Mechanism of charybdotoxin block of a voltage-gated K+ channel. *Biophys J* **65**, 1613-1619, doi:10.1016/S0006-3495(93)81200-1 (1993).

28 Wang, H. S. *et al.* KCNQ2 and KCNQ3 potassium channel subunits: molecular correlates of the M-channel. *Science* **282**, 1890-1893 (1998).

29 Rennie, K. J., Weng, T. & Correia, M. J. Effects of KCNQ channel blockers on K(+) currents in vestibular hair cells. *Am J Physiol Cell Physiol* **280**, C473-480 (2001).

30 Zaika, O. *et al.* Angiotensin II regulates neuronal excitability via phosphatidylinositol 4,5-bisphosphate-dependent modulation of Kv7 (M-type) K+ channels. *J Physiol* **575**, 49-67, doi:10.1113/jphysiol.2006.114074 (2006).

31 Brueggemann, L. I. *et al.* Kv7 potassium channels in airway smooth muscle cells: signal transduction intermediates and pharmacological targets for bronchodilator therapy. *Am J Physiol Lung Cell Mol Physiol* **302**, L120-132, doi:10.1152/ajplung.00194.2011 (2012).

32 Zagotta, W. N., Hoshi, T. & Aldrich, R. W. Restoration of inactivation in mutants of Shaker potassium channels by a peptide derived from ShB. *Science* **250**, 568-571 (1990).

33 Dorschner, H., Brekardin, E., Uhde, I., Schwanstecher, C. & Schwanstecher, M. Stoichiometry of sulfonylurea-induced ATP-sensitive potassium channel closure. *Molecular pharmacology* **55**, 1060-1066 (1999).

34 Russ, U. *et al.* Incomplete dissociation of glibenclamide from wild-type and mutant pancreatic K ATP channels limits their recovery from inhibition. *Br J Pharmacol* **156**, 354-361, doi:10.1111/j.1476-5381.2008.00005.x (2009).

35 Lamas, J. A., Selyanko, A. A. & Brown, D. A. Effects of a cognition-enhancer, linopirdine (DuP 996), on M-type potassium currents (IK(M)) and some other voltage- and ligand-gated membrane currents in rat sympathetic neurons. *Eur J Neurosci* **9**, 605-616 (1997).

Chapter Three

M-current preservation contributes to anticonvulsant effects of valproic acid

Introduction

Valproic acid (VPA) is used to treat epilepsy and bipolar disorder[1]. VPA is known to have multiple pharmacological actions such as prolongation of sodium channel inactivation[2], elevation of GABA content in the brain[3] and inhibition of HDAC activity[4]. However, underlying mechanisms for the anticonvulsant effect of VPA are still unclear.

The M-current is a low threshold non-inactivating voltage-gated potassium current widely expressed throughout the cortex[5,6]. Additionally, a recent study demonstrated that the Kv7.2/KCNQ2 is the dominant subunit in pyramidal neurons in the hippocampus[7], a focal point in temporal lobe epilepsy (TLE)[8,9]. Various neurotransmitters that activate Gq-coupled receptors, suppress the M-current and induce neuronal hyperexcitability. Accordingly, loss-of-function mutations in *KCNQ* genes are known to cause epilepsy and encephalopathy[5,10], and M-channel openers are used to treat epilepsy[11,12].

Intensive studies have been conducted to elucidate the molecular pathway mediating M-current suppression induced by neurotransmitters, especially by the muscarinic action of acetylcholine[5,6,13,14]. These studies revealed that multiple signaling pathways converge at the M-channel complex[14-17], further detailed in chapter 1. Specific

to this chapter is the mechanism mediated by PKC phosphorylation of KCNQ2 subunit, which reduces PIP2 efficacy. Upon activation of m1 muscarinic receptor, PKC bound to the KCNQ2 subunit via A-kinase anchoring protein (AKAP79/150) phosphorylates the KCNQ2 subunit. Phosphorylation of KCNQ2 dissociates calmodulin, destabilizing KCNQ2-PIP2 interaction and leads to the shut down of M-channel activity[17].

AKAP79/150 (human AKAP79/rodent AKAP150) is a critical signaling scaffold protein for the M-channel, which tethers several signaling enzymes, facilitating local signaling events. AKAP79/150 is known to be important not only for the M-channel but also for glutamate receptors as well as other ion channels[16,19,20]. AKAP150 *(Akap5)* gene knock-out mice show impaired learning and resistance to pilocarpine-induced seizures[21]. In addition, recent studies have shown that palmitoylation of AKAP79/150 plays essential roles in cellular signaling[22,23]. Palmitoylation is a reversible post-translational modification, which predominantly adds palmitic acid to selective cysteine residues[24]. Palmitoylation is required for neural plasticity as it targets relevant proteins to lipid rafts, which often creates signaling hot spots[25]. Furthermore, changes in neuronal activities induce de-palmitoylation[23,26]. Therefore, palmitoylation is gaining greater attention due to its dynamic regulation during signaling events.

We demonstrate that VPA treatment disrupted muscarinic acetylcholine receptor-induced M-current suppression, preventing receptor-induced hyperexcitability in neurons. Consistently, pharmacological blockade of M-current with XE991 diminished the anticonvulsant effect of VPA, but not that of diazepam. We show that retigabine, an M-channel opener, had anticonvulsant effect only when administered before induction of seizure in control mice. However, in VPA treated mice, anticonvulsant effect of

retigabine was maintained even when administered after seizure induction. We determined that disruption of receptor-induced M-current suppression was caused by reduced palmitoylation of AKAP79/150 by VPA treatment. These findings suggest that M-current suppression plays a role in the pathology of seizures and that disruption of M-current suppression is an integral part of the anticonvulsant mechanism of non-acute VPA treatment.

Experimental Procedures

Antibodies.

Antibodies used for quantitative immunoblots were as follows: Anti-V5 epitope monoclonal antibody (Catalog R960; Life technologies), anti-flag M2 antibody, HA monoclonal antibody, HA rabbit polyclonal antibody (Catalogs F3165, H3663, H6908, respectively; Sigma-Aldrich), PSD-95 (Catalog 041066; Millipore), flotillin-1, fyn, GRIP1, EAAT2 (Catalogs 041066, 610821, 611318, 611654, respectively; BD Transduction Laboratories), c-FOS (Catalog PC38; Calbiochem), mouse monoclonal AKAP150 (Catlog sc-377055; Santa Cruz Biotechnology) and Cy3 labeled goat anti-rabbit secondary antibody (Catalog AP187C; Millipore). Rabbit polyclonal antibody for AKAP150 is a gift from Dr. John D. Scott (University of Washington, lot VO88) and has been described[16,20,21,27].

Expression plasmids.

The following expression plasmids used in this study have been described: KCNQ2 and its mutants[16,17], AKAP79 and AKAP150[20], PKCβII(Δ1-32)-V5[28] and cytCKAR[28,29]. The plasmid for CFP-PH was obtained from Dr. Tobias Meyer (Stanford University) via addgene. HA-m1 muscarinic acetylcholine receptor was obtained from Missouri S&T cDNA resource center. A myristoylation consensus sequence (MGQSLTT)[30] was added to the N terminus of AKAP150 by PCR to generate Myr-AKAP79(C36S/C129C) and Myr-AKAP150(C36S/C123S). All PCR derived constructs were verified by sequencing.

Cell culture and VPA pretreatment.

HEK293A (Life Technologies) cells were grown in Dulbecco's modified Eagle medium with 10% fetal bovine serum. CHO hm1[16] cells were grown in alpha modified Eagle medium with 5% fetal bovine serum and 500 μg/ml G418 sulfate. SCG neurons were isolated from 14 to 19 day-old rats and cultured as described previously[16,17,20]. Rat neonatal hippocampal culture was prepared as described[20]. VPA solution was prepared daily from powder and was added to the medium at 500 μM unless indicated otherwise. A half volume of cultured medium was exchanged daily with freshly prepared VPA, vigabatrin or phenytoin containing media, and maintained for 3 to 4 days before recordings. For CHO hm1 cells, overnight incubation was sufficient to see VPA effects.

Immunoprecipitation.

HEK293A cells cultured in 10 cm dishes were transiently transfected with LT1 transfection reagent (Mirus) with various expression plasmids. Cells were harvested 48 h after transfection and lysed in 500 μl HSE buffer (150 mM NaCl, 5 mM EDTA, 5 mM EGTA, 20 mM HEPES (pH 7.4), 1% Triton X-100 and complete protease inhibitor cocktail (Roche)). Supernatants were incubated with anti-flag antibody conjugated resin or antibody and protein G conjugated resin. Following overnight incubation at 4ºC, immunoprecipitates were washed in HSE buffer. Bound proteins were analyzed by SDS-PAGE and immunoblotting.

Electrophysiological measurements and live cell imaging.

Patch clamp recordings were performed at room temperature on isolated cells using an Axopatch 200B patch-clamp amplifier (Molecular Devices). Signals were sampled at 2 kHz, filtered at 1 kHz, and acquired using pClamp software (version 7, Molecular Devices). Whole-cell patch clamp technique was used for KCNQ2 current

recording[17]. Cells were perfused with a solution containing 144 mM NaCl, 5 mM KCl, 2 mM $CaCl_2$, 0.5 mM $MgCl_2$, 10 mM glucose, and 10 mM HEPES (pH7.4). Patch pipettes (2-4 MΩ) were filled with intracellular solution containing 135 mM potassium aspartate, 2 mM $MgCl_2$, 3 mM EGTA, 1 mM $CaCl_2$, 4 mM ATP, 0.1 mM GTP, and 10 mM, HEPES (pH 7.2). KCNQ2 channels were activated from a holding potential of –70 mV by two-step test pulses to 0 mV followed by –60 mV with 500 ms duration for each step. KCNQ2 currents were measured at the end of the 0 mV step. For retigabine experiments, cells were held at –100 mV, jumped to –20 mV and then to –60 mV. For M-current in SCG as well as hippocampal neurons, perforated patch with amphotericin B was used as described[16,20]. Amplitudes of the M-currents were measured as deactivating currents during 500-ms test pulses to –60 mV from a holding potential of –30 mV. For current clamp experiments, membrane potentials were adjusted to –70 mV. During application of 20 μM XE991, cells were held at –30 mV for 1 min, then returned to –70 mV. Live cell imaging was performed as described previously[17]. Three filter methods were used to measure FRET between KCNQ2 and calmodulin as described[17]. PKC activity measurement using cytCKAR was conducted as described[28].

Palmitoylation assay.

ABE assay was performed following the protocol described by Wan et al.[31] with minor modifications. Briefly, cell and brain lysate were prepared in the presence of 10 mM N-ethylmaleimide (NEM) followed by denaturation with chloroform/methanol precipitation. Treated samples were further incubated overnight with 10 mM NEM. After extensive wash by chloroform/methanol precipitation, samples were subjected to hydroxylamine treatment. After each chloroform/methanol precipitation, protein pellets

were solubilized in aqueous buffers by sonication. After wash, HPDP-biotin (Pierce) was used for sulfhydryl biotinylation. Biotin exchanged samples were used for immunoprecipitation by mouse anti-AKAP150 antibody or affinity purification by NeutrAvidin resin (Pierce). Purified proteins were eluted by boiling in non-reducing SDS-PAGE loading buffer for detection with HRP-conjugated neutravidin, or with dithiothreitol for detection with antibodies.

Kainate-induced seizure.

For in vivo administration of VPA, adult C57BL/6 mice of both sexes (3-5 months old, Jackson lab) were administered (i.p.) either freshly prepared sodium valproate (250 mg/kg, VPA) or physiological saline solution twice daily for 4 days unless stated otherwise. For kainate-induced seizure experiments, 30 mg/kg kainate (s.c.) was injected 6 hours after the last VPA administration. One hour after kainate administration, mice were injected either with 2 mg/kg XE991 (i.p.) in Dulbecco's phosphate-buffered saline (DPBS), or DPBS alone. Mice were video-taped for the subsequent 4 hours after kainate injection, and behavior was scored by treatment-blind observers every 10 min according to a modified Racine scale with the following criteria: 1) immobility; 2) rigidity; 3) automatisms with scratching, head bobbing and circling; 4) intermittent rearing and falling; 5) continuous rearing and falling; 6) tonic-clonic whole body convulsions and rapid jumping. Animals that died during the experiments were assigned stage 6 thereafter.

c-FOS immunohistochemistry.

1 h after injection of kainate (30 mg/kg), mice were deeply anesthetized with isoflurane and perfused with 4% paraformaldehyde in PBS (pH 7.4). Brains were then

removed and post-fixed in 4% paraformaldehyde in PBS (pH 7.4) overnight at 4˚C. Brains were sectioned into coronal slices (30 μm) using a vibratome (Leica, VT-1200). Free-floating sections were washed with PBS in 24-well dishes and then incubated with PBS containing 0.3% hydrogen peroxide and 10% methanol for 10 min. After 3 washes with PBS, sections were incubated with a blocking buffer containing 0.5% Triton X-100 and 1% normal goat serum in PBS. Sections were then incubated with primary antibody mixture containing rabbit-anti c-FOS antibody (1:1000 dilution) in the blocking solution for 48 h at 4˚C. After 2 washes with PBS followed by 2 washes with Tris-buffered saline (TBS), sections were incubated with Cy3-conjugated anti-rabbit secondary antibody in TBS containing 0.5% Triton X-100 and 1% normal goat serum for 2 h at room temperature. After wash, sections were mounted onto glass slides using VECTASHIELD with DAPI (Vector Laboratories). Immunofluorescent images were acquired using a fluorescent light microscope (Leica, DM4000B) equipped with a CCD camera (Optronics MicroFire, OPTMIF). Areas around the dentate gyrus, CA1 and CA3 were selected and the average fluorescence intensity within each corresponding region of interest from DAPI and c-FOS staining images was quantified by observers blind to treatments using MetaMorph (Molecular devices). Nucleus-free regions in the stratum oriens were used as a background for DAPI and c-FOS staining.

Data analysis.

Data are presented as mean ± SEM. Statistical analyses were performed using GraphPad Prism. For comparing two groups, either unpaired or paired *t* tests were used with Welch's correction. For experiments with more than three groups, one-way ANOVA or Kruskal-Wallis test were used as follows. If variances were the same among groups,

as evaluated by Bartlett's test and Brown–Forsythe test, one-way ANOVA followed by Dunnett's multiple comparisons test was used. If variances were different among samples, Kruskal-Wallis test followed by Dunn's multiple comparisons test was used. When same cells received multiple treatments, repeated-measures one-way ANOVA followed by Turkey's multiple comparisons test was used. *P* values of less than 0.05 were considered significant.

Study approval. All animal experiments are approved by the Institutional Animal Care and Use Committee at the University of California, Irvine.

Results

Valproic acid prevents muscarinic agonist induced neuronal hyperexcitability by disrupting M-current suppression.

VPA has been used to treat epilepsy and bipolar disorder for several decades[32]. Accumulating genomic analyses indicate that these two neurological disorders are also linked with *KCNQ* gene mutations[5,33]. The similarity between the two motivated us to investigate whether VPA affects M-channel regulation.

Rat superior cervical ganglion (SCG) neurons were used in the initial assessment of VPA effects on the M-current since M-current regulation has been extensively characterized in this neuronal type, and neurons in the central nervous system are known to use the same regulatory mechanism[6,34]. SCG neurons were pretreated with 500 μM VPA for three days and M-current response to a muscarinic agonist, 0.1 μM oxotremorine-M (oxo-M) was measured. VPA treated neurons showed reduced muscarinic suppression of the M-current (Figure 3.1A). In contrast, pretreatment with a structurally similar short-chain fatty acid, valeric acid (500 μM), did not affect muscarinic suppression of the M-current (Figure 3.1B). In addition, other anti-epileptic compounds, 100 μM vigabatrin or 100 μM phenytoin did not change muscarinic suppression of the M-current (Figure 3.1B).

We next tested whether VPA also affects M-current mediated neuronal excitability in central neurons using hippocampal neurons. Cultured rat hippocampal neurons were pretreated with 500 μM VPA or 500 μM valeric acid for three days. Current clamp recording was used to measure neuronal excitability of these neurons. In control non-treated neurons, 50-pA current injections for 500 ms evoked action potential

firing (Figure 3.1C top row). Application of 1 μM oxo-M increased neuronal firing in control hippocampal neurons (Figure 3.1C). This oxo-M-induced hyperexcitability was apparent below 150 pA current injections in our conditions (Figure 3.1D). Similar hyperexcitability could be reproduced by the application of an M-channel inhibitor, XE991 (Figure 3.1, C and F).

In VPA treated neurons, we observed normal input-excitation relationships in the quiescent condition (Figure 3.1, C and E). However, oxo-M application did not increase neuronal excitability, as would be expected from attenuated muscarinic M-current suppression (Figure 3.1, C and E). The application of XE991 to VPA treated neurons induced hyperexcitation similar to that in VPA untreated neurons (Figure 3.1, C and F). On the other hand, valeric acid treated neurons did not show any difference from non-treated hippocampal neurons in basal excitability, oxo-M induced or XE991-induced hyperexcitability (Figure 3.1F). These results suggest that VPA treatment disrupted muscarinic suppression of the M-current and prevented receptor-induced hyperexcitability.

Preserved M-current contributes to anticonvulsant effects of VPA.

To test whether disruption of M-current suppression contributes to anticonvulsant effects of VPA, we evaluated the anticonvulsant effect of VPA in kainate-induced seizure model. In wild-type C57BL/6 mice, 30 mg/kg kainate induced seizures, which usually lead to generalized convulsions (stage 6, Figure 3.2, A and B) and often to mortality (7/9 mice). VPA treatment (250 mg/kg x 2/day x 3.5 days) diminished the severity to stage 3 (Figure 3.2, A and B) and prevented mortality (0/7 mice, $P = 0.0032$. Fisher's exact test).

Our in vitro experiments suggest that VPA counteracts receptor-induced M-current suppression. Therefore, we reasoned that XE991, an activated-subunit inhibitor of the M-channel, should diminish anticonvulsant effects of VPA. XE991 is a unique channel blocker that does not effectively inhibit the M-channel at membrane potentials below –65 mV, which is close to the resting membrane potential of neurons. Hence, it should have minimal effect on neurons showing sparse firing. Indeed, administration of XE991 (2 mg/kg) did not affect basic motor behaviors in mice (data not shown). However, this dose of XE991 transiently exacerbated kainate-induced seizure in VPA treated mice reaching stage 5 seizures (Figure 3.2C). In contrast, 2 mg/kg XE991 did not affect either the anticonvulsant effect of diazepam (Figure 3.2D) or stage 3 seizures in VPA non-treated mice induced by reduced kainate (25 mg/kg, Figure 3.2E). These results suggest that VPA shows anticonvulsant effect through preservation of the M-current. Inversely, since control kainate-induced seizures and diazepam treated seizures were not affected by XE991, these results also suggest that M-current is suppressed during seizures.

One caveat of above experiments is a possibility that observed effects of XE991 were derived from off-target inhibition of other potassium channels such as Kv4 channels that are partially inhibited by XE991 at high concentrations[36]. To specifically test whether M-current is involved in seizure pathology and VPA action, we performed a second set of experiments using retigabine as a probe, which does not affect Kv4 channels[37]. Retigabine is a recently approved anti-epileptic drug that opens the M-channel by shifting activation voltage close to the resting membrane potential[37]. Additionally, retigabine has been demonstrated to be ineffective at opening M-channels

under receptor-induced suppression[37]. We first tested whether VPA treatment modulates the pharmacological action of retigabine in vitro using transiently expressed KCNQ2 channels in Chinese hamster ovary cells stably expressing human m1 muscarinic receptor, CHO hm1 cells[38]. Homomeric KCNQ2 current was augmented by 5 μM retigabine when applied alone, but when applied together with 10 μM oxo-M, KCNQ2 current was decreased as reported[37] (Figure 3.3, A and B). In contrast, in 500 μM VPA treated CHO hm1 cells, KCNQ2 currents showed augmentation by retigabine even in the presence of 10 μM oxo-M (Figure 3.3, A and B). Similar results were obtained from KCNQ2/3 heteromeric channels (Figure 3.3C), which are considered to be a common form of the endogenous M-channels. Retigabine application augmented KCNQ2/3 current. However, the current amplitude was reduced when applied together with oxo-M. Notably, KCNQ2/3 currents from VPA treated cells showed augmentation by retigabine even in the presence of oxo-M. These results were consistent with our observation that VPA treatment preserves KCNQ current when m1 muscarinic receptor is activated. We then examined anticonvulsant effects of retigabine in kainate-induced seizures in mice. When retigabine was administered 5 min before application of kainate, it showed anticonvulsant effect on kainate-induced seizures as expected (Figure 3.3D). However, it did not show any anticonvulsant effect when applied 20 min after kainate injection (Figure 3.3D), which suggests retigabine-sensitive M-channels are reduced after induction of seizures.

To test whether VPA modulates retigabine efficacy, we used an increased kainate dose (35 mg/kg), which induced stage 6 seizures in VPA-treated mice (5/6 mice) (Figure 3.3E). Retigabine administration 5 min before kainate injection reduced

seizure severity similarly as observed in VPA non-treated mice. Importantly, retigabine administration 20 min after kainate also reduced severity of seizures in VPA treated mice (Figure 3.3E). These results further support that the anticonvulsant effect of VPA involves preservation of M-current during seizures.

Pharmacological modulation of behavioral seizure severity in the above experiments may merely reflect changes at the motor cortex without altering generalized seizure activity in other brain regions. Therefore, we evaluated accumulative neural hyperactivity in the brain during kainate-induced seizures by quantifying c-fos expression in the hippocampus, a primary target brain region for administered kainate[39]. We observed strong expression of c-FOS in the CA1 region and the dentate gyrus of the hippocampus 60 min after kainate injection, which would correspond to neuronal activity during status epilepticus in control mice as reported previously (Figure 3.4)[40,41]. Kainate-induced c-FOS expression was reduced in VPA treated mice. However, when XE991 was administered to VPA treated mice, c-FOS expression showed equivalent induction as compared to control (Figure 3.4). These results suggest that neuronal activity in the hippocampus correlates with behavioral seizures in our experimental conditions.

VPA interfered with the PKC mediated pathway of muscarinic suppression of KCNQ2 current.

Since VPA effects could be reconstituted in CHO hm1 cells expressing homomeric KCNQ2 channels (Figure 3.3, A and B), we used this heterologous expression system to further characterize the molecular process that is disrupted by VPA treatment. Overnight treatment with 500 μM VPA reduced muscarinic suppression

of KCNQ2 current (Figure 3.5A) similar to the effects observed in SCG neurons. Dose response experiments showed that VPA disrupted muscarinic suppression of KCNQ2 current with EC_{50} of 213 $\pm$ 9 μM (n = 7) (Figure 3.5B). Importantly, short exposure (5 min) to 500 μM VPA did not alter muscarinic suppression of KCNQ2 current (Figure 3.5C). In addition, pretreatment with lithium chloride (1 mM) or HDAC inhibitors (1 mM sodium butyrate or 2 μM SAHA) did not affect muscarinic suppression of the KCNQ2 current [relative currents with oxo-M were, 26.3 $\pm$ 4.6% control (Figure 3.5C, n = 8), 23.5 $\pm$ 5.6% lithium (n = 6), 33.9 $\pm$ 2.7% SAHA (n = 9), 27.0 $\pm$ 5.8% butyrate (n = 9), $P >$ 0.05, respectively].

We have previously demonstrated that PKC mediated KCNQ2 subunit phosphorylation of serine 541 is important for suppression of the M-current[17]. Therefore, we tested a mutant channel that lacks the phosphorylation acceptor residue, an alanine substitution of serine 541 in the KCNQ2 subunit, KCNQ2(S541A). As we reported previously[17], KCNQ2(S541A) exhibited smaller responses to oxo-M compared to the wild-type KCNQ2 current (Figure 3.5C). Importantly, VPA treatment did not further modify oxo-M responses of KCNQ2(S541A) current (Figure 3.5C), which suggests that the KCNQ2(S541A) mutation occluded VPA effects.

Since PKC mediated phosphorylation of KCNQ2(S541) triggers calmodulin (CaM) dissociation from KCNQ2 channel[17], we measured KCNQ2-CaM dissociation by total internal reflection fluorescence FRET analysis (TIRF-FRET) using KCNQ2-mCitrine (KCNQ2-mCit) and calmodulin-mCerulean (CaM-mCer). Basal FRET efficiency showed positive FRET signals between KCNQ2-mCit and CaM-mCer, indicating association of these proteins as we previously reported[17]. These basal FRET

efficiencies were not altered by VPA treatment [0.18 ± 0.02 (n = 28) for VPA non-treated cells, 0.16 ± 0.01 (n = 34) for VPA treated cells, *P* = 0.327, *t* test]. Application of oxo-M reduced FRET signal in control cells, which corresponds to dissociation of CaM as described[17] (Figure 3.5D). However, VPA treatment abolished oxo-M induced decrease in FRET efficiency (Figure 3.5D). These results support the hypothesis that VPA treatment disrupts PKC dependent KCNQ2 regulation.

Next we asked whether this effect was due to the general inhibition of PKC activation or focal inhibition within the KCNQ2 channel complex. To address this question, we measured oxo-M induced cellular PKC activity using a cytosolic version of FRET based PKC kinase activity reporter, cytCKAR[29]. Cellular PKC activity induced by muscarinic agonist was not altered by VPA treatment (Figure 3.5E), suggesting that interference of PKC signaling occurred only within the KCNQ2 channel complex.

Another key pathway of muscarinic suppression of the M-current is through PIP2 depletion. Therefore, we examined whether VPA treatment altered PIP2 depletion after muscarinic stimulation using CFP-PH, a CFP fusion protein with the PH domain of PLCδ[42]. In control CHO hm1 cells, PIP2 depletion, triggered by 3 μM oxo-M, induced translocation of CFP-PH into the cytoplasm (Figure 3.5F). VPA treatment did not evoke any changes in oxo-M induced translocation of CFP-PH (Figure 3.5F). These results suggest that VPA selectively disrupted local PKC mediated phosphorylation of the KCNQ2 channel without interfering with global PKC activation or phosphatidylinositol turnover.

VPA inhibited palmitoylation of AKAP150 and other neuronal proteins.

AKAP79/150 anchors PKC to the KCNQ2 subunit and is critical for PKC mediated KCNQ2(S541) phosphorylation[16,20]. Therefore, we next focused on AKAP79/150 dependent mechanisms. We first suspected that VPA decreased AKAP150 expression since similar disruption of PKC mediated KCNQ2 phosphorylation was observed in AKAP150 deficient cells[20,21]. However, VPA treatment did not change AKAP150 protein expression or protein interaction profiles of AKAP150 binding proteins (Figure 3.6).

Accumulating evidence suggests that palmitoylation of AKAP150 is important for AKAP150 mediated signaling[22,23]. Therefore, we measured palmitoylation of AKAP150 by acyl-biotin exchange (ABE) analyses[31] in cultured hippocampal neurons. This technique uses hydroxylamine (NH_2OH) treatment to cleave palmitic acid from palmitoylated cysteine residues, followed by biotin labeling of newly exposed cysteine thiols. Therefore, biotin labeling of hydroxylamine treated samples indicates specific detection of palmitoylation. We observed that 1 mM VPA treatment reduced palmitoylation of AKAP150 (Figure 3.7A, $P = 0.038$, n = 3, paired *t* test). Interestingly, VPA treatment did not drastically alter the overall palmitoylation patterns in hippocampal neuron lysates (Figure 3.7B), suggesting some degree of selectivity for VPA sensitive palmitoylation.

We next examined the effects of in vivo administration of VPA on AKAP150 palmitoylation. After administering VPA (i.p., 250 mg/kg/day x 3.5 days) to mice, cerebrums were collected and used for ABE analyses combined with immunoblots. Consistent with our results from cultured neurons, VPA treatment reduced palmitoylation of AKAP150 (Figure 3.7C). We also found that VPA suppressed

palmitoylation of PSD95, Flotillin-1, Fyn and GRIP, but not EAAT2, confirming some degree of selectivity for VPA sensitive palmitoylation (Figure 3.7C).

Palmitoylation of AKAP150 is required for muscarinic regulation of the M-current.

One remaining question was whether palmitoylation of AKAP79/150 is involved in muscarinic suppression of the M-current. We addressed this question by using AKAP150 silenced SCG neurons. Endogenous AKAP150 was silenced in rat SCG neurons using a silencing plasmid, pSAKAP150i[20]. In these AKAP150 silenced neurons, various versions of the human orthologue, AKAP79, which are resistant to rat AKAP150 RNAi, were expressed to examine whether they can restore AKAP79/150 signaling. AKAP150 silenced SCG neurons showed attenuated muscarinic responses as we reported previously[20] (Figure 3.8). The muscarinic response was rescued by expression of wild-type AKAP79, as expected (Figure 3.8). Two cysteine residues in AKAP79, C36 and C129, have been identified as the palmitoylation sites[22,23]. Expression of the double serine-substituted mutant for the palmitoylation sites, AKAP79(C36S/C129S), could not restore the oxo-M response of KCNQ2 current (Figure 3.8, A and B).

It has been shown that myristoylation can mimic constitutive palmitoylation[30]. Therefore, a myristoylation consensus site was added to the N-terminus of AKAP79(C36S/C129S), Myr-AKAP79(C36S/C129S). Expression of Myr-AKAP79(C36S/C129S) restored muscarinic suppression of the M-current (Figure 3.8B). These results confirmed that palmitoylation of AKAP150 is critical for AKAP150 mediated regulation of KCNQ2 channel.

AKAP150 mutants carrying a myristoylation site were resistant to VPA treatment.

Since distinct enzymes regulate myristoylation and palmitoylation, we wondered if the myristoylated AKAP150-restored M-channel pathway becomes resistant to VPA treatment. To test this, we overexpressed rat Myr-AKAP150(C36S/C123S), which corresponds to human Myr-AKAP79(C36S/C129S), in SCG neurons, then treated neurons with 2 mM VPA for three days and tested for muscarinic responses to 1 μM oxo-M (Figure 3.9). In control experiments with overexpression of wild-type AKAP150, VPA pretreatment attenuated the muscarinic response of the M-current as expected (Figure 3.9A). In contrast, muscarinic responses in Myr-AKAP150(C36S/C123S) expressing SCG neurons became insensitive to 2 mM VPA (Figure 3.9, B and C). These results further support that VPA disrupts receptor-induced M-current suppression by interfering with palmitoylation of AKAP150.

Discussion

In the present study, we report that disruption of M-current suppression during seizure contributes to the non-acute anticonvulsant action of VPA. Conversely, we report that M-current suppression is involved in the pathophysiology of seizures. VPA has been demonstrated to have many pharmacological effects. However, some known effects require high concentrations of VPA. Therefore, it is important to evaluate effects at the concentration of VPA that is within the therapeutic range in human (28–700 μM)[1]. We were able to demonstrate that VPA in this concentration range prevented muscarinic receptor-induced suppression of the M-current, as well as M-current dependent hyperexcitability in primary neurons.

Previously, we showed that AKAP79/150 is important for receptor-induced suppression of the M-current[16,20]. In the present study, we demonstrate that palmitoylation of AKAP79/150 is critical for M-current regulation and that VPA disrupts AKAP79/150 mediated M-current regulation by interfering with palmitoylation of AKAP79/150. Palmitoylation of AKAP79/150 has been shown to stabilize its membrane localization[22], which may be required during the rearrangement of the multiprotein KCNQ2 channel complex that occurs during muscarinic suppression of the M-current[17].

We also demonstrate that VPA suppressed palmitoylation of a minor fraction of neuronal proteins including several synaptic proteins. Interestingly, kainate-induced seizures have been demonstrated to increase palmitoylation of PSD-95, SNAP25, as well as AKAP150, which promotes synaptic potentiation[23]. Therefore, in addition to VPA effects on the M-channel, inhibited palmitoylation of synaptic proteins may also contribute to the anticonvulsant action of VPA. Palmitoylation is mediated by palmitoyl

acyltransferases, which consist of over 20 subtypes of DHHC (Asp-His-His-Cys) proteins[25]. GRIP1b has been shown to be palmitoylated by DHHC5 and DHHC8, while Fyn is palmitoylated by other DHHC enzymes[30]. VPA suppressed palmitoylation of GRIP1 and Fyn to a similar degree, which indicates that VPA affects multiple DHHC subtypes. Therefore, VPA should be considered a palmitoyl acyltransferase inhibitor with moderate selectivity.

Although KCNQ subunit mutations have been linked to epilepsy, modulation of the wild-type M-channel has never been implicated in the pathophysiology of seizures. Our results suggest that M-current is suppressed during seizures. As described in chapter 2, XE991 is an activated-subunit inhibitor that is becomes efficacious when the membrane potential is depolarized above –65 mV. Therefore, M-channels become sensitive to XE991 only when neurons are depolarized by neuronal activities such as high frequency firing. Indeed, we showed that XE991 aggravated kainate-induced seizures in VPA treated mice. In contrast, XE991 administration did not show any effects in control kainate-induced seizures. This would be the case if the M-current were already suppressed by seizure activity in affected regions leaving few M-channels to be inhibited. Further support came from retigabine experiments. Retigabine has been shown to activate M-channels by shifting the activation voltage below the resting membrane potential range. However, retigabine-activated M-current can undergo receptor-induced suppression and is not efficacious in neurons already suppressed by neurotransmitters[37]. Our experiments confirmed that retigabine could augment KCNQ2 or KCNQ2/3 currents when applied without a muscarinic agonist but when applied together with a muscarinic agonist, muscarinic suppression overwhelmed retigabine-

induced augmentation. However, when cells were pretreated with VPA, retigabine could augment KCNQ2 and KCNQ2/3 currents even in the presence of muscarinic agonist. In addition, efficacy of retigabine in kainate-induced seizures also supports this view. In non-treated mice, retigabine could suppress kainate-induced seizures only when applied before induction of seizures. In contrast, in VPA treated mice, retigabine did not lose efficacy even when administered after seizure induction. These results suggest that administration of retigabine to VPA treated patients would be a powerful procedure to cease status epilepticus. However, since M-current suppression has also been implicated in cognitive function, careful evaluation of long-term effects of this combination therapy would need to be performed. Together, these results suggest that M-current is suppressed during seizures and that VPA treatment preserves M-current by disrupting its receptor-induced suppression.

One scenario for M-current suppression during seizure is that seizures provoke excess neurotransmitter release that activates Gq-coupled receptors thereby suppressing the M-current. Such seizure-induced M-current suppression increases the excitability of relevant neurons, which, in turn, facilitates propagation of ictal activities. Indeed, microdialysis studies have shown that several neurotransmitters are elevated during seizures including acetylcholine[43,44], serotonin[43,45], noradrenaline[45,46] and glutamate[47,48]. In addition, corresponding Gq-coupled receptors for these transmitters have been identified in hippocampal neurons: m1 acetylcholine receptor[49,50], serotonin 5-HT2 receptor[51], α1 adrenergic receptor[51] and group 1 metabotropic glutamate receptor[52]. However, noradrenaline and serotonin are considered to have

anticonvulsant actions through distinct receptors[53,54]. Further studies are required to identify responsible neurotransmitters that suppress the M-current during seizures.

It has been reported that some VPA metabolites, which are primarily generated in the liver[55], have more potent anticonvulsant action[56]. In our case, anti-hyperexcitation effects were reproduced in cultured cells. Therefore, we believe that VPA is the primary compound for the inhibition of palmitoylation in our conditions. However, we do not rule out the possibility that active VPA metabolites could be more potent palmitoylation inhibitors.

In summary, M-current suppression contributes to the pathophysiology of seizures and preserved M-current during seizures is involved in the anticonvulsant effect of VPA, which is mediated by interfering with palmitoylation of AKAP79/150. These findings would provide novel insights and biochemical targets for developing better antiepileptic treatments.

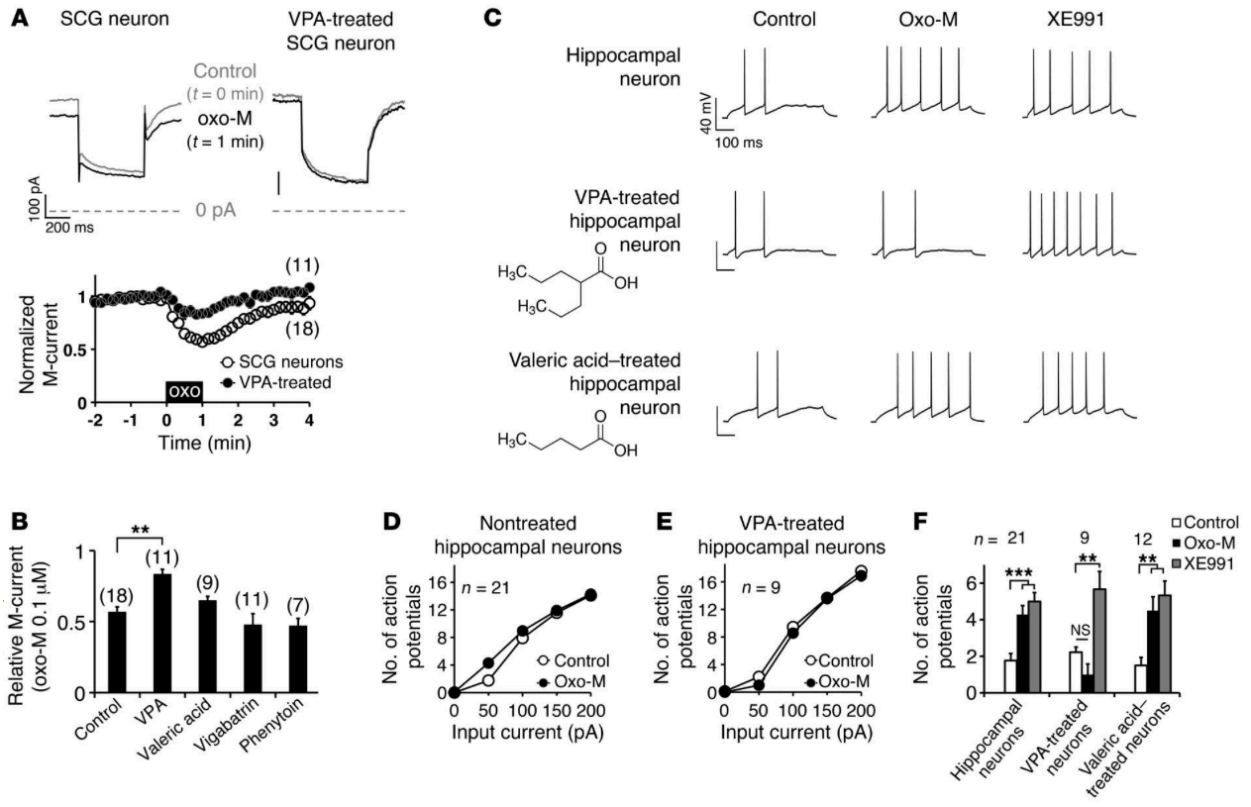

Figure 3.1. VPA attenuated muscarinic suppression of the M-current and prevented oxo-M induced hyperexcitability in cultured SCG and hippocampal neurons.

A. Representative voltage-clamp current traces from SCG neurons (top) and pooled results (bottom) showing M-current suppression by 0.1 μM oxo-M and its disruption by 500 μM VPA pretreatment. Amplitudes of the M-currents are normalized to those at t = 0. Black box indicates presence of 0.1 μM oxo-M. **B.** Summary of muscarinic suppression of the M-current at t = 1 min including results shown in A. Muscarinic suppression is attenuated by 500 μM VPA but not by 500 μM valeric acid, 100 μM vigabatrin or 100 μM phenytoin. ** < 0.01, Kruskal-Wallis one-way ANOVA followed by Dunn's multiple comparisons test. **C.** Current clamp traces showing action potential firing in response to 50-pA current injection. Traces from VPA non-treated (top), 500 μM VPA treated (middle), and 500 μM valeric acid treated (bottom) hippocampal neurons are shown. Control (left), presence of 1 μM oxo-M (middle), or presence of 20 μM XE991 (right). **D, E.** Input-excitation relationships from hippocampal neurons before (open circle) and after application of oxo-M (filled circle) from non-treated neurons (D) or 500 μM VPA treated neurons (E). **F.** Summary of neural firing by 50-pA current injection shown in C-E. * < 0.05, ** < 0.01, *** < 0.001, NS: not significant, repeated measures one-way ANOVA followed by Turkey's multiple comparisons test. Error bars show SEM.

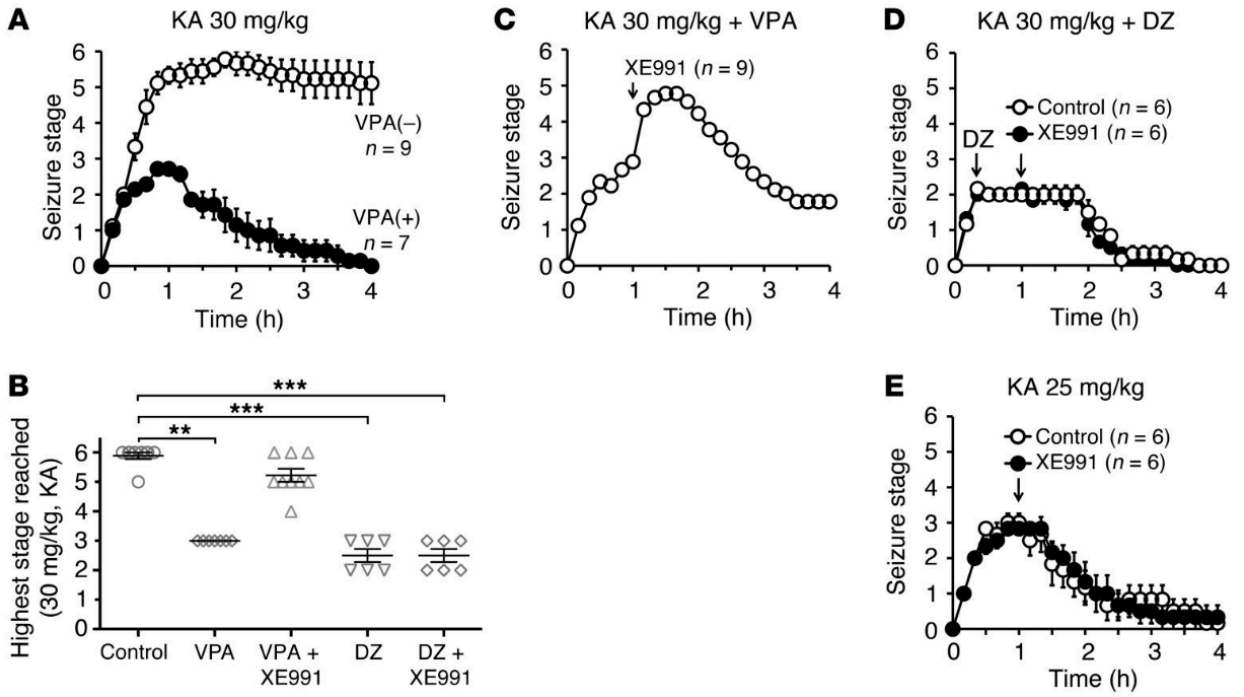

Figure 3.2. XE991 transiently removed anticonvulsant effect of VPA in kainate-induced seizure in mice.

A. Pretreatment with VPA decreased seizure stages of kainate-induced seizure (KA, 30 mg/kg, t=0) in adult mice. **B.** Distribution of highest seizure stages reached in experiments shown in A, C, and D. ** < 0.01, *** < 0.001, Kruskal-Wallis one-way ANOVA followed by Dunn's multiple comparisons test. **C.** Administration of XE991 (2 mg/kg) transiently removed anticonvulsant effects of VPA. **D.** Anticonvulsant effect of diazepam (DZ, 5 mg/kg) was not affected by XE991 (2 mg/kg). **E.** 2 mg/kg XE991 did not affect stage 3 seizure induced by 25 mg/kg kainate in VPA non-treated mice. Arrows show time points for injection of indicated compounds. KA is injected at t = 0. Error bars show SEM.

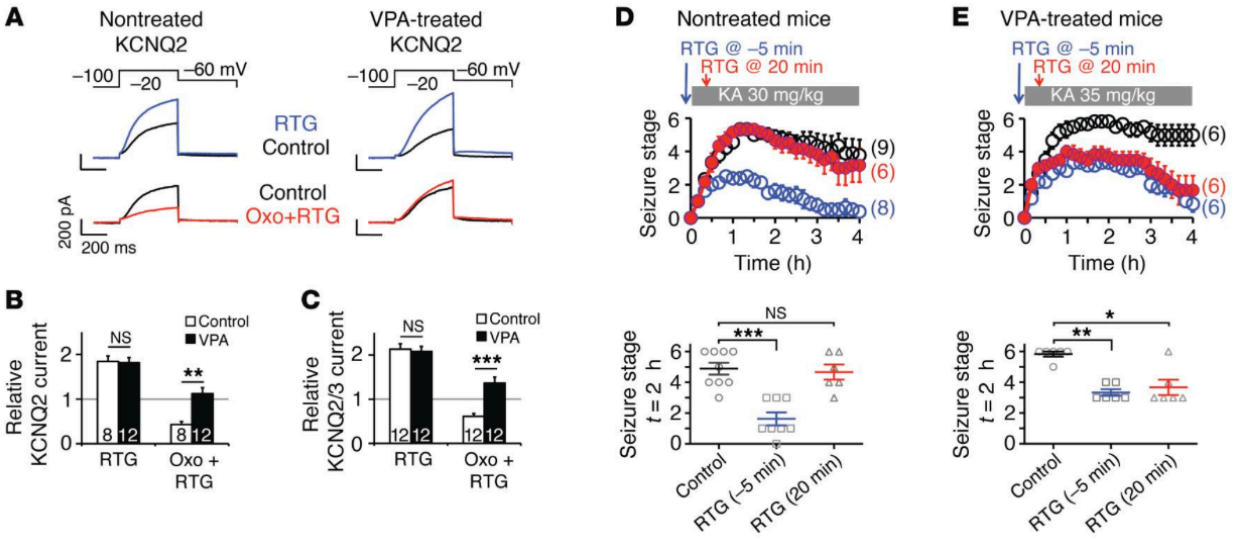

Figure 3.3. VPA protected retigabine-induced augmentation of KCNQ currents in the presence of oxo-M as well as anticonvulsant effects with post-seizure administration of retigabine.

A. Representative current traces showing 5 μM retigabine (RTG)-induced augmentation of KCNQ2 currents (top) and its modulation by oxo-M (bottom). In VPA non-treated CHO hm1 cells (left), 10 μM oxo-M + 5 μM retigabine induced current suppression (left). In contrast, in VPA treated cells, retigabine augmented KCNQ2 current even in the presence of 10 μM oxo-M (right). **B.** Summary of experiments shown in A for homomeric KCNQ2 channel. **C.** Retigabine and oxo-M showed similar effects in heterologous KCNQ2/3 channels. Currents were normalized to the current before applying drugs. **<0.01, ***<0.001, unpaired *t* test. **D.** Retigabine (10 mg/kg) showed anticonvulsant effects only when applied prior (t = –5 min) to KA injection (30 mg/kg, t = 0). Lower panel shows seizure stages at t = 2h. **E.** Increased KA (35 mg/kg) was used to induce stage 6 seizures in VPA treated mice. In these VPA treated mice, retigabine showed anticonvulsant effect even when applied after the induction of seizures. Lower panel shows seizure stages at t = 2h. Kruskal-Wallis one-way ANOVA followed by Dunn's multiple comparisons test. Error bars show SEM.

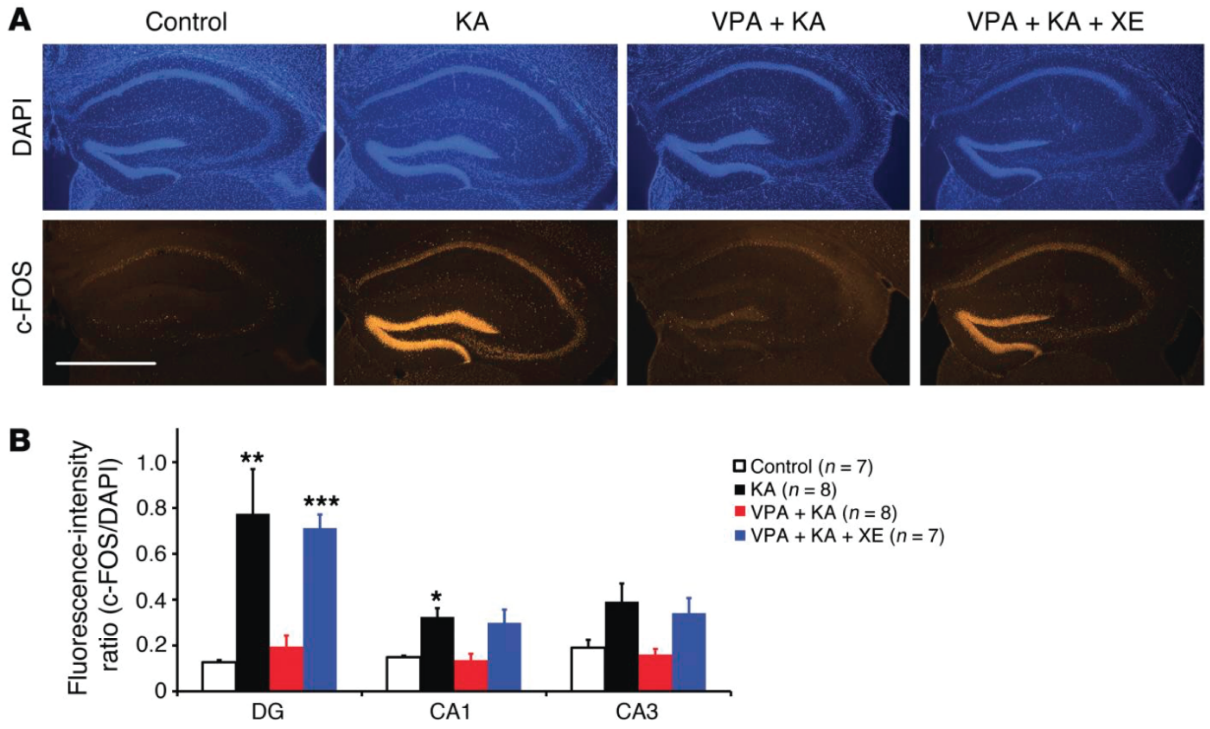

Figure 3.4. Induction of c-FOS expression in the hippocampus corresponded with behavioral seizures.

A. DAPI staining and c-FOS immunofluorescence staining in the hippocampus. Scale bar shows 1 mm. **B.** Histogram summarizing quantification of kainate-induced c-FOS expression. Reduced induction of c-FOS expression in the hippocampus was observed in VPA treated mice. Restored induction of c-FOS was observed in VPA treated mice co-administrated with XE991 (2 mg/kg) and KA (30 mg/kg). Fluorescent intensities from corresponding regions of DAPI and c-FOS images were quantified and used to evaluate c-FOS expression relative to DAPI signals. * < 0.05, ** < 0,01 *** < 0.001, Kruskal-Wallis one-way ANOVA followed by Dunn's multiple comparisons test. Error bars show SEM.

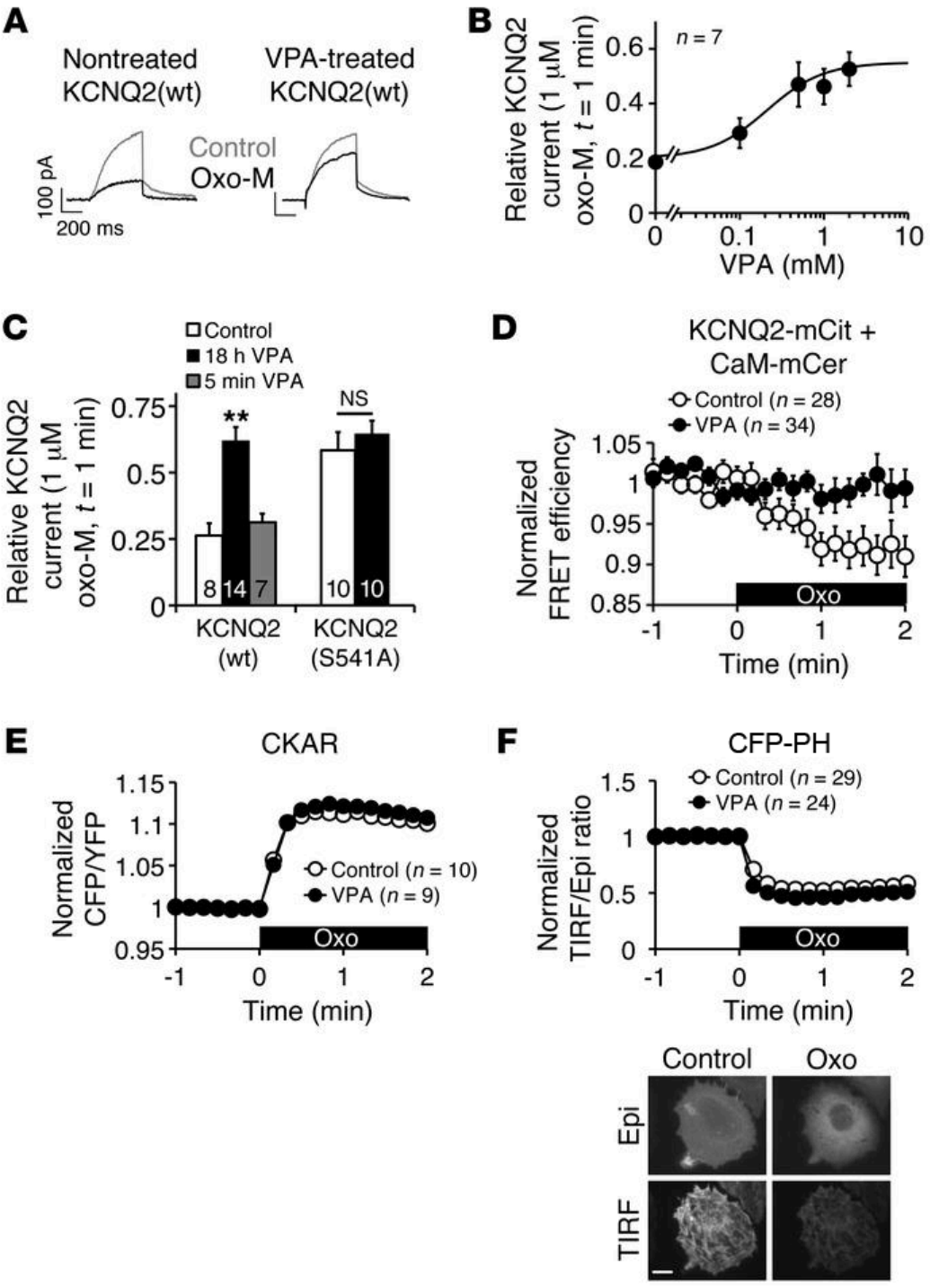

Figure 3.5. VPA disrupted PKC mediated KCNQ2 regulation.

A) KCNQ2 current traces showing that 500 μM VPA treatment attenuated 1 μM oxo-M induced current suppression in KCNQ2 channels. **B)** Dose response curve for VPA and oxo-M induced KCNQ2 current suppression. **C)** Relative KCNQ2 currents 1 min after

oxo-M application. 18 h treatment with 500 μM VPA reduced muscarinic suppression. 5 min incubation with 500 μM VPA did not attenuate oxo-M response. KCNQ2(S541A) channels were more resistant to oxo-M. Notably, 18 h treatment with 500 μM VPA had no effects. Amplitudes of currents are relative to those before oxo-M application. ** < 0.01, Kruskal-Wallis one-way ANOVA followed by Dunn's multiple comparisons test. **D)** TIRF-FRET analysis between KCNQ2-mCitrine (mCit) and CaM-mCerulean (mCer). Application of oxo-M decreased FRET signal corresponding to dissociation of CaM from KCNQ2 channel in control (open circle). VPA treatment prevented CaM dissociation (filled circle). Black box indicates presence of 3 μM oxo-M. **E)** Oxo-M induced PKC activity measured by FRET based PKC probe, cytCKAR. VPA did not have any effects. Black box indicates presence of 3 μM oxo-M. **F)** PIP2 depletion measured by CFP-PH and EPI/TIRF microscope. 3 μM oxo-M induced translocation of CFP-PH. Inset shows fluorescent images for epi fluorescence (EPI) and TIRF channel before (control) and after oxo-M (oxo) application. Scale bar shows 10 μm. Error bars indicate SEM.

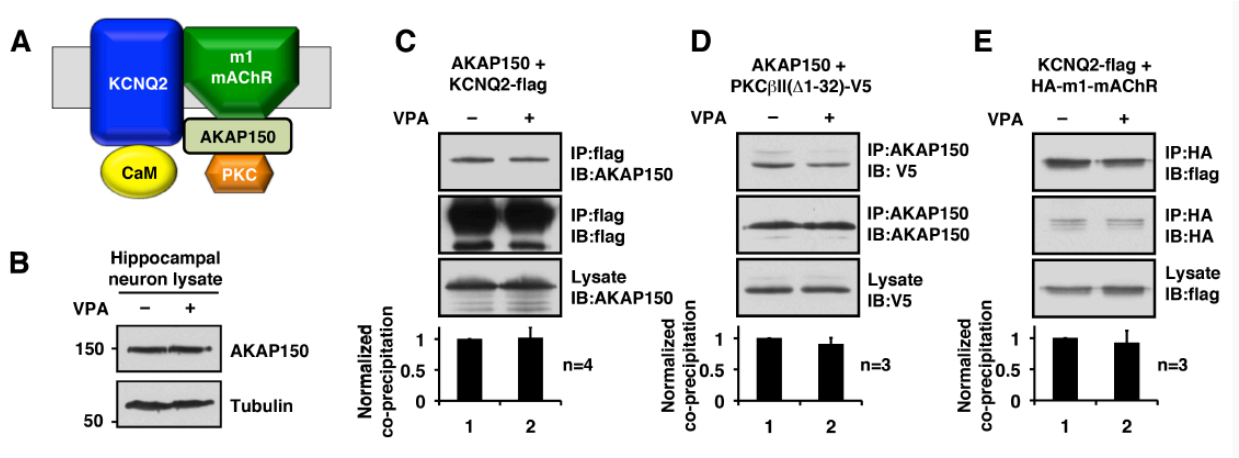

Figure 3.6. VPA treatment did not change AKAP150 protein expression or AKAP150 protein interaction.

A. Schematic diagram showing the KCNQ2 channel complex. **B.** Immunoblots showing equal protein expression between control and VPA treated cultured neurons. Tubulin blotting confirmed equal loading. **C.** Co-immunoprecipitation of AKAP150 with KCNQ2-flag from transiently transfected HEK293 cells. The histogram summarizes quantification from 4 independent experiments. VPA did not disturb KCNQ2-AKAP150 interaction. **D.** Co-immunoprecipitation of V5 tagged PKCβII(Δ1-32) with AKAP150 from transiently transfected HEK293 cells. The histogram summarizes 3 independent experiments. VPA did not disturb AKAP150- PKCβII interaction. **E.** Co-immunoprecipitation of KCNQ2-flag with HA-tagged m1 muscarinic receptors from transiently transfected HEK293 cells. The histogram summarizes 3 independent experiments. Error bars show SEM.

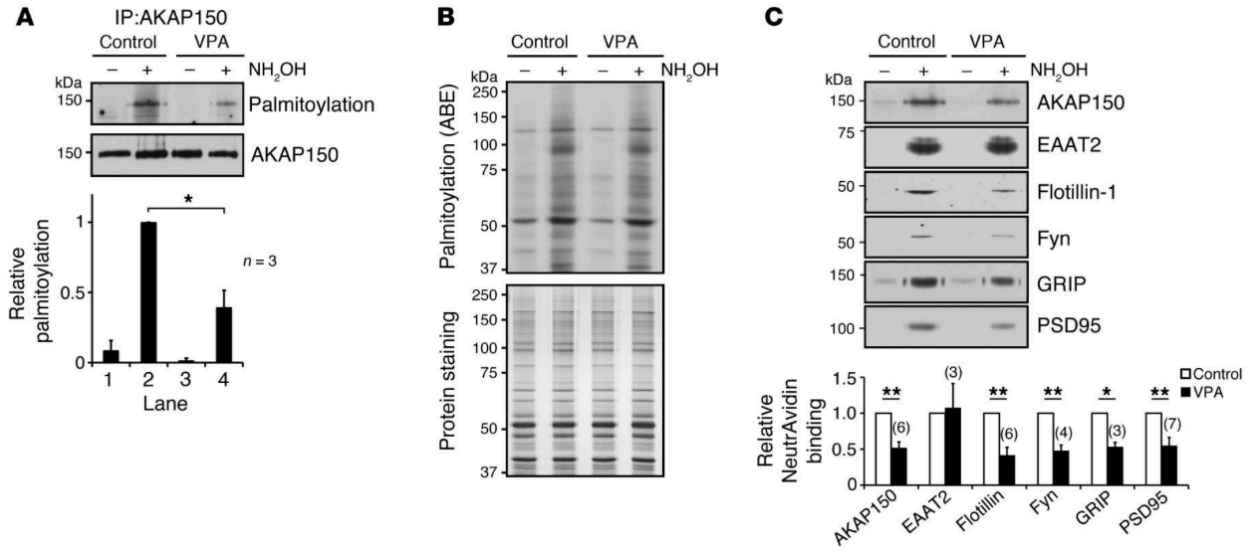

Figure 3.7. VPA selectively reduced palmitoylation of AKAP150 and several neuronal proteins.

A. Palmitoylation of AKAP150 was evaluated using cultured hippocampal neurons. After ABE labeling, AKAP150 protein was purified by immunoprecipitation using monoclonal anti-AKAP150 antibody. Palmitoylation was detected by NeutrAvidin-HRP (upper panel). Middle panel shows equal recovery of AKAP150 among treatments assessed by immunoblots using rabbit anti-AKAP150 antibody. Bottom histogram shows summary of three independent experiments. Palmitoylation of AKAP150 was reduced in VPA treated neurons. Requirement of hydroxylamine, NH_2OH, for biotinylation verified selective labeling of palmitoylation. * < 0.05, paired *t* test to control. **B.** VPA treatment had minimal effect on overall palmitoylation in cultured hippocampal neuronal lysates. **C.** ABE labeling was performed on mouse brain extracts followed by purification of labeled proteins by NeutrAvidin-beads. Palmitoylation of indicated neural proteins was assessed by immunobloting. VPA reduced palmitoylation of several but not all neuronal proteins. * < 0.05, ** < 0.01, paired *t* test to control. Error bars show SEM.

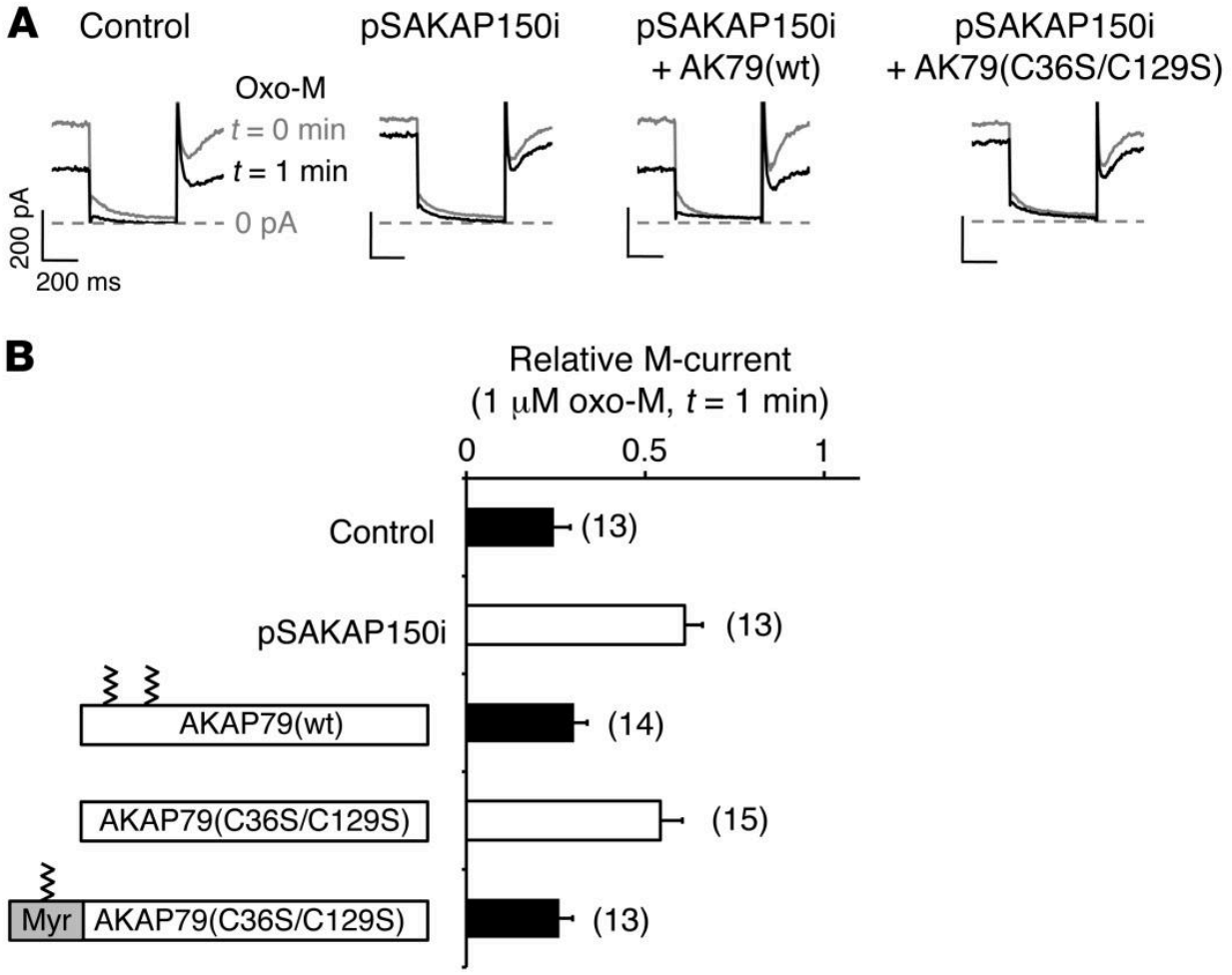

Figure 3.8. Lipid modification of AKAP150 is required for muscarinic suppression of the M-current.

A. Representative current traces showing muscarinic response of the M-current in AKAP150 silenced rat SCG neurons. Silencing of endogenous AKAP150 attenuated 1 μM oxo-M induced suppression of the M-current. Co-expression of wild-type AKAP79, AK79(wt), but not palmitoylation deficient AKAP79(C36S/C129S), AK79(C36S/C129S), rescued oxo-M induced suppression of the M-current. **B.** Summary of the ability of AKAP79 mutants to restore muscarinic M-current suppression in AKAP150 silenced neurons. Open bars indicate $P < 0.001$ from AKAP150-silenced control evaluated by one-way ANOVA followed by Dunnett's multiple comparisons test. AKAP79(C36S/C129S) did not restore AKAP150 mediated muscarinic signaling. Attachment of a myristoylation site to AKAP79(C36S/C129S) restored signaling. Error bars show SEM.

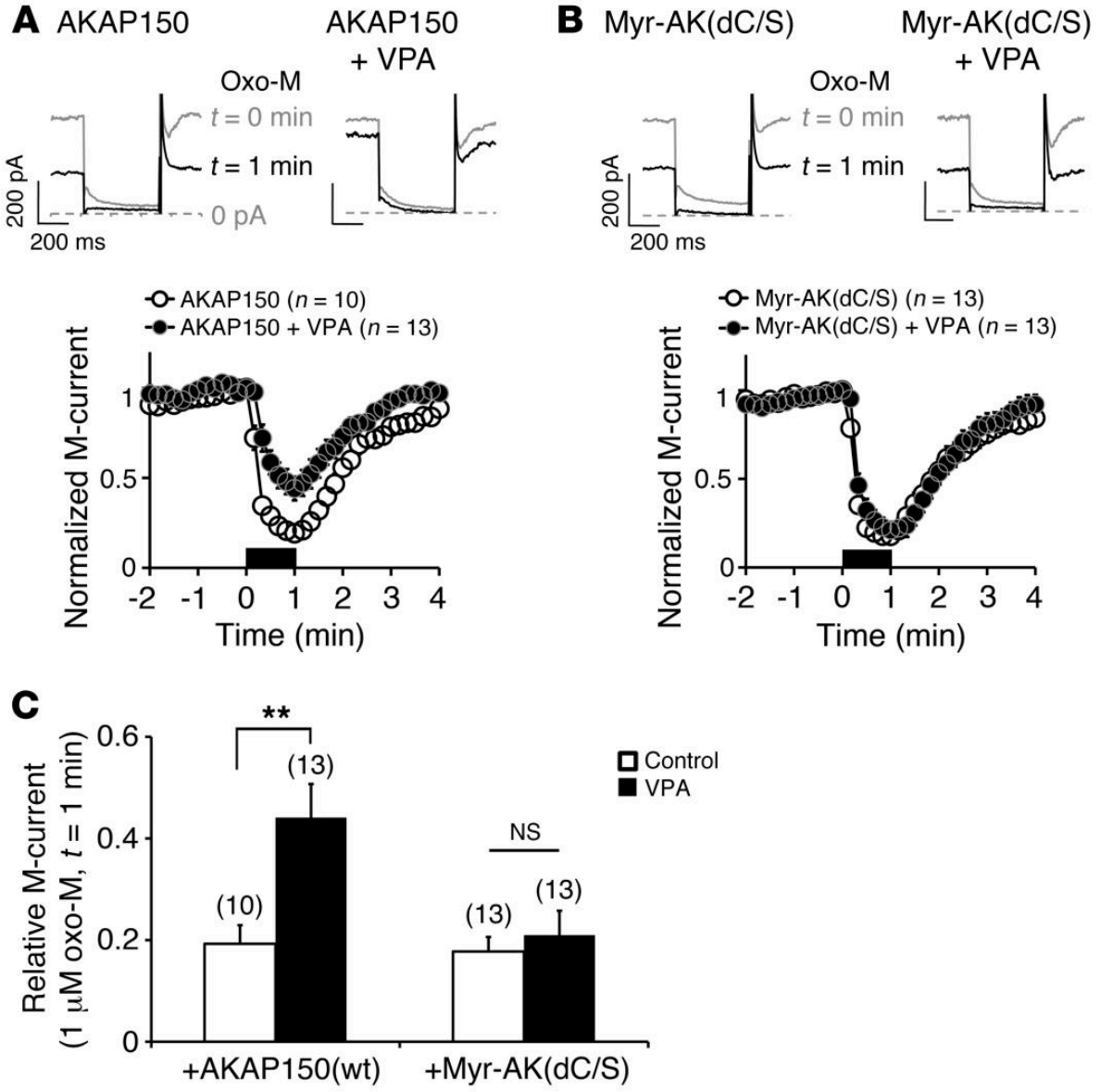

Figure 3.9. M-current suppression became resistant to VPA treatment when a myristoylated AKAP150 mutant was overexpressed in SCG neurons.

A. Current traces (top) and pooled results (bottom) showing oxo-M responses of the M-current in rat SCG neurons overexpressing wild-type AKAP150. 2 mM VPA treatment attenuated responses to 1 μM oxo-M. Black box indicates presence of oxo-M. **B.** Current traces (top) and pooled results (bottom) showing oxo-M responses of the M-current from SCG neurons overexpressing the myristoylation site-attached AKAP150(C36S/C123S), Myr-AK(dC/S). 2 mM VPA treatment did not affect muscarinic response in Myr-AK(dC/S) overexpressed neurons. **C.** Histogram summarizing results shown in A and B. ** < 0.01, NS: not significant, unpaired *t* test with Welch's correction. Error bars show SEM.

References

1 French, J. A. & Pedley, T. A. Clinical practice. Initial management of epilepsy. *N Engl J Med* **359**, 166-176, doi:10.1056/NEJMcp0801738 (2008).

2 McLean, M. J. & Macdonald, R. L. Sodium valproate, but not ethosuximide, produces use- and voltage-dependent limitation of high frequency repetitive firing of action potentials of mouse central neurons in cell culture. *J Pharmacol Exp Ther* **237**, 1001-1011 (1986).

3 Nau, H. & Loscher, W. Valproic acid: brain and plasma levels of the drug and its metabolites, anticonvulsant effects and gamma-aminobutyric acid (GABA) metabolism in the mouse. *J Pharmacol Exp Ther* **220**, 654-659 (1982).

4 Phiel, C. J. *et al.* Histone deacetylase is a direct target of valproic acid, a potent anticonvulsant, mood stabilizer, and teratogen. *J Biol Chem* **276**, 36734-36741, doi:10.1074/jbc.M101287200 (2001).

5 Jentsch, T. J. Neuronal KCNQ potassium channels: physiology and role in disease. *Nat Rev Neurosci* **1**, 21-30, doi:10.1038/35036198 (2000).

6 Delmas, P. & Brown, D. A. Pathways modulating neural KCNQ/M (Kv7) potassium channels. *Nat Rev Neurosci* **6**, 850-862, doi:10.1038/nrn1785 (2005).

7 Soh, H., Pant, R., LoTurco, J. J. & Tzingounis, A. V. Conditional deletions of epilepsy-associated KCNQ2 and KCNQ3 channels from cerebral cortex cause differential effects on neuronal excitability. *J Neurosci* **34**, 5311-5321, doi:10.1523/JNEUROSCI.3919-13.2014 (2014).

8 Avoli, M. The Epileptic Hippocampus Revisited: Back to the Future. *Epilepsy Curr* **7**, 116-118, doi:10.1111/j.1535-7511.2007.00194.x (2007).

9 Bell, B., Lin, J. J., Seidenberg, M. & Hermann, B. The neurobiology of cognitive disorders in temporal lobe epilepsy. *Nature reviews. Neurology* **7**, doi:10.1038/nrneurol.2011.3 (2011).

10 Miceli, F. *et al.* Genotype-phenotype correlations in neonatal epilepsies caused by mutations in the voltage sensor of K(v)7.2 potassium channel subunits. *Proc Natl Acad Sci U S A* **110**, 4386-4391, doi:10.1073/pnas.1216867110 (2013).

11 Rundfeldt, C. & Netzer, R. The novel anticonvulsant retigabine activates M-currents in Chinese hamster ovary-cells tranfected with human KCNQ2/3 subunits. *Neurosci Lett* **282**, 73-76 (2000).

12 Raol, Y. H., Lapides, D. A., Keating, J. G., Brooks-Kayal, A. R. & Cooper, E. C. A KCNQ channel opener for experimental neonatal seizures and status epilepticus. *Ann Neurol* **65**, 326-336, doi:10.1002/ana.21593 (2009).

13 Marrion, N. V. Control of M-current. *Annu Rev Physiol* **59**, 483-504, doi:10.1146/annurev.physiol.59.1.483 (1997).

14 Gamper, N. & Shapiro, M. S. Calmodulin mediates Ca2+-dependent modulation of M-type K+ channels. *J Gen Physiol* **122**, 17-31, doi:10.1085/jgp.200208783 (2003).

15 Suh, B. C. & Hille, B. Recovery from muscarinic modulation of M current channels requires phosphatidylinositol 4,5-bisphosphate synthesis. *Neuron* **35**, 507-520 (2002).

16 Hoshi, N. *et al.* AKAP150 signaling complex promotes suppression of the M-current by muscarinic agonists. *Nat Neurosci* **6**, 564-571, doi:10.1038/nn1062 (2003).

17 Kosenko, A. *et al.* Coordinated signal integration at the M-type potassium channel upon muscarinic stimulation. *EMBO J* **31**, 3147-3156, doi:10.1038/emboj.2012.156 (2012).

18 Suh, B. C. & Hille, B. PIP2 is a necessary cofactor for ion channel function: how and why? *Annu Rev Biophys* **37**, 175-195, doi:10.1146/annurev.biophys.37.032807.125859 (2008).

19 Wong, W. & Scott, J. D. AKAP signalling complexes: focal points in space and time. *Nat Rev Mol Cell Biol* **5**, 959-970, doi:10.1038/nrm1527 (2004).

20 Hoshi, N., Langeberg, L. K. & Scott, J. D. Distinct enzyme combinations in AKAP signalling complexes permit functional diversity. *Nat Cell Biol* **7**, 1066-1073, doi:10.1038/ncb1315 (2005).

21 Tunquist, B. J. *et al.* Loss of AKAP150 perturbs distinct neuronal processes in mice. *Proc Natl Acad Sci U S A* **105**, 12557-12562, doi:10.1073/pnas.0805922105 (2008).

22 Delint-Ramirez, I., Willoughby, D., Hammond, G. R., Ayling, L. J. & Cooper, D. M. Palmitoylation targets AKAP79 protein to lipid rafts and promotes its regulation of calcium-sensitive adenylyl cyclase type 8. *J Biol Chem* **286**, 32962-32975, doi:10.1074/jbc.M111.243899 (2011).

23 Keith, D. J. *et al.* Palmitoylation of A-kinase anchoring protein 79/150 regulates dendritic endosomal targeting and synaptic plasticity mechanisms. *J Neurosci* **32**, 7119-7136, doi:10.1523/JNEUROSCI.0784-12.2012 (2012).

24 Resh, M. D. Fatty acylation of proteins: new insights into membrane targeting of myristoylated and palmitoylated proteins. *Biochim Biophys Acta* **1451**, 1-16 (1999).

25 Fukata, Y. & Fukata, M. Protein palmitoylation in neuronal development and synaptic plasticity. *Nat Rev Neurosci* **11**, 161-175, doi:10.1038/nrn2788 (2010).

26 Kang, R. *et al.* Neural palmitoyl-proteomics reveals dynamic synaptic palmitoylation. *Nature* **456**, 904-909, doi:10.1038/nature07605 (2008).

27 Dell'Acqua, M. L., Faux, M. C., Thorburn, J., Thorburn, A. & Scott, J. D. Membrane-targeting sequences on AKAP79 bind phosphatidylinositol-4, 5-bisphosphate. *EMBO J* **17**, 2246-2260, doi:10.1093/emboj/17.8.2246 (1998).

28 Smith, I. M. & Hoshi, N. ATP competitive protein kinase C inhibitors demonstrate distinct state-dependent inhibition. *PLoS One* **6**, e26338, doi:10.1371/journal.pone.0026338 (2011).

29 Gallegos, L. L., Kunkel, M. T. & Newton, A. C. Targeting protein kinase C activity reporter to discrete intracellular regions reveals spatiotemporal differences in agonist-dependent signaling. *J Biol Chem* **281**, 30947-30956, doi:10.1074/jbc.M603741200 (2006).

30 Thomas, G. M., Hayashi, T., Chiu, S. L., Chen, C. M. & Huganir, R. L. Palmitoylation by DHHC5/8 targets GRIP1 to dendritic endosomes to regulate AMPA-R trafficking. *Neuron* **73**, 482-496, doi:10.1016/j.neuron.2011.11.021 (2012).

31 Wan, J., Roth, A. F., Bailey, A. O. & Davis, N. G. Palmitoylated proteins: purification and identification. *Nat Protoc* **2**, 1573-1584, doi:10.1038/nprot.2007.225 (2007).

32 Belmaker, R. H. Bipolar disorder. *N Engl J Med* **351**, 476-486, doi:10.1056/NEJMra035354 (2004).

33 Borsotto, M. *et al.* PP2A-Bgamma subunit and KCNQ2 K+ channels in bipolar disorder. *Pharmacogenomics J* **7**, 123-132, doi:10.1038/sj.tpj.6500400 (2007).

34 Brown, D. A. Muscarinic acetylcholine receptors (mAChRs) in the nervous system: some functions and mechanisms. *Journal of molecular neuroscience : MN* **41**, 340-346, doi:10.1007/s12031-010-9377-2 (2010).

35 Romero, M., Reboreda, A., Sanchez, E. & Lamas, J. A. Newly developed blockers of the M-current do not reduce spike frequency adaptation in cultured mouse sympathetic neurons. *Eur J Neurosci* **19**, 2693-2702, doi:10.1111/j.1460-9568.2004.03363.x (2004).

36 Wang, H. S. *et al.* KCNQ2 and KCNQ3 potassium channel subunits: molecular correlates of the M-channel. *Science* **282**, 1890-1893 (1998).

37 Tatulian, L., Delmas, P., Abogadie, F. C. & Brown, D. A. Activation of expressed KCNQ potassium currents and native neuronal M-type potassium currents by the anti-convulsant drug retigabine. *J Neurosci* **21**, 5535-5545 (2001).

38 Hoshi, N., Langeberg, L. K., Gould, C. M., Newton, A. C. & Scott, J. D. Interaction with AKAP79 modifies the cellular pharmacology of PKC. *Mol Cell* **37**, 541-550, doi:10.1016/j.molcel.2010.01.014 (2010).

39 Ben-Ari, Y. & Cossart, R. Kainate, a double agent that generates seizures: two decades of progress. *Trends Neurosci* **23**, 580-587 (2000).

40 Popovici, T. *et al.* Effects of kainic acid-induced seizures and ischemia on c-fos-like proteins in rat brain. *Brain Res* **536**, 183-194 (1990).

41 Gall, C., Murray, K. & Isackson, P. J. Kainic acid-induced seizures stimulate increased expression of nerve growth factor mRNA in rat hippocampus. *Brain Res Mol Brain Res* **9**, 113-123 (1991).

42 Botelho, R. J. *et al.* Localized biphasic changes in phosphatidylinositol-4,5-bisphosphate at sites of phagocytosis. *J Cell Biol* **151**, 1353-1368 (2000).

43 Zis, A. P., Nomikos, G. G., Brown, E. E., Damsma, G. & Fibiger, H. C. Neurochemical effects of electrically and chemically induced seizures: an in vivo microdialysis study in the rat hippocampus. *Neuropsychopharmacology* **7**, 189-195 (1992).

44 Baptista, T., Weiss, S. R., Zocchi, A., Sitcoske, M. & Post, R. Electrical kindling is associated with increases in amygdala acetylcholine levels: an in vivo microdialysis study. *Neurosci Lett* **167**, 133-136 (1994).

45 Shouse, M. N., Staba, R. J., Ko, P. Y., Saquib, S. F. & Farber, P. R. Monoamines and seizures: microdialysis findings in locus ceruleus and amygdala before and during amygdala kindling. *Brain Res* **892**, 176-192 (2001).

46 Kokaia, M., Kalen, P., Bengzon, J. & Lindvall, O. Noradrenaline and 5-hydroxytryptamine release in the hippocampus during seizures induced by hippocampal kindling stimulation: an in vivo microdialysis study. *Neuroscience* **32**, 647-656 (1989).

47 Lehmann, A., Isacsson, H. & Hamberger, A. Effects of in vivo administration of kainic acid on the extracellular amino acid pool in the rabbit hippocampus. *J Neurochem* **40**, 1314-1320 (1983).

48 Pena, F. & Tapia, R. Relationships among seizures, extracellular amino acid changes, and neurodegeneration induced by 4-aminopyridine in rat hippocampus: a microdialysis and electroencephalographic study. *J Neurochem* **72**, 2006-2014 (1999).

49 Yamasaki, M., Matsui, M. & Watanabe, M. Preferential localization of muscarinic M1 receptor on dendritic shaft and spine of cortical pyramidal cells and its anatomical evidence for volume transmission. *J Neurosci* **30**, 4408-4418, doi:10.1523/jneurosci.5719-09.2010 (2010).

50 Martinello, K. *et al.* Cholinergic afferent stimulation induces axonal function plasticity in adult hippocampal granule cells. *Neuron* **85**, 346-363, doi:10.1016/j.neuron.2014.12.030 (2015).

51 Felder, C. C., Kanterman, R. Y., Ma, A. L. & Axelrod, J. Serotonin stimulates phospholipase A2 and the release of arachidonic acid in hippocampal neurons by a type 2 serotonin receptor that is independent of inositolphospholipid hydrolysis. *Proc Natl Acad Sci U S A* **87**, 2187-2191 (1990).

52 Lujan, R., Nusser, Z., Roberts, J. D., Shigemoto, R. & Somogyi, P. Perisynaptic location of metabotropic glutamate receptors mGluR1 and mGluR5 on dendrites and dendritic spines in the rat hippocampus. *Eur J Neurosci* **8**, 1488-1500 (1996).

53 Clinckers, R., Smolders, I., Meurs, A., Ebinger, G. & Michotte, Y. Anticonvulsant action of hippocampal dopamine and serotonin is independently mediated by D and 5-HT receptors. *J Neurochem* **89**, 834-843, doi:10.1111/j.1471-4159.2004.02355.x (2004).

54 Giorgi, F. S., Pizzanelli, C., Biagioni, F., Murri, L. & Fornai, F. The role of norepinephrine in epilepsy: from the bench to the bedside. *Neuroscience and biobehavioral reviews* **28**, 507-524, doi:10.1016/j.neubiorev.2004.06.008 (2004).

55 Silva, M. F. *et al.* Valproic acid metabolism and its effects on mitochondrial fatty acid oxidation: a review. *J Inherit Metab Dis* **31**, 205-216, doi:10.1007/s10545-008-0841-x (2008).

56 Bialer, M. & Yagen, B. Valproic Acid: second generation. *Neurotherapeutics : the journal of the American Society for Experimental NeuroTherapeutics* **4**, 130-137, doi:10.1016/j.nurt.2006.11.007 (2007).

Chapter Four

Role of M-current suppression in seizures and the process of epileptogenesis

Introduction

Cognitive and motor functions are dependent on neural circuits communicating with precise spatial and temporal resolution. On the other hand, epilepsy abruptly and sporadically disrupts normal cognitive functions with excessive synchronous activity in cerebral neurons[1]. Presently, epilepsy is among the more debilitating pathologies that affects nearly 1% of the population and can develop at all stages of life[2]. Numerous conditions are described under the broad heading of epilepsy, developing from either genetic or acquired sources[3]. Epileptic conditions are diagnosed by their distinctive behavioral characteristics, electrographic activity, affected molecular mechanisms and focal points[4,5]. To date, numerous therapeutics have been developed to treat seizures, however, the underlying mechanisms that contribute to this pathology are still a topic of heated debate, and many forms of epilepsy remain resistant to available therapeutics.

Of the known mechanisms linked to epilepsy, channelopathies predominate, with the majority being derived from mutations in potassium channels. Notably, over 30 mutations in Kv7 channels have been reported to be associated with or the cause of epilepsy and encephalopathies[6-8]. These mutations have been reported to cause development of epilepsy through the reduction of M-current surface expression,

changing voltage dependence of channel activity or altering subcellular localization[7,9,10]. However, rare mutations that augment M-current activity also increase the susceptibility to seizure induction[11,12]. This suggests that basal M-current activity plays an important role in prevention of pathological hyperexcitability and that a delicate balance must be maintained to ensure normal function in the brain. We hypothesized that hyperexcitability within the cortex during seizures induces the release of neurotransmitters that in turn suppress the M-current.

In a previous work, our lab identified a PKC phosphorylation site on the Kv7.2 subunit that is key for channel suppression through Gq-coupled receptor activation[13,14], further detailed in chapter 1. Thus, we developed a transgenic mouse line with an alanine substitution for this residue, KCNQ2(S559A), that maintains normal M-current activity while being resistant to neurotransmitter-induced suppression. In chapter 3 we gave evidence that the M-current is normally suppressed during seizures[15], and that one of the mechanisms for the anticonvulsive action of valproic acid is the consequence of interfering with Kv7.2 phosphorylation by PKC, thereby preventing channel suppression. Here, we investigated the pathological role of M-current suppression in seizures and epileptogenesis. Using kainic acid model of chemically induced status epilepticus we confirmed our proposed mechanism for the anticonvulsant action of valproic acid and provide further evidence that the M-current is normally suppressed during ictal activities. We also utilize a pilocarpine model of temporal lobe epilepsy[16] to determine if there is prolonged suppression of the M-current after status epilepticus and whether channel suppression plays a role in the process of epileptogenesis.

Experimental Procedures

Generation of KCNQ2(S559A) mice.

Generation of the targeting vector was performed at BAC Recombineering Core, Duke Comprehensive Cancer Center (Duke University). An alanine mutation of serine residue 559 of the kcnq2 gene (transcript variant 1) was introduced to the vector KCNQ2(S559A). Homologous recombination of the targeting vector was performed using a C57BL/6NTac derived ES cell line (JM8.N4) from the UC Irvine Transgenic Mouse Facility. Successful recombination was confirmed by Southern blots and the embryonic stem cell clone with the strongest karyotyping signal was used to generate chimeric mice. The offspring of these chimeras were screened for germline transmission by genomic PCR (Fig. 4.1A). This floxed Kv7.2(S559A) mouse line, Q2E13(S559A)/neo, was then crossed with C57BL/6 background Cre mice that express Cre in oocytes, C57BL/6-Tg (Zp3-cre)93Knw/j, to generate global knock-in mice. Excision of the neo cassette was confirmed by genomic PCR. Mice were continually backcrossed with C57BL/6J mice.

Electrophysiological measurement of hippocampal neurons.

Mouse neonatal hippocampal culture was prepared as described[17]. For measurement of the M-current in hippocampal neurons, perforated patch with amphotericin B was used as described[13,17]. Briefly, amplitudes of the M-currents were measured as deactivating currents during 500-ms test pulses to –60 mV from a holding potential of –30 mV. For XE991 experiments, application of 20 μM XE991 was given while cells were held at –30 mV for 1 min, then returned to –70 mV.

Kainate-induced seizures.

For seizure experiments C57BL/6 and KCNQ2(S559A) transgenic mice of both sexes (3-5 months old) were used. For kainate-induced seizure experiments, kainate (s.c.) was injected at the indicated dose. One hour after kainate administration, mice were injected either with 2 mg/kg XE991 (i.p.) in Dulbecco's phosphate-buffered saline (DPBS), or DPBS alone. For VPA experiments, adult mice were administered (i.p.) either freshly prepared sodium valproate (250 mg/kg, VPA) or physiological saline solution twice daily for 3.5 days. Kainate treatment started 6 hours after the final VPA administration. Mice were video-taped for the subsequent 4 hours after kainate injection, and behavior was scored by treatment and genotype blind observers every 10 minutes according to a previously described[15] modified Racine scale with the following criteria: 1) immobility; 2) rigidity; 3) automatisms with scratching, head bobbing and circling; 4) intermittent rearing and falling; 5) continuous rearing and falling; 6) tonic-clonic whole body convulsions and rapid jumping. All mice that died during the experiments were assigned stage 6 thereafter.

Pilocarpine-induced seizures.

C57BL/6 and KCNQ2(S559A) transgenic mice of both sexes (2-3 months old) were used. For pilocarpine-induced seizure experiments, methyl scopolamine (1 mg/kg i.p.) was administered 10 minutes before injecting pilocarpine (289 mg/kg i.p.). 30 minutes after pilocarpine administration, mice were injected either with 2 mg/kg XE991 (i.p.) in Dulbecco's phosphate-buffered saline (DPBS), or DPBS alone. Mice were video-taped for the subsequent 2 hours after pilocarpine injection, and behavior was scored by treatment-blind observers every 10 min according to a modified Racine scale with the following criteria: 1) immobility and facial twitching; 2) head bobbing, Straub tail,

“wet dog shakes”; 3) unilateral forelimb myoclonus; 4) bilateral forelimb myoclonus, rearing; 5) total loss of balance, generalized convulsions. Animals that died during the experiments were assigned stage 5 thereafter. For seizure survival experiments, mice were administered diazepam (5 mg/kg i.p.) to terminate seizures and were given 5% glucose infusions until body weight stabilized.

Spontaneous recurrent seizures

Pilocarpine-experienced wild-type and Q2KI mice that underwent status epilepticus were selected to observe for development of spontaneous ictal activity. Status epilepticus was determined by behavioral seizures that reach stage 5 within the two-hour observation period with at least two additional incidences of stage 4 - 5 seizures. Two weeks following status epilepticus animals were observed for 3 hours/day for the proceeding 3 weeks by a treatment and genotype blind observer. Animals that underwent $\geq$ stage 4 seizure were recorded and the frequency of ictal activity was evaluated.

Antibodies.

Antibodies used for immunohistochemistry are as follows: c-fos (Cat No. PC38; Calbiochem), GAD67 (Cat. No. MAR5406; EMD Millipore), ZnT3 (Cat. No. 197002; Synaptic Systems), Cy3 labeled goat anti-rabbit secondary antibody (Cat. No. AP187C; Millipore), and Alexa Fluor 568 goat anti-mouse secondary antibody (Cat. No. A11004; Invitrogen.

Immunohistochemistry.

Immunohistochemistry protocol was followed as previously described[15]. 1 h after injection of kainate/pilocarpine, mice were deeply anesthetized with isoflurane before

being transcardially perfused with iced cold 4% paraformaldehyde in PBS (pH 7.4). Brains were then removed and post-fixed in 4% paraformaldehyde in PBS (pH 7.4) overnight at 4˚C. Brains were sectioned into coronal slices (30 μm) using a vibratome (Leica, VT-1200). Free-floating sections were washed with PBS in 24-well dishes and then incubated with PBS containing 0.3% hydrogen peroxide and 10% methanol for 10 min. After 3 washes with PBS, sections were incubated with a blocking buffer containing 0.5% Triton X-100 and 1% normal goat serum in PBS. Sections were then incubated with primary antibody mixture containing: rabbit anti-c-FOS antibody (1:1000 dilution) or rabbit anti-ZnT3 antibody (1:1000 dilution) or mouse anti-GAD67 antibody (1:5000 dilution) in the blocking solution for 48 h at 4˚C. After 2 washes with PBS followed by 2 washes with Tris-buffered saline (TBS), sections were incubated with a 1:500 dilution of Cy3-conjugated anti-rabbit secondary antibody (c-fos and ZnT3) or Alexa Fluor 568 anti mouse secondary antibody (GAD67) in TBS containing 0.5% Triton X-100 and 1% normal goat serum for 2 h at room temperature. After wash, sections were mounted onto glass slides using VECTASHIELD with DAPI (Vector Laboratories). Immunofluorescent images were acquired using a fluorescent light microscope (Leica, DM4000B) equipped with a CCD camera (Optronics MicroFire, OPTMIF). Areas around the dentate gyrus, CA1 and CA3 were selected and the average fluorescence intensity within each corresponding region of interest from DAPI and c-FOS staining images was quantified by observers blind to treatments using MetaMorph (Molecular devices). Nucleus-free regions in the stratum oriens were used as a background for immunofluorescent staining.

Fluoro jade C staining.

Fixed coronal brain slices were incubated with PBS in 24-well dishes for 4 washes of 5 minutes before being mounted onto gelatin-coated slides. Slides were then dried at 50˚C for 30 minutes before being immersed for 5 minutes in a basic alcohol solution (0.5% NaOH, 80% EtOH). Slides were then washed with 70% EtOH for 2 minutes followed by a 2 minute wash with deionized water. Tissue was counterstained with a 0.06% solution of $KMnO_4$ for 10 minutes and then washed twice with deionized water for 2 minutes. Degenerating neurons were selectively labeled by incubating with 0.0001% Fluoro jade C (Cat. No. 1FJC; Histo-Chem Inc.) dissolved in 0.1% acetic acid for 20 minutes. Slides were then washed four times in deionized water for 1 minute, dried at 50˚C for 10 minutes before clearing in xylene for 4 minutes and mounting with DPX mounting medium. Immunofluorescent images were acquired using a fluorescent light microscope (Leica, DM4000B) equipped with a CCD camera (Optronics MicroFire, OPTMIF). Fluorescent neurons were then counted within the areas of the dentate gyrus, CA1 and CA3.

Results

Generation of KCNQ2(S559A) mice.

The KCNQ2(S559A) targeting vector was used for homologous recombination in C57BL/6 embryonic stem cells (Figure 4.1A). Recombination was confirmed by Southern blots and embryonic stem cells with successful recombination were used to generate chimeras using C57BL/6 mouse lines. Germline transmission was determined using genomic PCR with primers flanking the loxP sites. KCNQ2(S559A)/neo mice were crossed with mice that express Cre in oocytes, C57BL/6-Tg (Zp3-cre)93Knw/j, to generate global knock-in mice, which were used in the proceeding experiments.

Characterization of M-current in KCNQ2(S559A) mice.

Our lab previously confirmed that KCNQ2(S559A) knock-in (Q2KI) mice behave same as wild-type littermates, with normal growth and no differences in gross brain morphology (unpublished results). Macroscopic currents from cultured hippocampal neurons revealed that Q2KI mice have normal M-current densities (Figure 4.1B). Importantly, suppression of the M-current through muscarinic stimulation with oxotremorine-M was greatly attenuated in Q2KI mice (Figure 4.1B & C). However, the M-current could still be suppressed directly with the Kv7 specific inhibitor XE991. These data indicate that we have developed a mouse line with normal M-current activity that is resistant to suppression from Gq-coupled receptor activation.

M-current is suppressed during seizure but preserved in KCNQ2(S559A) mice.

We have previously demonstrated that the anticonvulsive action of valproic acid (VPA) is owed in part to preserved M-current[15]. This alternatively suggests that the M-current is normally suppressed as a consequence of seizure activity. If suppression of

the M-current contributes to the propagation of ictal activities then our Q2KI mice should have an anticonvulsant phenotype. For confirmation, a kainate model of induced status epilepticus was used. Kainic acid (30 mg/kg s.c.) induced generalized convulsions in wild-type mice (stage 6, Fig 4.2A & B) that typically ended in mortality (8/11). Q2KI mice showed reduced seizure severity as well as duration (Figure 4.2B & C) with no incidence of mortality. To confirm that the anticonvulsive effect is M-current specific, mice were treated with XE991 (2 mg/kg i.p.) 60 minutes after administering kainic acid. As expected, XE991 transiently exacerbated seizure severity in Q2KI mice to levels equivalent with wild-type (Figure 4.2).

As described in chapter 3, we hypothesized that the anticonvulsant action of VPA is through interfering with the phosphorylation of serine residue 559 in the Kv7.2 subunit. Since Q2KI mice lack this phosphorylation acceptor, VPA should provide no additional anticonvulsive action in Q2KI mice if our hypothesis is correct. To test this, we utilized the same experimental condition of sub-chronic valproic acid in Q2KI mice (250 mg/kg VPA × 2/day × 3.5 days)[15]. If other proposed mechanisms for valproic acid contribute to its action then treatment of Q2KI mice with VPA should provide stronger anticonvulsive action. Since Q2KI mice are resistant to kainate seizure an elevated dose of kainic acid (34 mg/kg s.c.) was used to increase seizure severity throughout the period of observation, however no differences were detected, as expected (Figure 4.3). A control group of Q2KI mice were treated with diazepam (5 mg/kg i.p.) 20 minutes after kainate, which transiently reduced seizure severity (Figure 4.3C). These results suggest that VPA provided no additional protection in Q2KI mice, confirming that a key

mechanism underlying valproic acid's chronic anticonvulsive effect is through interference of phosphorylation of Kv7.2 S559 residue.

When using global knock-in animals, compensation or developmental changes due to expression of mutant channel is a potential issue, which may underlie the anticonvulsive phenotype. To exclude this possibility, we examined the effect of transient removal of the M-current in Q2KI mice by XE991 (Figure 4.3). Treatment with XE991 coincided with transient removal of the anticonvulsant phenotype in Q2KI mice, suggesting that it is through a M-current specific mechanism. We previously demonstrated in wild-type mice that treatment with retigabine before seizure induction is protective, however, treatment during ictal activity was not efficacious since retigabine cannot open suppressed M-current (chapter 3). Therefore as an additional confirmation, we tested whether the Kv7 channel opener retigabine augments the protective phenotype of Q2KI mice after induction of seizure. We used an elevated dose of kainic acid (35 mg/kg s.c.) that induced generalized convulsions in the majority of Q2KI mice (4/5 mice, Figure 4.4A & B). If Q2KI mice indeed retain M-current throughout the duration of the seizure, the anticonvulsant effect of retigabine should be effective regardless of when retigabine is administered. As expected, treatment of Q2KI mice with retigabine (10 mg/kg i.p.) reduced seizure severity and duration when administered either before or during seizures (Figure 4.4).

M-current suppression in a pilocarpine model of temporal lobe epilepsy.

In order to investigate the role of M-current suppression in the pathology of epileptogenesis we developed a model of temporal lobe epilepsy using our Q2KI mice. One caveat of using mice with a C57BL/6 background is their innate resistance to

spontaneously recurring seizures when induced with kainic acid[18,19]. However, it has been shown that pilocarpine can generate spontaneous recurrent seizures (SRS) in C57BL/6 mice[20]. To this end, we assayed seizure severity of wild-type and Q2KI mice using pilocarpine. Pilocarpine is an agonist for the M1 muscarinic receptor that elevates glutamate levels and destabilizes excitatory and inhibitory transmission inducing generalized convulsions[20].

To confirm the protective phenotype of Q2KI mice, wild-type and Q2KI mice were compared using a separate Racine scale (stages 1-5) established specifically for the distinct characteristics of pilocarpine-induced seizures. Mice were first pretreated with methyl scopolamine (1 mg/kg i.p.) to block peripheral side effects of pilocarpine. Approximately 10 minutes later mice were treated with pilocarpine (289 mg/kg i.p.). A subset of Q2KI mice also treated with XE991 (2 mg/kg i.p., t = 30 min) to determine M-current contribution to anticonvulsive phenotype (Figure 4.5A). Wild-type mice developed limbic seizures typically within the first 60 minutes with intermittent bouts of generalized convulsions (stage 5), the majority developing status epilepticus (7/9 mice). Q2KI mice showed reduced seizure severity with no occurrence of status epilepticus. However XE991-treated Q2KI mice (2 mg/kg i.p., t = 30 min) developed the same seizure severity as wild-type mice (Figure 4.5B & C).

The Pilocarpine model of acquired epilepsy has been shown to be an effective tool for determining mechanisms involved in temporal lobe epilepsy[21]. In order to effectively determine the role of M-current suppression during the process of epileptogenesis, wild-type and Q2KI mice must first undergo equivalent status epilepticus (SE). To this end animals were given the same condition described above

with both groups receiving XE991 to effectively suppress the M-current for the duration of the seizure. Wild-type and Q2KI mice demonstrated equivalent seizure severity throughout the time course of pilocarpine-induced seizure, with no differences in occurrence of status epilepticus[22-24] (P = 0.078, Fisher exact test) or mortality (P = 0.178, Fisher exact test). Put together, these results suggest that this condition provides equivalent status epilepticus between genotypes. For termination of seizures animals were administered a positive allosteric modulator of $GABA_A$ receptors[25] (5 mg/kg i.p.) 120 minutes after pilocarpine treatment. Animals that reached stage 5 with at least two additional occurrences of $\geq$ stage 4 during the observation period were considered to have undergone status epilepticus[22-24] and were further analyzed for development of epileptogenesis.

Pilocarpine-induced c-fos expression corresponded with seizure severity.

Behavioral observations may not accurately describe seizure severity, and instead may merely indicate hyperactivity in the motor cortex. We have previously shown that induction of c-fos is well correlated with accumulative neural activity during seizures[15,26-28]. Therefore, we quantified c-fos expression in the hippocampus, a focal point of pilocarpine-induced seizures[26,29]. Brains were collected 1 hour after termination of pilocarpine-induced seizure. Strong expression of c-fos was observed in the dentate gyrus, CA3 and CA1 of pilocarpine-treated wild-type mice, corresponding to hyperactivity within the hippocampus during seizure (Figure 4.6). Pilocarpine-induced c-fos expression was greatly reduced in Q2KI mice in all areas of the hippocampus. Importantly, XE991 did not alter c-fos expression in wild-type mice, but elevated expression of c-fos to wild-type levels in Q2KI mice (Figure 4.6B-D). Taken together

with scored behavioral seizures, these results suggest that co-treatment of pilocarpine and XE991 is sufficient to produce equivalent seizure in both genotypes. Accordingly, this treatment was then used to investigate the role of M-current suppression in the period of time following status epilepticus.

Spontaneous recurrent seizures and comorbidities of epileptogenesis.

Epileptogenesis after status epilepticus involves multiple changes within the cortex. In the first days following the initial insult neurodegeneration can be observed in the hippocampus[22-24]. There is typically a latent period where no ictal activity is observed, which develops into spontaneous recurrent seizures whose frequency plateaus within the first month after the initial insult[21]. At the time when SRS is observed development of new synaptic connections[30] and loss of inhibitory interneurons[31,32] become apparent.

As explained, neurodegeneration and apoptosis are common consequences of status epilepticus observable within the first days following the initial induced seizure[22-24]. Using our established model of pilocarpine-induced temporal lobe epilepsy, the aforementioned comorbidities of epileptogenesis were investigated. We investigated the degree of neurodegeneration 3 days after inducing status epilepticus using fluoro jade C (FJC) as a selective marker of neurodegeneration[33]. SE-experienced wild-type animals showed FJC staining in the dentate gyrus, CA3 and CA1 regions, being most pronounced in the CA1 region (Figure 4.7A & D). However, in SE-experienced Q2KI mice FJC labeling was sparse in all areas of the hippocampus (Figure 4.7A lower, B-D). These data suggest that even when M-current is inhibited during the initial induction of SE, recovery of M-current after metabolism of XE991 reduced neurodegeneration.

Another cohort of animals that underwent pilocarpine+XE991 induced status epilepticus was analyzed for development of spontaneous recurrent seizures (SRS). It is known that there is a latent period after the initial insult where no behavioral pathology is observed that proceeds to development of SRS, typically lasting 2 weeks after SE[21]. Therefore, two weeks following status epilepticus, wild-type and Q2KI mice were recorded 3 hours/day for three weeks and any occurrences of stage 4-5 seizures were noted. All wild-type mice developed SRS (11/11 mice) with a frequency of occurrence at 0.127 $\pm$ 0.001 seizures/hour (Figure 4.8), a rate that is in agreement with other studies of pilocarpine-induced SRS in C57BL/6 mice[34,35]. As would be expected from reduced neurodegeneration, we observed near-absence of observable seizures in Q2KI mice (1/10 mice) as well as a near null rate of occurrence at 0.0022 $\pm$ 0.0022 seizures/hour (Figure 4.8).

Seven weeks after pilocarpine-induced seizure, hippocampi from all animals were collected and assayed by immunohistochemistry. It has been reported that there is a high correlation between the presence of SRS and synaptogenesis[30,36]. This “mossy fiber sprouting” of axonal processes is largely specific to the inner molecular layer of the dentate gyrus[24,37] and can be visualized by upregulation of the zinc transporter, ZnT3[38,39]. In good agreement with the literature, wild-type mice showed elevated levels of ZnT3 compared to no treatment control. In contrast, ZnT3 expression in Q2KI mice remained unchanged (Figure 4.9). These results suggest that disruption of neurotransmitter-induced suppression of the M-current prevents epileptogenesis after SE insult.

Prolonged pathological excitability is suspected to cause neurodegeneration of inhibitory interneurons after seizure, which may not become evident for several weeks proceeding the initial trauma[31,32]. Therefore, to further assess consequences of M-current suppression after status epilepticus the loss of GABAergic interneurons was measured. GABAergic interneurons function in diverse ways including timing of firing and silencing of neural circuits throughout the brain[40,41]. Disinhibition within the cortex via the loss of GABAergic interneurons is thought to contribute to the exacerbation of excitatory neural activity, creating a permissive environment for seizure propagation[42,43]. As Kv7 channels are expressed in both excitatory and inhibitory interneurons[44], M-current suppression during the process of epileptogenesis may contribute to prolonged excitotoxicity that reduces survival in these neurons. Loss of inhibitory interneurons was detected by immunolabeling cells expressing glutamic acid decarboxylase (GAD67) 7 weeks after pilocarpine-induced seizure. In non-treated mice, strong signal of GAD67-positive neurons was seen in the dentate gyrus, CA3 and CA1 region of the hippocampus. SE-experienced wild-type mice showed reduction in all areas of the hippocampus. In contrast SE-experienced Q2KI mice showed no difference in GAD67 fluorescence compared to non-treated control (Figure 4.10).

Discussion

Despite the numerous Kv7 mutations known to cause epilepsy, the contribution of Kv7 channel suppression to the generation and propagation of seizures and epileptogenesis had not been elucidated. Our KCNQ2(S559A) knock-in mice demonstrated removal of the majority of M-current suppression from Gq-coupled receptor activation while preserving basal channel. Ablation of M-current suppression provided and important tool for investigating the pathological consequences of Kv7 channel transitions between the activated and suppressed states. We used this mouse line to investigate the behavioral, cellular and molecular outcomes of M-current suppression during and after ictal activity, utilizing two methods of induced status epilepticus. Kainic acid induced seizures directly activate ionotropic kainate receptors, especially within the hippocampus, and give a comparable model for pathological neural hyperexcitability seen in generalized seizures[45]. Alternatively, excitotoxic damage induced by pilocarpine-induced status epilepticus has been shown to produce numerous comorbidities associated with acquired epilepsy, including neuronal loss, synaptogenesis and development of spontaneous seizures[21].

Our Q2KI mice demonstrated a protective phenotype against chemoconvulsants. When using transgenic animals there is always a possibility of phenotypes occurring through off target effects during development. However, two major results support that the observed anticonvulsive phenotype is M-current specific: 1) the protective phenotype was transiently removed from Q2KI mice when treated with the M-current specific inhibitor XE991 (Figures 4.2 & 4.5), which in chapter 2 was demonstrated to selectively target activated channels, and 2) M-current activity could be augmented by

retigabine in Q2KI mice even when treated 20 minutes after induction of seizure (Figure 4.4). In chapter 3 we demonstrated that seizures in wild-type mice could not be attenuated by retigabine when treated after seizures manifested. Here, we were able to confirm that the anticonvulsive action of valproic acid is through preservation of the M-current (Figure 4.3). This is evident as VPA treatment showed no additional benefit compared to VPA-untreated Q2KI mice. Thus, we concluded that the M-current is not suppressed in Q2KI mice during seizure, which alternatively confirmed our hypothesis in chapter 3 that wild-type M-current is suppressed during seizures. We believe that pathological M-current suppression is a consequence of the abnormal and excessive release of neurotransmitters that activate Gq-coupled receptors, which in turn suppress the M-current. As explained in chapter 3, microdialysis studies in the hippocampus after seizure have revealed elevated levels of numerous neurotransmitters such as acetylcholine, glutamate and dopamine that activate Gq-coupled receptors remained elevated even after seizure activity subsided[46-49].

We also investigated the role of M-current suppression during the latent period after status epilepticus where epileptogenesis occurs. We found that even when the M-current is pharmacologically suppressed during seizure insult, Q2KI mice have a drastically reduced incidence of acquired epilepsy in the weeks following (Figure 4.8). This suggests that wild-type M-current remains suppressed even after ictal activities subside. Little is known about seizure-induced changes in Kv7 channel activity or expression. However, sustained elevation in the levels of neurotransmitters due to synchronous ictal activity could account for prolonged M-current suppression. In a recent study, persistent elevation of glutamate lead to pronounced internalization of the

M-current through a PKC-dependent pathway[50]. If the target of this PKC pathway of Kv7 channel internalization involves phosphorylation of S559 of the Kv7.2 subunit, then the absence of epileptogenesis in Q2KI mice may be due to lack of M-current internalization after SE. Alternatively, it was reported that cholinergic fiber stimulation onto hippocampal granule neurons induce pronounced suppression of axonal Kv7 channels, which was largely irreversible[51]. In this condition, seizure activity may over-stimulate these cholinergic fibers and induce suppression of the M-current, lasting long after ictal activities subside.

Numerous comorbidities accompany acquired epilepsy. Previous studies have suggested that epileptogenesis occurs through a series of processes which occur during the latent period between the initial insult and development of spontaneous recurrent seizures[22,23]. Even though wild-type and Q2KI mice experienced equivalent status epilepticus, Q2KI mice showed drastic reductions in all morbidities assayed (Figure 4.7-10). Q2KI mice recover M-current activity as XE991 is metabolized. As discussed above, there is evidence to suggest that wild-type Kv7 channels would have sustained suppression after seizures subside. That Q2KI mice were protected from epileptogenesis suggest that, at least in this model of acquired epilepsy, prolonged and pronounced suppression of the M-current occurs after the initial episode of status epilepticus and is required for the process of epileptogenesis.

In summary, the M-current is an important deterrent to pathological neural hyperexcitability[52,53]. Namely, synchronous hyperactivity at the focal point of seizure induction leads to release of excessive neurotransmitters into the surrounding area, many of which activate Gq-coupled receptors. In relevant neurons, activating Gq-

coupled receptors leads to activation of AKAP5 anchored PKC, which in turn phosphorylates and suppresses the M-current. Finally, suppression of the M-current promotes hyperexcitability and further release of neurotransmitters that propagate ictal activities throughout the brain. We demonstrated that preserving the M-current after status epilepticus is sufficient to drastically reduce numerous mechanisms involved in epileptogenesis. A remaining question is whether preservation of the M-current after establishment of epilepsy is capable of reducing the frequency and severity of ictal activities. The therapeutic potential of this pathway has yet to be fully explored.

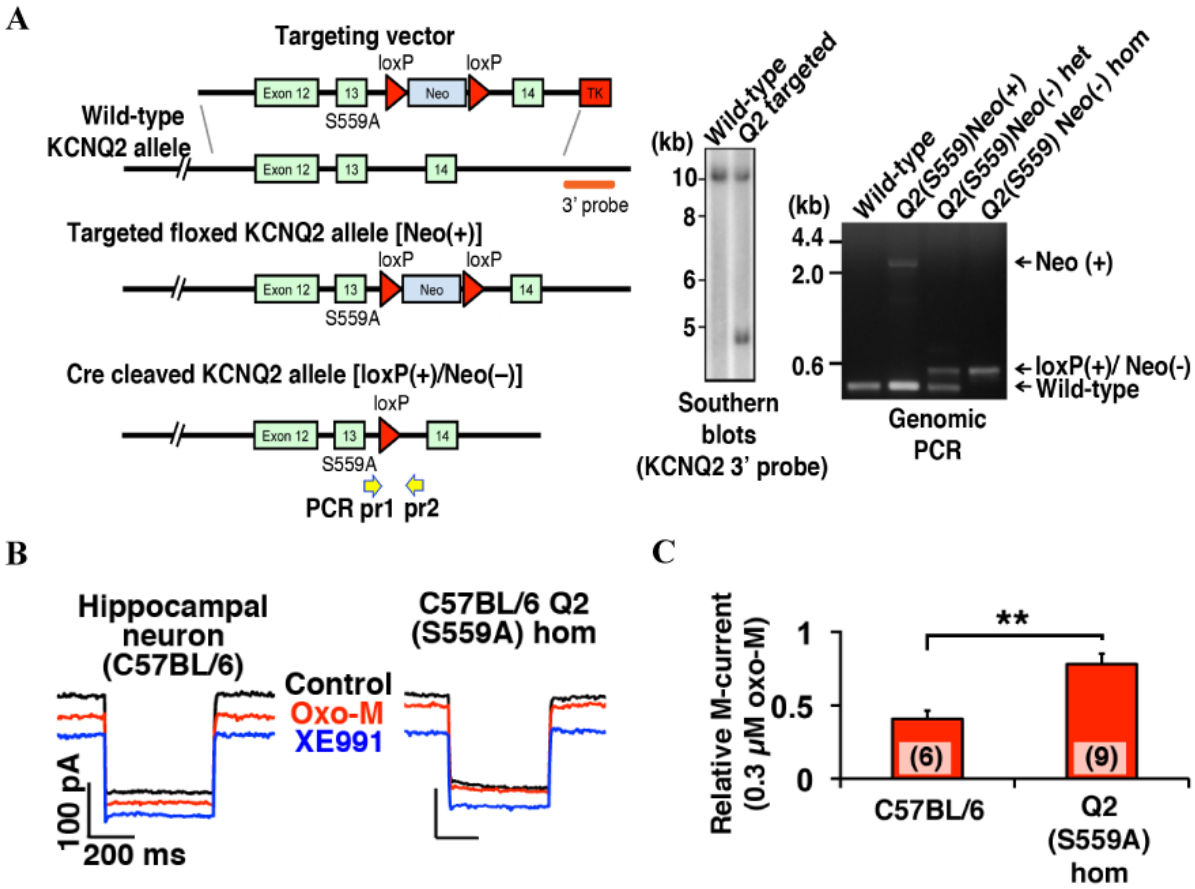

Figure 4.1. Generation of global KCNQ2(S559A) knock-in mice and characterization of M-current suppression.

A. Illustration showing alanine substitution of serine 541 on exon 13 of KCNQ2 gene. Genomic Southern blots confirmed presence of the Neo cassette with KCNQ2(S559A) mutation in floxed heterozygous knock-in mutants. Gel electrophoresis confirms genotypes of wild-type, floxed, and Cre cleaved global heterozygous and homozygous KCNQ2(S559A) mice. **B.** Current traces recorded from cultured hippocampal neurons. KCNQ2(S559A) neurons show attenuated response to oxo-M treatment compared to wildtype. **C.** Pooled results of current suppression induced by 0.3 μM oxo-M. **P < 0.01 using unpaired t test with Welch's correction. Error bars show SEM.

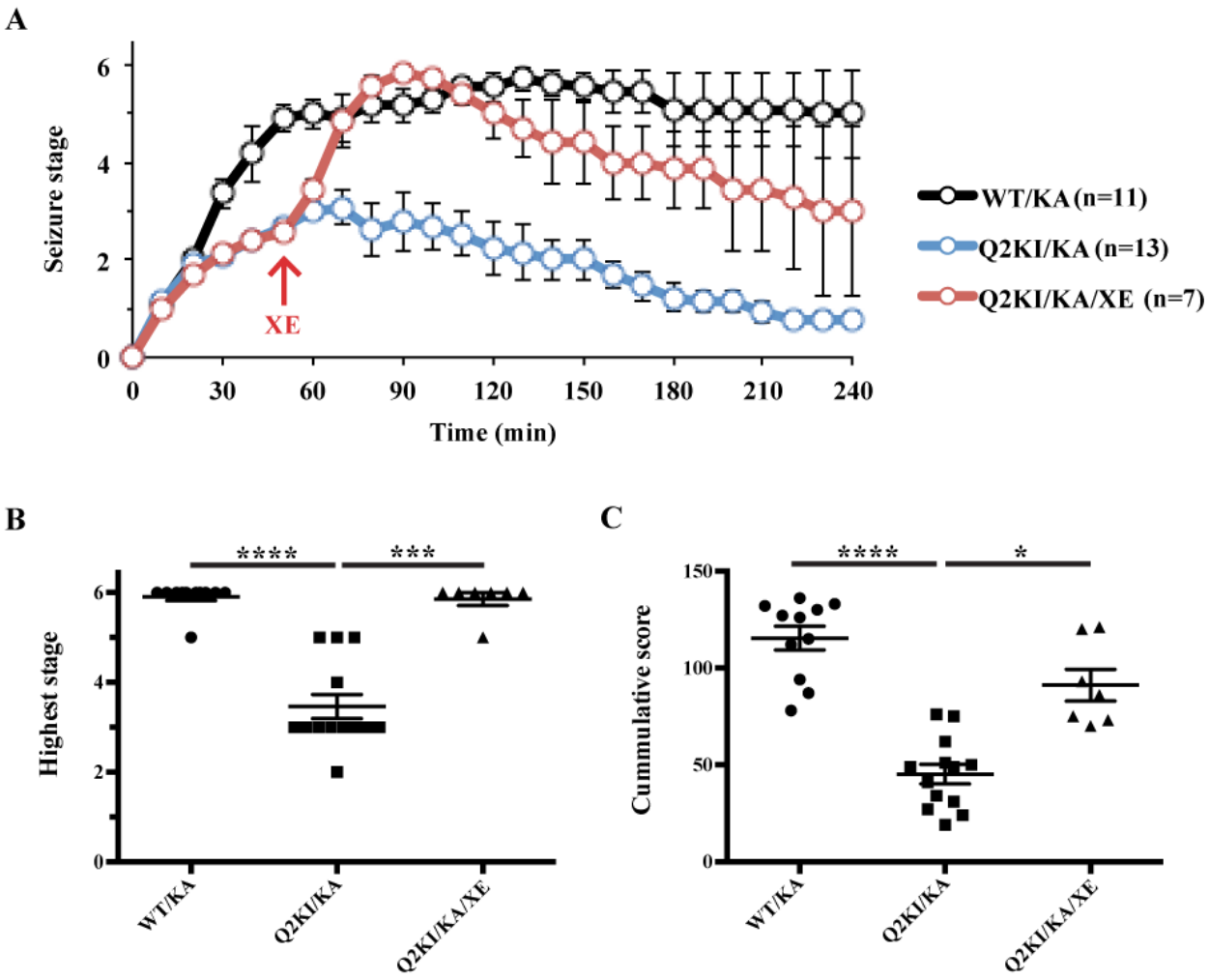

Figure 4.2. XE991 transiently removed anticonvulsive phenotype of Q2KI mice in kainate-induced seizure.

A. Time course of seizure severity during kainate-induced seizure (30 mg/kg KA, t = 0). Knock-in mice have protective phenotype that is transiently removed when treated with M-current-specific inhibitor XE991 (XE 2mg/kg, t = 60 minutes). **B.** Distribution of highest seizure stage reached throughout observation period, knock-in mice show lower seizure severity, removed when M-current is suppressed by XE991. ***P < 0.001 and ****P < 0.0001 using Kruskal-Wallis one-way ANOVA followed by Dunn's multiple comparisons test. **C.** Distribution of the sum of seizure scores from each 10-minute observation, knock-in mice show lower total seizure severity, which is removed when treated with XE991. ****P < 0.0001 and *P < 0.05 using Kruskal-Wallis one-way ANOVA followed by Dunn's multiple comparisons test. Error bars show SEM.

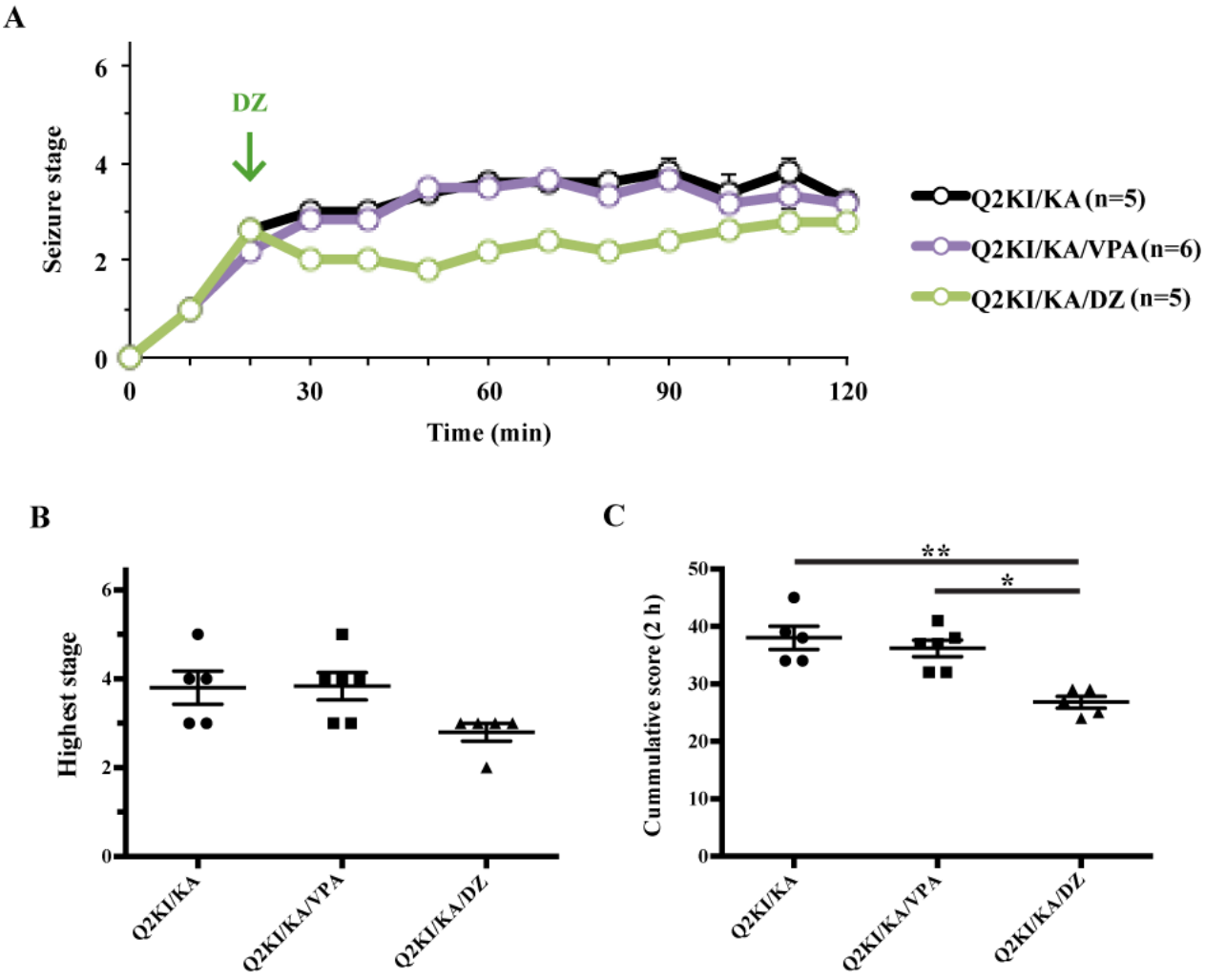

Figure 4.3. Interference of M-current suppression occludes anticonvulsant effect of valproic acid.

A. Time course of seizure severity during kainate-induced seizure (34 mg/kg KA, t = 0). Sub-chronic treatment with valproic acid showed no additional effect. Treatment with diazepam (5 mg/kg DZ, t = 20 minutes) transiently reduced seizure severity. **B.** Distribution of highest seizure stage reached throughout observation period. No difference between groups using Kruskal-Wallis one-way ANOVA. **C.** Distribution of the sum of seizure scores from each 10-minute observation. No difference between groups using Kruskal-Wallis one-way ANOVA. Error bars show SEM.

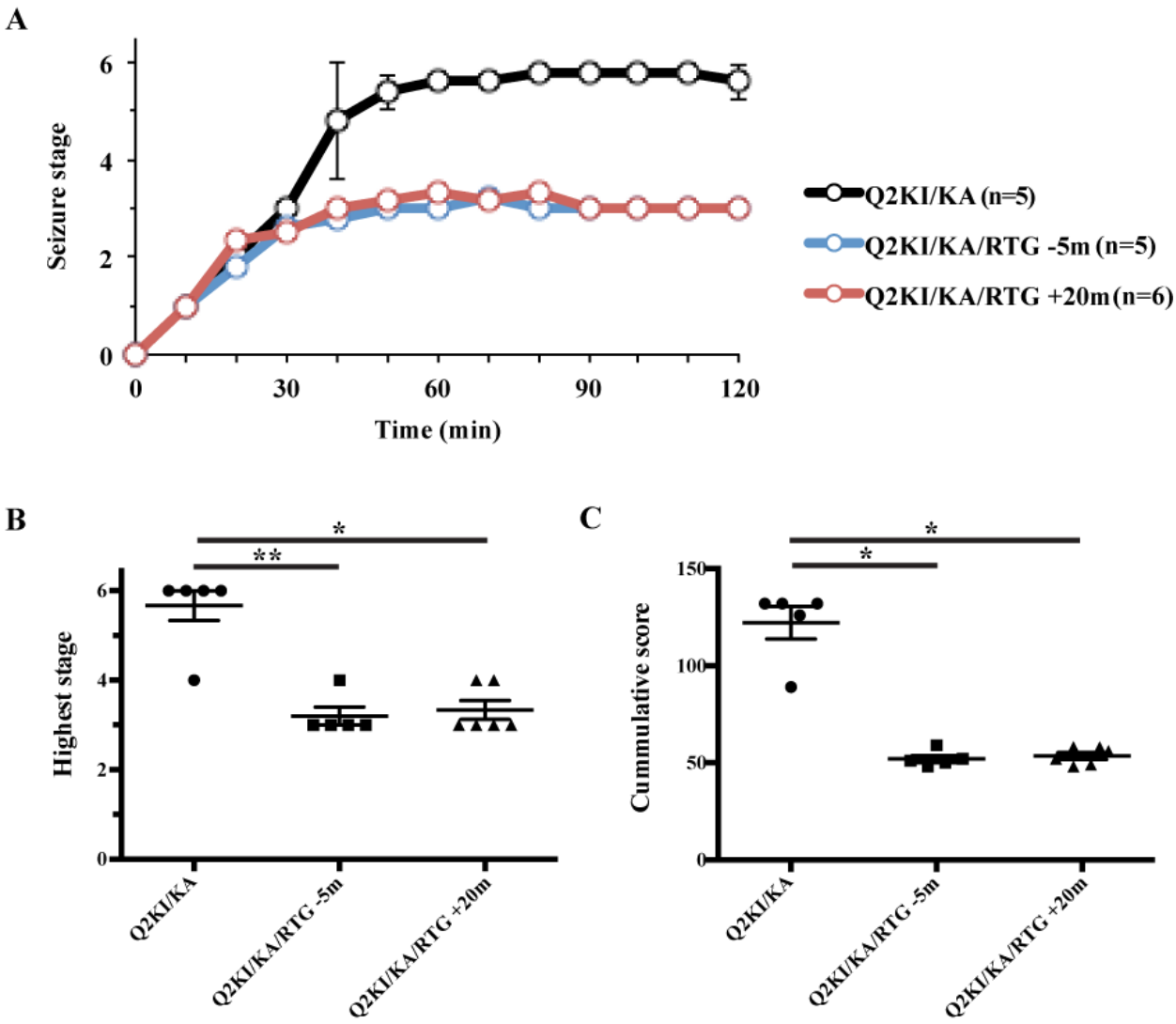

Figure 4.4. Interference of M-current suppression protected retigabine augmentation of the M-current after seizure induction.

A. Time course of seizure severity during first 2 hours of kainate-induced seizure (35 mg/kg KA, t = 0). Treatment with retigabine (10 mg/kg RTG) both 5 minutes prior to and 20 minutes after induction of seizures reduced seizure activity. **B.** Distribution of highest seizure stage reached throughout observation period, RTG treatment showed lower seizure severity in both dose times. *$P < 0.05$ and **$P < 0.01$ using Kruskal-Wallis one-way ANOVA followed by Dunn's multiple comparisons test. **C.** Distribution of the sum of seizure scores from each 10-minute observation, RTG-treated knock-in mice show lower total seizure severity. *$P < 0.05$ using Kruskal-Wallis one-way ANOVA followed by Dunn's multiple comparisons test. Error bars show SEM.

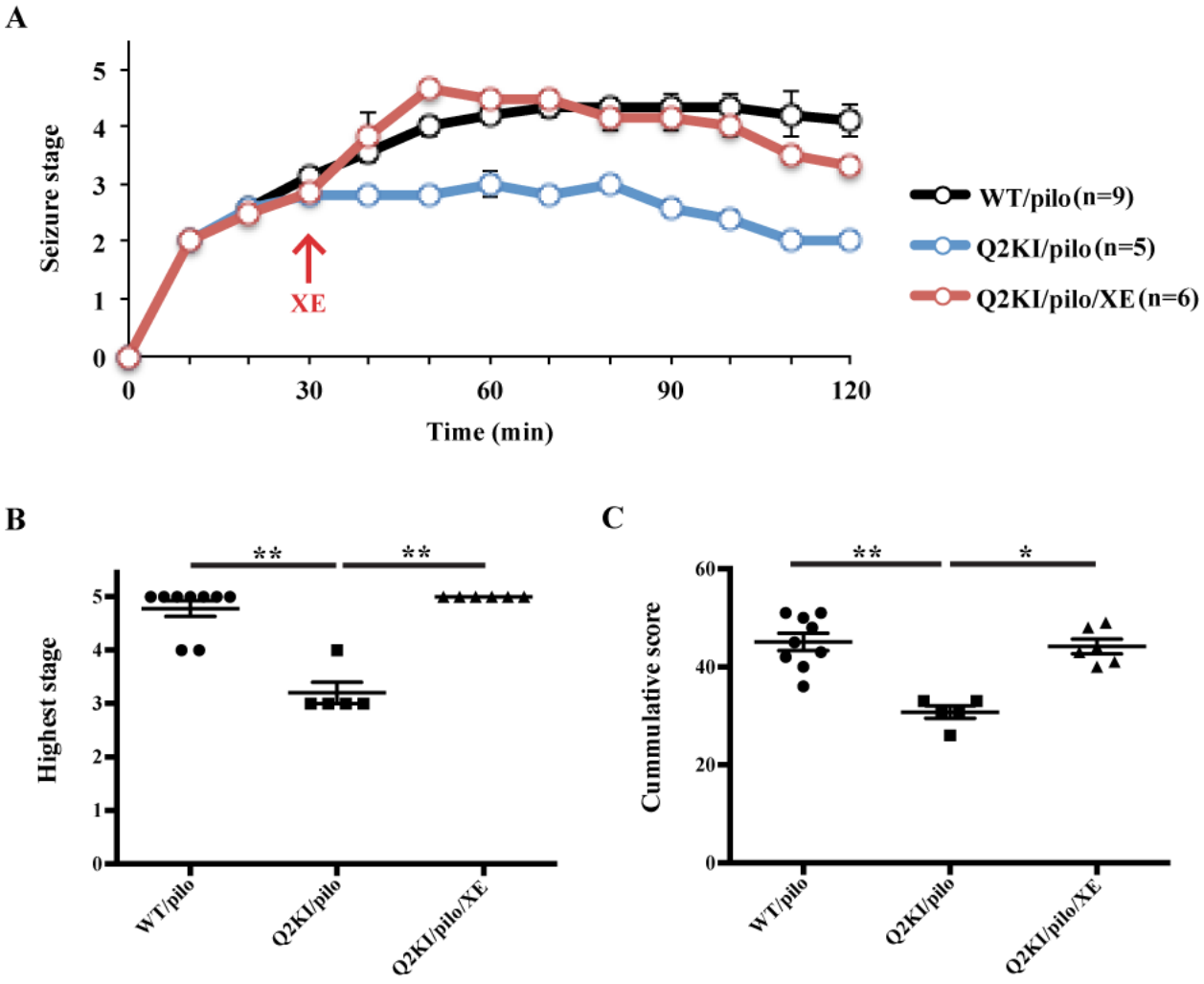

Figure 4.5. Interference of M-current suppression is protective against pilocarpine-induced seizure.

A. Time course of seizure severity during pilocarpine-induced seizure (289 mg/kg Pilo, t = 0). Treatment with M-current-specific inhibitor XE991 (XE 2mg/kg, t = 30 minutes) removed protective phenotype. **B.** Distribution of highest seizure stage reached throughout observation period, knock-in mice show lower seizure severity, removed when M-current is suppressed by XE991. $^{**}P < 0.01$ using Kruskal-Wallis one-way ANOVA followed by Dunn's multiple comparisons test. **C.** Distribution of the sum of seizure scores from each 10-minute observation, knock-in mice show lower total seizure severity, which is removed when treated with XE991. $^{*}P < 0.05$ and $^{**}P < 0.01$ using Kruskal-Wallis one-way ANOVA followed by Dunn's multiple comparisons test. Error bars show SEM.

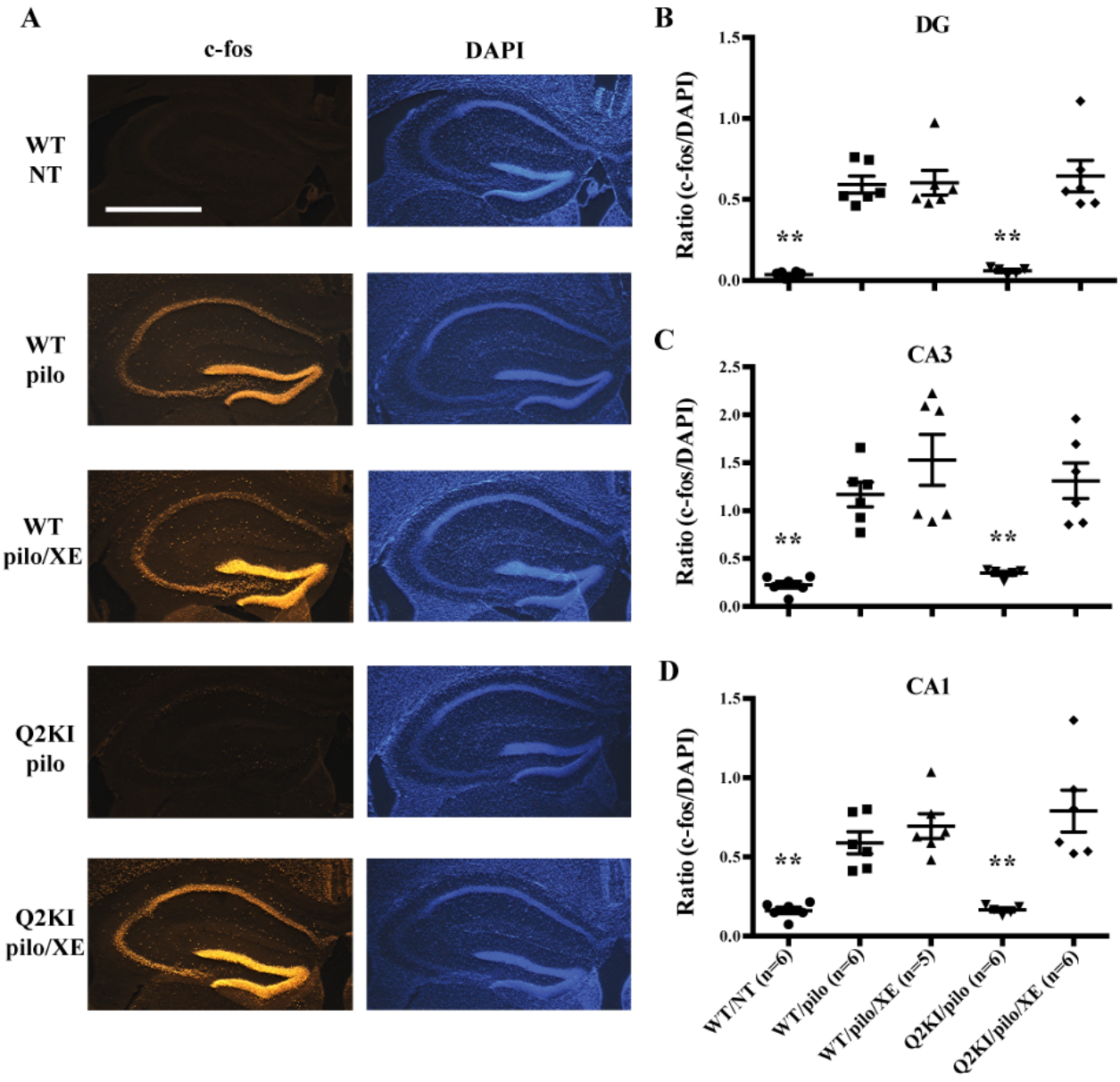

Figure 4.6. Cumulative neural activity shown by c-fos induction corresponded with behavioral seizures.

A. DAPI staining and immunofluorescence staining of c-fos in the hippocampus. Scale bar shows 1 mm. Equivalent induction of c-fos seen in wt and KCNQ2(S559A) mice when co-administered XE991 (B-D). **B.** Distribution of pilocarpine-induced c-fos expression in the dentate gyrus. Low c-fos expression in non-treated mice. Low c-fos induction was observed in KCNQ2(S559A) mice, which was restored when co-administered XE991. **C.** Same as B in the CA3 region. **D.** Same as B in the CA1 region. **P < 0.01 using Kruskal-Wallis one-way ANOVA then each group was compared to WT XE using Mann Whitney test. Error bars show SEM.

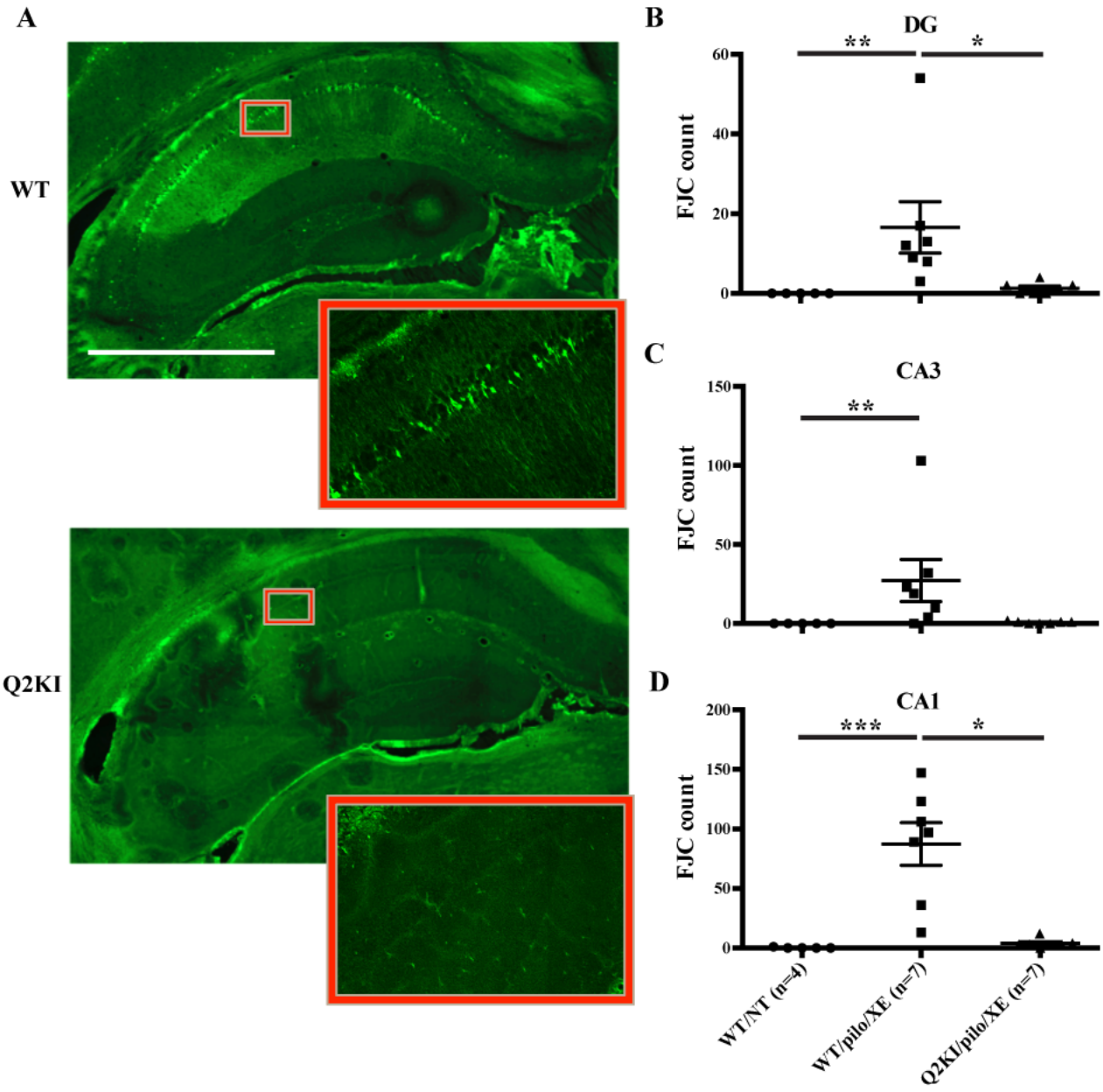

Figure 4.7. Neurodegeneration prevented when M-current preserved after status epilepticus.

A. Staining of neurodegeneration in the hippocampus by Fluoro Jade C. Scale bar shows 1 mm. CA1 region magnified in red box. FJC elevated in wild-type mice but minimal in KCNQ2(S559A) mice. **B.** Distribution of pilocarpine-induced FJC staining in the dentate gyrus. FJC staining observed in wild-type mice, but not in KCNQ2(S559A) or non-treated controls. **C.** Same as B in the CA3 region. **D.** Same as B in the CA1 region. *P < 0.05 and **P < 0.01 using Kruskal-Wallis one-way ANOVA followed by Dunn's multiple comparisons test. Error bars show SEM.

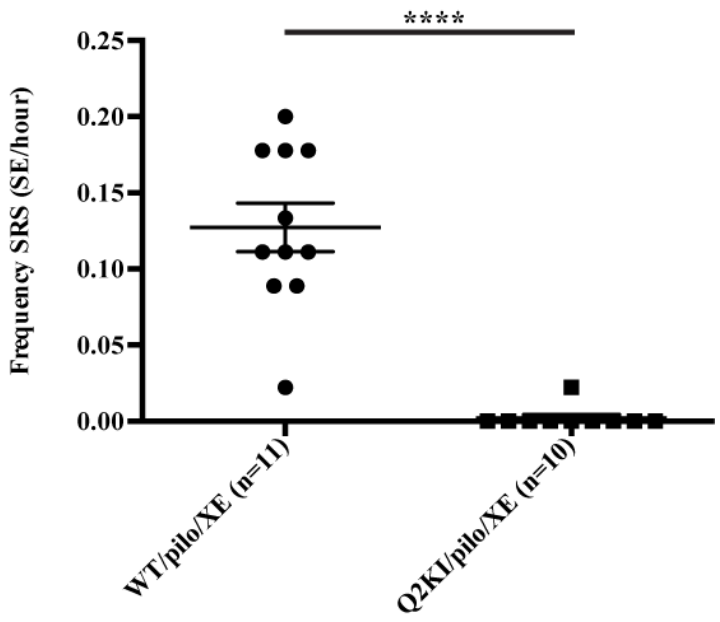

Figure 4.8. Reduced frequency of spontaneous recurrent seizures when M-current preserved after status epilepticus.

Mice observed 3 hours/day from week 2-5 after status epilepticus to observe occurrence of spontaneous seizures. KCNQ2(S559A) mice showed drastic reduction of observable seizures throughout the period of observation. ****$P < 0.0001$ using Kruskal-Wallis one-way ANOVA followed by Dunn's multiple comparisons test. Error bars show SEM.

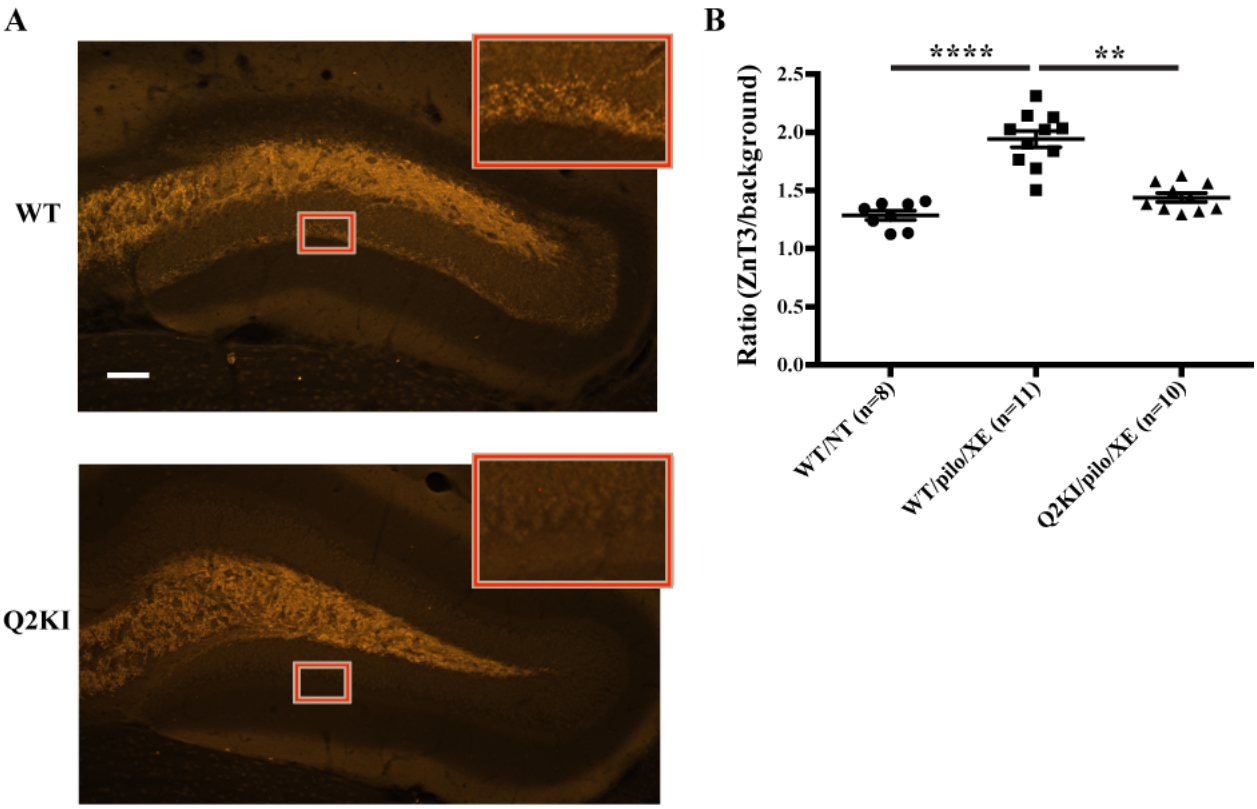

Figure 4.9. Attenuation of synaptogenesis in the granule cell layer of the dentate gyrus when M-current preserved after status epilepticus.

A. Immunofluorescence staining of ZnT3 in the dentate gyrus of the hippocampus 6 weeks after pilocarpine-induced seizure. Scale bar shows 0.1 mm. Granule cell layer magnified in red inset. **B.** Distribution of ZnT3 in the granule layer of the dentate gyrus. ZnT3 fluorescence in the granule cell layer was elevated in wild-type mice but not in KCNQ2(S559A). **P < 0.01 and ****P < 0.0001 using Kruskal-Wallis one-way ANOVA followed by Dunn's multiple comparisons test. Error bars show SEM.

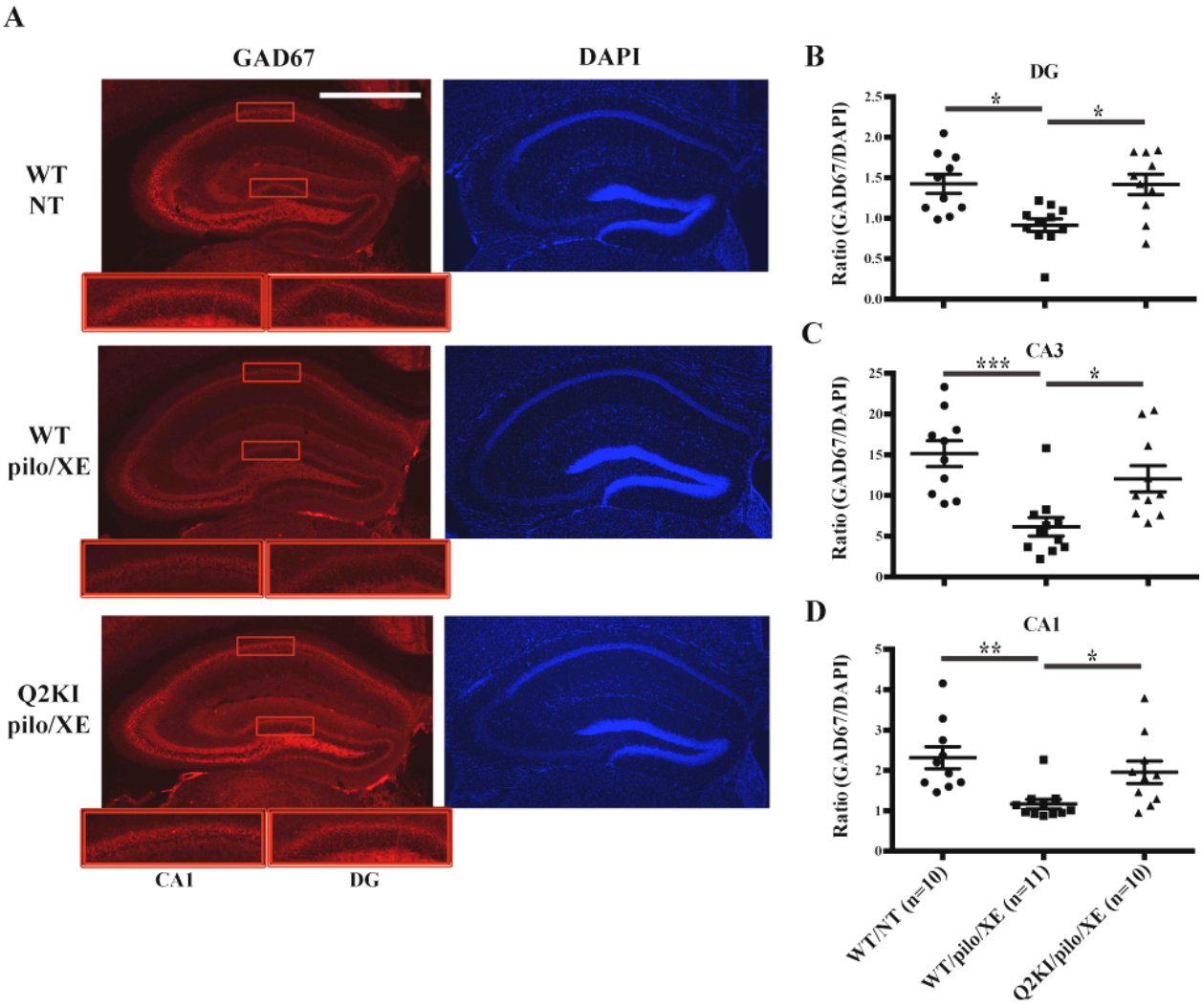

Figure 4.10. Loss of inhibitory interneurons reduced when M-current preserved after status epilepticus.

A. DAPI staining and Immunofluorescence staining of GAD67 in the hippocampus 6 weeks after pilocarpine-induced seizure. CA1 and DG magnified in red insets. Scale bar shows 1 mm. **B.** Distribution of GAD67 in the dentate gyrus. GAD67 fluorescence reduced in wild-type mice but not in KCNQ2(S559A) mice. **C.** Same as B in the CA3 region. **D.** Same as B in the CA1 region. *P < 0.05, **P < 0.01 and ***P < 0.001 using Kruskal-Wallis one-way ANOVA followed by Dunn's multiple comparisons test. Error bars show SEM.

References

1 Purpura, D. P. *Experimental models of epilepsy--a manual for the laboratory worker*. (Raven Press, 1972).

2 Hirtz, D. *et al.* How common are the "common" neurologic disorders? *Neurology* **68**, 326-337, doi:10.1212/01.wnl.0000252807.38124.a3 (2007).

3 Shorvon, S. D., Andermann, F. & Guerrini, R. *The causes of epilepsy : common and uncommon causes in adults and children*. (Cambridge University Press, 2011).

4 Stafstrom, C. E. & Carmant, L. Seizures and epilepsy: an overview for neuroscientists. *Cold Spring Harbor perspectives in medicine* **5**, doi:10.1101/cshperspect.a022426 (2015).

5 Staley, K. Molecular mechanisms of epilepsy. *Nat Neurosci* **18**, 367-372, doi:10.1038/nn.3947 (2015).

6 Cooper, E. C. in *Jasper's Basic Mechanisms of the Epilepsies* (eds J. L. Noebels *et al.*) (2012).

7 Schwake, M., Pusch, M., Kharkovets, T. & Jentsch, T. J. Surface expression and single channel properties of KCNQ2/KCNQ3, M-type K+ channels involved in epilepsy. *J Biol Chem* **275**, 13343-13348 (2000).

8 Jentsch, T. J., Schroeder, B. C., Kubisch, C., Friedrich, T. & Stein, V. Pathophysiology of KCNQ channels: neonatal epilepsy and progressive deafness. *Epilepsia* **41**, 1068-1069 (2000).

9 Ambrosino, P. *et al.* Epilepsy-causing mutations in Kv7.2 C-terminus affect binding and functional modulation by calmodulin. *Biochim Biophys Acta* **1852**, 1856-1866, doi:10.1016/j.bbadis.2015.06.012 (2015).

10 Watanabe, H. *et al.* Disruption of the epilepsy KCNQ2 gene results in neural hyperexcitability. *J Neurochem* **75**, 28-33 (2000).

11 Miceli, F. *et al.* Early-onset epileptic encephalopathy caused by gain-of-function mutations in the voltage sensor of Kv7.2 and Kv7.3 potassium channel subunits. *J Neurosci* **35**, 3782-3793, doi:10.1523/JNEUROSCI.4423-14.2015 (2015).

12 Devaux, J. *et al.* A Kv7.2 mutation associated with early onset epileptic encephalopathy with suppression-burst enhances Kv7/M channel activity. *Epilepsia*, doi:10.1111/epi.13366 (2016).

13 Hoshi, N. *et al.* AKAP150 signaling complex promotes suppression of the M-current by muscarinic agonists. *Nat Neurosci* **6**, 564-571, doi:10.1038/nn1062 (2003).

14 Kosenko, A. *et al.* Coordinated signal integration at the M-type potassium channel upon muscarinic stimulation. *EMBO J* **31**, 3147-3156, doi:10.1038/emboj.2012.156 (2012).

15 Kay, H. Y., Greene, D. L., Kang, S., Kosenko, A. & Hoshi, N. M-current preservation contributes to anticonvulsant effects of valproic acid. *J Clin Invest* **125**, 3904-3914, doi:10.1172/JCI79727 (2015).

16 Cavalheiro, E. A., Santos, N. F. & Priel, M. R. The pilocarpine model of epilepsy in mice. *Epilepsia* **37**, 1015-1019 (1996).

17 Hoshi, N., Langeberg, L. K. & Scott, J. D. Distinct enzyme combinations in AKAP signalling complexes permit functional diversity. *Nat Cell Biol* **7**, 1066-1073, doi:10.1038/ncb1315 (2005).

18 McKhann, G. M., 2nd, Wenzel, H. J., Robbins, C. A., Sosunov, A. A. & Schwartzkroin, P. A. Mouse strain differences in kainic acid sensitivity, seizure behavior, mortality, and hippocampal pathology. *Neuroscience* **122**, 551-561 (2003).

19 McLin, J. P. & Steward, O. Comparison of seizure phenotype and neurodegeneration induced by systemic kainic acid in inbred, outbred, and hybrid mouse strains. *Eur J Neurosci* **24**, 2191-2202, doi:10.1111/j.1460-9568.2006.05111.x (2006).

20 Clifford, D. B., Olney, J. W., Maniotis, A., Collins, R. C. & Zorumski, C. F. The functional anatomy and pathology of lithium-pilocarpine and high-dose pilocarpine seizures. *Neuroscience* **23**, 953-968 (1987).

21 Curia, G., Longo, D., Biagini, G., Jones, R. S. & Avoli, M. The pilocarpine model of temporal lobe epilepsy. *J Neurosci Methods* **172**, 143-157, doi:10.1016/j.jneumeth.2008.04.019 (2008).

22 Hattiangady, B., Kuruba, R. & Shetty, A. K. Acute Seizures in Old Age Leads to a Greater Loss of CA1 Pyramidal Neurons, an Increased Propensity for Developing Chronic TLE and a Severe Cognitive Dysfunction. *Aging Dis* **2**, 1-17 (2011).

23 Nobili, P. *et al.* Continuous neurodegeneration and death pathway activation in neurons and glia in an experimental model of severe chronic epilepsy. *Neurobiol Dis* **83**, 54-66, doi:10.1016/j.nbd.2015.08.002 (2015).

24 Furtado, M. A., Castro, O. W., Del Vecchio, F., de Oliveira, J. A. & Garcia-Cairasco, N. Study of spontaneous recurrent seizures and morphological alterations after status epilepticus induced by intrahippocampal injection of pilocarpine. *Epilepsy Behav* **20**, 257-266, doi:10.1016/j.yebeh.2010.11.024 (2011).

25 Walters, R. J., Hadley, S. H., Morris, K. D. & Amin, J. Benzodiazepines act on GABAA receptors via two distinct and separable mechanisms. *Nat Neurosci* **3**, 1274-1281, doi:10.1038/81800 (2000).

26 Barone, P. *et al.* Expression of c-fos protein in the experimental epilepsy induced by pilocarpine. *Synapse* **14**, 1-9, doi:10.1002/syn.890140102 (1993).

27 Dube, C. *et al.* C-Fos, Jun D and HSP72 immunoreactivity, and neuronal injury following lithium-pilocarpine induced status epilepticus in immature and adult rats. *Brain Res Mol Brain Res* **63**, 139-154 (1998).

28 Motte, J., Fernandes, M. J., Baram, T. Z. & Nehlig, A. Spatial and temporal evolution of neuronal activation, stress and injury in lithium-pilocarpine seizures in adult rats. *Brain Res* **793**, 61-72 (1998).

29 Peng, Z. & Houser, C. R. Temporal patterns of fos expression in the dentate gyrus after spontaneous seizures in a mouse model of temporal lobe epilepsy. *J Neurosci* **25**, 7210-7220, doi:10.1523/jneurosci.0838-05.2005 (2005).

30 Ribak, C. E., Tran, P. H., Spigelman, I., Okazaki, M. M. & Nadler, J. V. Status epilepticus-induced hilar basal dendrites on rodent granule cells contribute to recurrent excitatory circuitry. *The Journal of comparative neurology* **428**, 240-253 (2000).

31 Dingledine, R., Varvel, N. H. & Dudek, F. E. When and How Do Seizures Kill Neurons, and Is Cell Death Relevant to Epileptogenesis? *Advances in experimental medicine and biology* **813**, 109-122, doi:10.1007/978-94-017-8914-1_9 (2014).

32 Fujikawa, D. G. Prolonged seizures and cellular injury: understanding the connection. *Epilepsy Behav* **7 Suppl 3**, S3-11, doi:10.1016/j.yebeh.2005.08.003 (2005).

33 Vignoli, T. *et al.* Consequences of pilocarpine-induced status epilepticus in immunodeficient mice. *Brain Res* **1450**, 125-137, doi:10.1016/j.brainres.2012.02.028 (2012).

34 Shibley, H. & Smith, B. N. Pilocarpine-induced status epilepticus results in mossy fiber sprouting and spontaneous seizures in C57BL/6 and CD-1 mice. *Epilepsy Res* **49**, 109-120 (2002).

35 Hunt, R. F., Girskis, K. M., Rubenstein, J. L., Alvarez-Buylla, A. & Baraban, S. C. GABA progenitors grafted into the adult epileptic brain control seizures and abnormal behavior. *Nat Neurosci* **16**, 692-697, doi:10.1038/nn.3392 (2013).

36 Nadler, J. V., Perry, B. W. & Cotman, C. W. Selective reinnervation of hippocampal area CA1 and the fascia dentata after destruction of CA3-CA4 afferents with kainic acid. *Brain Res* **182**, 1-9 (1980).

37 Davenport, C. J., Brown, W. J. & Babb, T. L. Sprouting of GABAergic and mossy fiber axons in dentate gyrus following intrahippocampal kainate in the rat. *Exp Neurol* **109**, 180-190 (1990).

38 Buckmaster, P. S. & Lew, F. H. Rapamycin suppresses mossy fiber sprouting but not seizure frequency in a mouse model of temporal lobe epilepsy. *J Neurosci* **31**, 2337-2347, doi:10.1523/JNEUROSCI.4852-10.2011 (2011).

39 Pierce, J. P., Melton, J., Punsoni, M., McCloskey, D. P. & Scharfman, H. E. Mossy fibers are the primary source of afferent input to ectopic granule cells that are born after pilocarpine-induced seizures. *Exp Neurol* **196**, 316-331 (2005).

40 Hu, H., Gan, J. & Jonas, P. Interneurons. Fast-spiking, parvalbumin(+) GABAergic interneurons: from cellular design to microcircuit function. *Science* **345**, 1255263, doi:10.1126/science.1255263 (2014).

41 Kelsom, C. & Lu, W. Development and specification of GABAergic cortical interneurons. *Cell & bioscience* **3**, 19, doi:10.1186/2045-3701-3-19 (2013).

42 Kobayashi, M. & Buckmaster, P. S. Reduced inhibition of dentate granule cells in a model of temporal lobe epilepsy. *J Neurosci* **23**, 2440-2452 (2003).

43 Hofmann, G., Balgooyen, L., Mattis, J., Deisseroth, K. & Buckmaster, P. S. Hilar somatostatin interneuron loss reduces dentate gyrus inhibition in a mouse model of temporal lobe epilepsy. *Epilepsia*, doi:10.1111/epi.13376 (2016).

44 Klinger, F., Gould, G., Boehm, S. & Shapiro, M. S. Distribution of M-channel subunits KCNQ2 and KCNQ3 in rat hippocampus. *Neuroimage* **58**, 761-769, doi:10.1016/j.neuroimage.2011.07.003 (2011).

45 Reddy, D. S. & Kuruba, R. Experimental models of status epilepticus and neuronal injury for evaluation of therapeutic interventions. *International journal of molecular sciences* **14**, 18284-18318, doi:10.3390/ijms140918284 (2013).

46 Mark, G. P. & Finn, D. A. The relationship between hippocampal acetylcholine release and cholinergic convulsant sensitivity in withdrawal seizure-prone and withdrawal seizure-resistant selected mouse lines. *Alcoholism, clinical and experimental research* **26**, 1141-1152, doi:10.1097/01.alc.0000024125.23287.ca (2002).

47 Acon-Chen, C. *et al.* Evaluation of acetylcholine, seizure activity and neuropathology following high-dose nerve agent exposure and delayed neuroprotective treatment drugs in freely moving rats. *Toxicology mechanisms and methods* **26**, 378-388, doi:10.1080/15376516.2016.1197992 (2016).

48 Meurs, A., Clinckers, R., Ebinger, G., Michotte, Y. & Smolders, I. Seizure activity and changes in hippocampal extracellular glutamate, GABA, dopamine and serotonin. *Epilepsy Res* **78**, 50-59, doi:10.1016/j.eplepsyres.2007.10.007 (2008).

49 Roosevelt, R. W., Smith, D. C., Clough, R. W., Jensen, R. A. & Browning, R. A. Increased extracellular concentrations of norepinephrine in cortex and hippocampus following vagus nerve stimulation in the rat. *Brain Res* **1119**, 124-132, doi:10.1016/j.brainres.2006.08.048 (2006).

50 Li, C. *et al.* Activity-dependent downregulation of M-Type (Kv7) K(+) channels surface expression requires the activation of iGluRs/Ca(2)(+)/PKC signaling pathway in hippocampal neuron. *Neuropharmacology* **95**, 154-167, doi:10.1016/j.neuropharm.2015.03.004 (2015).

51 Martinello, K. *et al.* Cholinergic afferent stimulation induces axonal function plasticity in adult hippocampal granule cells. *Neuron* **85**, 346-363, doi:10.1016/j.neuron.2014.12.030 (2015).

52 Lothman, E. W., Bertram, E. H., 3rd & Stringer, J. L. Functional anatomy of hippocampal seizures. *Prog Neurobiol* **37**, 1-82 (1991).

53 Meriaux, C. *et al.* Human temporal lobe epilepsy analyses by tissue proteomics. *Hippocampus* **24**, 628-642, doi:10.1002/hipo.22246 (2014).

Chapter Five

Summary and Conclusions

Investigations continue to uncover new mechanisms responsible for controlling activity within the cortex as well as enrich our understanding of debilitating pathologies that plague the brain. Despite all our efforts, there is still much work to be done. I endeavored to increase our knowledge, emphasizing on the pathological roles of the M-current. In this dissertation, I characterized the mechanism of inhibition for XE991 and linopirdine, two commonly used M-current blockers, identified a molecular mechanism underlying the anticonvulsive effect of valproic acid and utilized a novel transgenic mouse line to determine the role of M-current suppression during seizure and epileptogenesis.

Mechanism of inhibition and use of pharmacological compounds

Insufficient characterization of pharmacological compounds can confound results leading to poor interpretation. Conversely, robust understanding of pharmacological compounds can provide a greater degree of manipulation during experiments. M-channel inhibitors, especially XE991, are increasingly being used in animal experiments. However, lack of information concerning this compound has lead to conflicting reports regarding its effectiveness to inhibit as well as what tissues express functional Kv7 channels, which motivated me to characterize this inhibitor. Characterization of the mechanism of inhibition of XE991 and linopirdine were covered in chapter 2. Both inhibitors were not efficacious around the resting membrane potential

of cells in physiological conditions. Furthermore, inhibition of Kv7.2 and Kv7.2/3 channels by XE991 was closely related with its activation threshold, indicating the need to manipulate tissue in order to have effective inhibition. When voltage dependence of activation was left-shifted by retigabine or right-shifted by the mutation, Kv7.2(R214D), the shift in half activation voltage proportionally coincided with the half-effective potential for XE991 inhibition. Inhibition kinetics during XE991 wash-in were facilitated at depolarized potentials. Ten-minute washout resulted in partial recovery, most of which was attributed to surface transport of Kv7.2 channels. Linopirdine also exhibited similar features with the notable difference that it could be washed out if cells were held at potentials above the activation range of Kv7.2 channels.

Binding and dissociation kinetics of both XE991 and linopirdine were far less sensitive to voltage than what would be predicted when modeling for open channel binding. Instead, they were well explained by binding to a single activated subunit. We demonstrated that XE991 and linopirdine are activated-subunit inhibitors rather than voltage-dependent inhibitors of Kv7/KCNQ channels. We conclude that XE991 and linopirdine are activated-subunit inhibitors. The characteristics of XE991 were taken into account when this M-channel inhibitor was used in our models of status epilepticus.

Seizures occur due to excessive synchronous activity that perpetuates itself throughout the cortex. To understand the role of M-current inhibition in epilepsy, XE991 allowed for the selective inhibition of Kv7 channels in neurons contributing to ictal activities while having minimal effect in silent or sparsely spiking neurons.

Pathway underlying anticonvulsant action of valproic acid

Valproic acid has been widely used to treat epilepsy for decades. Accordingly, numerous studies have proposed mechanisms responsible for its mechanism of action. Unfortunately, the majority of reports used doses of valproic acid many fold higher than the therapeutic concentration, typically focusing on pathways affected by acute use. As such, this compound has remained poorly understood. In chapter 3 we demonstrate that the anticonvulsant effects of non-acute valproic acid treatment involve interfering with the process of M-current suppression during seizures.

Suppression of the M-current induces hyperexcitability in a wide variety of neurons downstream of Gq-coupled receptor activation, including the m1 muscarinic acetylcholine receptor. We demonstrated that valproic acid treatment disrupts muscarinic suppression of the M-current and prevents resultant agonist-induced neuronal hyperexcitability. We also identify the mechanism. Namely, that valproic acid treatment interferes with M-channel signaling by inhibiting palmitoylation of a signaling scaffold protein within the M-channel complex, AKAP79/150.

In a kainate model of induced status epilepticus, administration of a dose XE991 that did not affect seizure severity in control mice transiently eliminated anticonvulsant effects of valproic acid. Retigabine, an M-channel opener that is not effective on receptor-suppressed M-channels, showed anticonvulsant effects only when administered before seizure induction in control mice. In contrast, in valproic acid treated mice, retigabine showed anticonvulsant effects even when administered after induction of seizures. That valproic acid was able to further augment the anticonvulsant activity of retigabine suggests that combinational treatment with these two compounds would provide powerful suppression of neural hyperactivity, even if administered during

a seizure episode. Taken together, these results suggest that receptor-induced M-current suppression plays a role in the pathophysiology of seizures and that preservation of the M-current during seizures is an effective therapeutic strategy.

Role of M-current suppression in pathology of epilepsy

A major drawback of using valproic acid to investigate the contribution of M-current suppression in seizures is the fact that the compound has been reported to affect a multitude of pathways. In order to circumvent this issue we generated a transgenic mouse line using an alanine substitution for the target of AKAP79/150-anchored PKC on serine residue 559 of the KCNQ2/Kv7.2 subunit, KCNQ2(S559A). This mutation allowed us to develop a mouse line that removed the majority of M-current suppression from Gq-coupled receptor activation. In chapter 4 these mice were used to investigate the role of pathological M-current suppression during seizure and epileptogenesis.

As we expected, KCNQ2(S559A) knock-in (Q2KI) mice were resistant to pharmacologically-induced seizures compared to wild-type C57BL/6 mice. Moreover, valproic acid treatment was occluded by the anticonvulsive phenotype in Q2KI mice. If other pathways affected by valproic acid are major contributors to its therapeutic effect it is reasonable to assume that VPA-treated Q2KI mice would have a cumulative effect resulting in less severe seizures than VPA non-treated. This provided further evidence that a key mechanism underlying the effectiveness of valproic acid is indeed through preservation of the M-current. Indeed, XE991 and retigabine experiments confirmed that the anticonvulsive phenotype was derived from the selective mutation of the PKC phosphorylation site in Q2KI mice, and not from compensatory changes that may occur

during development in transgenic animals. We can conclude from these results the wild-type M-current is suppressed during seizures.

In order to investigate whether prolonged suppression of the M-current after initial status epilepticus contributes to epileptogenesis we utilized a pilocarpine model of temporal lobe epilepsy. In order to ensure equivalent severity of seizure between genotypes it was necessary to pharmacologically suppress the M-current with XE991 in conjunction with inducing seizures with pilocarpine. If the M-current normally recovers after status epilepticus then it would be expected that both genotypes would undergo the same degree of epileptogenesis. While wild-type mice progressed to develop spontaneous recurrent seizures (SRS), observed episodes were almost nonexistent in Q2KI mice. It is possible that the absence of SRS in Q2KI mice may not be an indication of the absence of ictal activities but instead possibly due to the anticonvulsive phenotype of Q2KI mice attenuating seizure severity below what is observable. In future experiments electroencephalogram (EEG) recordings will be utilized to detect ictal activity directly from the cortex. However, the lack of common morbidities that normally occur alongside and contribute to epileptogenesis provide strong evidence that preservation of the M-current after status epilepticus is sufficient to attenuate the development of epilepsy. It will be interesting to see where investigations into the pathological consequences of the transition of the channel to the activated and suppressed states progress.